66-14,248

SCIANCE, Carroll Thomas, 1939-

POOL BOILING HEAT TRANSFER TO
LIQUEFIED HYDROCARBON GASES.

The University of Oklahoma, Ph.D., 1966
Engineering, chemical

University Microfilms, Inc., Ann Arbor, Michigan

THE UNIVERSITY OF OKLAHOMA

GRADUATE COLLEGE

POOL BOILING HEAT TRANSFER TO LIQUEFIED HYDROCARBON GASES

A DISSERTATION

SUBMITTED TO THE GRADUATE FACULTY

in partial fulfillment of the requirements for the

degree of

DOCTOR OF PHILOSOPHY

BY

CARROLL THOMAS SCIANCE

Norman, Oklahoma

1966

POOL BOILING HEAT TRANSFER TO

LIQUEFIED HYDROCARBON GASES

APPROVED BY

C. M. Sliepcevich

Frank Canfield

F. M. Townsend

[illegible signature]

Sherril D. Christian

DISSERTATION COMMITTEE

ACKNOWLEDGEMENT

The author wishes to express his sincere appreciation to all of those who have helped him to complete the experimental work and prepare this dissertation. Particular thanks are due to the following persons:

Dr. C. M. Sliepcevich for his direction of this research and his continuing advice and encouragement.

Dr. C. Phillip Colver for his suggestions and help with this manuscript and the paper on methane boiling.

Dr. Frank Canfield, Dr. Sherril Christian, and Dr. Mark Townsend for their advice and assistance.

Mr. Arlin Lee, Mr. Paul Johnson, Mr. Calvin Hurst, Mrs. Marlys Tucker and Mrs. Charlotte Levendosky of the University of Oklahoma High Speed Computer Project for their assistance in treating the experimental data.

Mr. Woodrow Porter for his unfailing industry in constructing, modifying and repairing the heater.

Mrs. Billy Ann Brown for expediting the purchase of equipment and supplies, among many other things.

Mr. Kenneth R. Hall for the use of his ORNOR curve-fitting program.

Dr. Jerry Lott and Mr. Robert Loeffler for their advice and assistance.

Dr. Efton Park for his work in initiating the study of cryogenic boiling at this university.

Finally, to my wife Anita, who typed this thesis and more than a hundred others; who prepared the computer tapes of the data; who raised four children; and who never complained once.

The author is indebted to the National Aeronautics and Space Administration for their financial support for three years and to Conch Methane, Ltd. and the Continental Oil Company for furnishing part of the supplies and equipment.

TABLE OF CONTENTS

TABLE OF CONTENTS--Continued

TABLE OF CONTENTS--Continued

LIST OF TABLES

LIST OF TABLES--Continued

LIST OF TABLES--Continued

LIST OF ILLUSTRATIONS

LIST OF ILLUSTRATIONS--Continued

LIST OF ILLUSTRATIONS--Continued

POOL BOILING HEAT TRANSFER TO LIQUEFIED HYDROCARBON GASES

CHAPTER I

INTRODUCTION

Boiling heat transfer may occur in a variety of complex situations. In this work, data were taken for saturated pool boiling outside an electrically heated cylinder. The significance of each of these qualifications is described below.

"Saturated" boiling occurs when the bulk fluid is at its saturation temperature. "Saturated pool boiling" means that the heater is immersed in the boiling liquid; it further implies that the liquid has a free surface and no forced convection is present.

Most saturated pool boiling data are taken from flat plates, cylinders or wires. Differentiating between cylinders and wires is arbitrary, but necessary; hydrodynamic aspects change radically depending upon the size of the bubbles relative to that of the surface on which they form. The gold-plated cylinder used in this work had a diameter of 0.811 inch and a length of 4 inches. This diameter, slightly over two centimeters, is large enough so that the data can be

directly compared with that from pipes or flat plates [10].

The use of an electric heater normally limits study to the nucleate and film boiling regimes described below. An electric heater is essentially a constant-flux device which is inherently unstable in the transition boiling regime [86].

Study of saturated pool boiling for several substances, over a range of pressures, and on the same surface, permits isolation of the effects of fluid properties on boiling heat transfer. The disadvantage of such a simplified situation is that data are not directly applicable to industrial problems unless the effect of each complicating factor can be calculated separately.

Boiling Regimes

The pool boiling heat transfer coefficient h_b and the driving force ΔT are defined by equation (1-1).

$$q \equiv h_b(T_w - T_{sat}) \equiv h_b \Delta T \qquad (1\text{-}1)$$

The flux q has units Btu/ft^2-hr, T_w is the temperature of the solid surface, and T_{sat} is the saturation temperature of the fluid. Temperatures are in degrees Fahrenheit.

Equation (1-1) is not the definition of ΔT that is always encountered; an alternate definition would be $(T_w - T_\infty)$, with T_∞ the bulk fluid temperature. Westwater [85] has pointed out that the former definition of ΔT is more significant than the latter, because the very important

critical heat fluxes, described below, seem to occur at a particular value of T_w, regardless of the fact that the bulk fluid may be subcooled or superheated slightly. The practice used in this work will be to use equation (1-1). Deviations of T_∞ from T_{sat} were always very small for the data taken in this work.

Pool boiling heat transfer data are traditionally presented on log-log plots of q vs. ΔT or h_b vs. ΔT. (A well-known example of misleading correlation is to plot q vs. h_b [50,55].) In 1934, Nukiyama [64] demonstrated, with curves of the type shown in Figure 1, that there were different kinds (regimes) of boiling. The discussion which follows refers to Figure 1.

Nucleate Boiling

Nucleate boiling is characterized by bubbles forming at isolated points (nucleation sites). Fluxes are very high; for organic liquids 150,000 Btu/ft^2-hr is not uncommon. Temperature differences are usually less than 100 F°. Surface characteristics have a pronounced effect. The nucleate boiling curves are those on the left in Figure 1. The ΔT at a given flux decreases with increasing pressure. The theory of nucleate boiling is discussed in Chapter II.

First Critical Point

As the heat flux is increased in the nucleate boiling regime, more and more nucleation sites become activated. The population of active sites eventually becomes so dense that

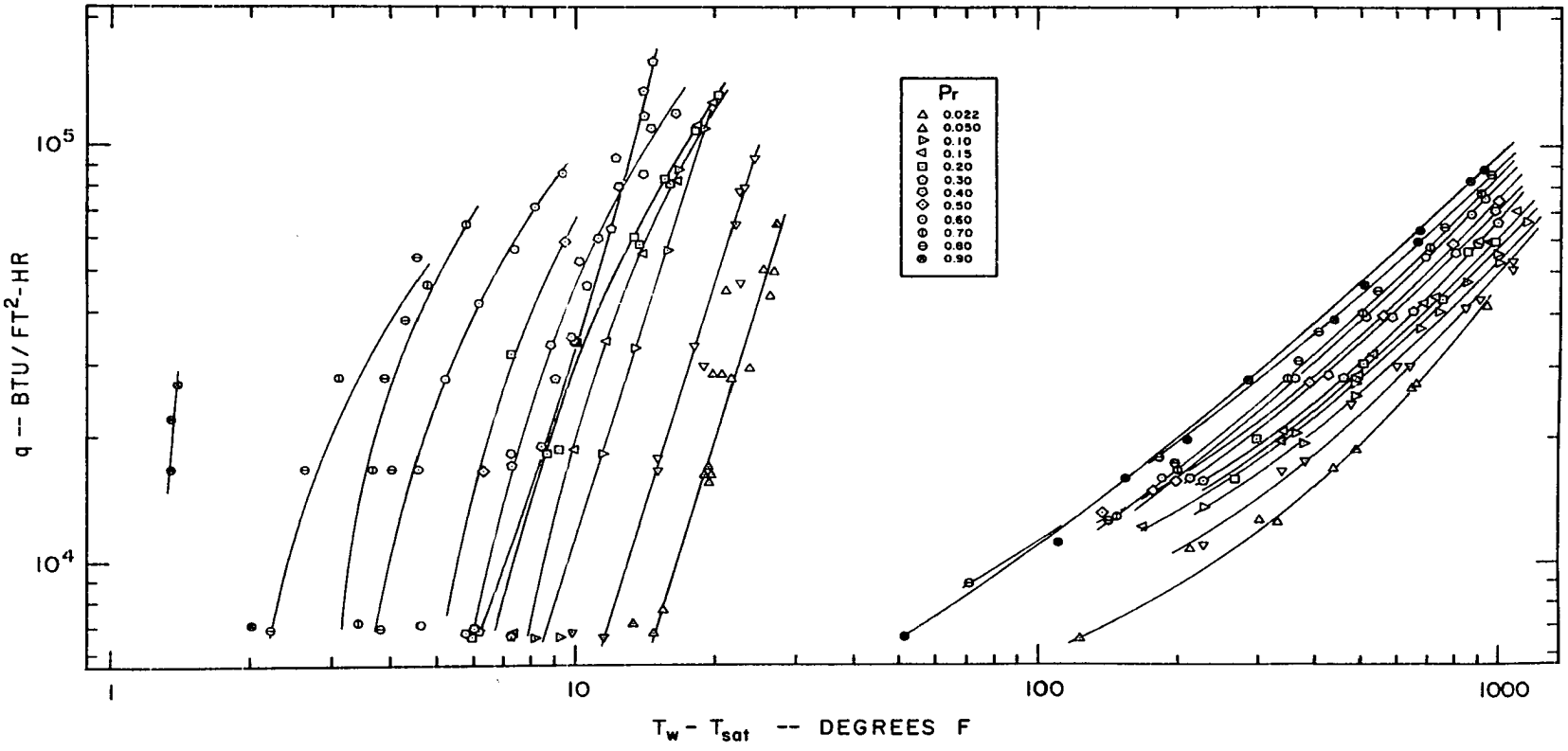

Figure 1. Typical Boiling Heat Transfer Curves (the Methane Data Taken in this Work) for Both Stable Nucleate and Film Boiling at Several Pressures

the surface becomes blanketed with vapor. A subsequent increase of ΔT reduces the flux. This point is of great practical and theoretical significance and has probably received more attention than any other aspect of boiling heat transfer. It is sometimes called the "burnout point," because a constant-flux device, such as an electric heater, tries to compensate for the decreasing heat transfer coefficient by increasing T_w. If the flux of a heater operating at the critical flux is increased slightly, the heat transfer coefficient will drop sharply, and the resulting increase in surface temperature may result in the melting, or burnout, of the heater. Theories and correlations involving the first critical point are discussed in Chapter II.

Transition Boiling

The transition boiling regime would be represented in Figure 1 by lines connecting the nucleate and film boiling curves at each pressure. It was not studied in this work because an electric heater was used. The transition boiling regime can be investigated with a source of constant T_w, such as a condensing vapor. Farber and Scorah [23] were able to establish all three boiling regimes on a heated wire, and some electric heaters can be controlled or stabilized, but the one used in this work was not. Westwater [86] cites photographs which indicate that the surface is always blanketed by vapor in this region; Rohsenow [75] describes the film as collapsing and reforming under the action of circulation currents.

Film Boiling and the Second Critical Point

At very high values of ΔT, the surface becomes blanketed by a stable vapor film of rather low conductivity. Since the surface temperature is much higher than the fluid temperature, radiation becomes an important contributor to the total flux. The minimum film boiling point is sometimes called the "Leidenfrost point," and sometimes the "second critical point." The second critical point and stable film boiling regime are treated more thoroughly in Chapter III.

Effect of Pressure

Cichelli and Bonilla [22], in 1945, showed that the first critical heat flux q_{lc} varies regularly with reduced pressure Pr; it is zero at Pr = 1 and Pr = 0, and passes through a maximum at about Pr = 0.3.

Increasing pressure moves both the nucleate and film boiling curves in Figure 1 to the left.

Beyond these generalities, existing correlations do not account for the pressure effect very well, especially at reduced pressures above 0.5. Data are also rather scarce at high reduced pressures.

At pressures above the critical pressure a "boiling-like" heat transfer may occur because of the large density gradients near the heated surface. It can be considered to be a special case of natural convective heat transfer.

Purpose of this Work

In Chapters II and III the extant theories are taken

up in detail. At this point, however, it is appropriate to explain why this research was undertaken.

A great amount of experimental work has been done during the past thirty years in the field of boiling heat transfer. However, efforts to predict boiling heat transfer coefficients, or even to correlate them, have met with only limited success.

An exhaustive analysis of the literature of pool boiling heat transfer to cryogenic liquids by Brentari, Giarratano and Smith [11] led to the following conclusions:

1. Predictive correlations for nucleate boiling at high pressures are of marginal success.

2. Peak flux predictions are inaccurate at reduced pressures above 0.6.

3. Insufficient data are available to discuss the effect of pressure on film boiling.

4. More detailed and better controlled experiments are required.

There exists a real need for boiling heat transfer data for a series of simple substances boiling over a range of pressures on the same surface. The low molecular weight saturated hydrocarbons are ideal substances, partly because of their simple molecular structure, but more importantly because of the wealth of accurate data on their physical and transport properties. Correlation of even the most accurate heat transfer data cannot succeed unless the properties used in the correlations are known accurately.

The object of this work was to obtain accurate data on saturated pool boiling of methane, ethane, propane and butane over the range of pressure between one atmosphere and the critical pressure. It was particularly desired to test existing film boiling correlations since so little high pressure work had been done in this area. Data were taken in both the nucleate and stable film boiling regimes, and at both the first and second critical fluxes.

CHAPTER II

NUCLEATE POOL BOILING AND THE FIRST CRITICAL POINT

Theories Based on Turbulence

Early efforts to describe nucleate boiling were based on the mechanism known as "microconvection in the sublayer." Measurements by Gunther and Kreith [35] and Rohsenow and Clark [77] had indicated that the large fluxes encountered in nucleate boiling were due primarily to bubble-induced agitation near the heated surface.

Dimensional analysis indicated that data could be correlated using the Prandtl Number Pr*, the Nusselt number Nu*, and the Reynolds number Re*:

$$Pr^* \equiv C_p\mu/k \tag{2-1}$$

$$Nu^* \equiv hL^*/k \tag{2-2}$$

$$Re^* \equiv G^*L^*/\mu \tag{2-3}$$

where L* is a characteristic length, G* a characteristic mass velocity, k is thermal conductivity, μ is viscosity, C_p is the heat capacity at constant pressure, and h is the heat transfer coefficient. By analogy with correlations used for nonboiling heat transfer, the correlating form selected was

$$Nu^* = m_1(Re^*)^{m_2}(Pr^*)^{m_3} \tag{2-4}$$

where the m_i's are empirical constants. The theoretical problem was to select appropriate values of G* and L*. Because data are often presented in graphs of q vs. ΔT, as mentioned in Chapter I, it is worth noting that at a particular pressure equations of the type (2-4) can be approximated by the form (2-5).

$$q = m_4(\Delta T)^{m_5} \tag{2-5}$$

In 1952, Rohsenow [75] chose bubble diameter and vapor mass velocity as the characteristic quantities G* and L*. Rohsenow's characteristic length L* was B, the "Laplace Reference Length"

$$B \equiv \sqrt{\frac{g_c \sigma}{g(\rho_\ell - \rho_v)}} \tag{2-6}$$

where σ is surface tension, ρ_ℓ is the saturated liquid density, ρ_v the saturated vapor density, and g the acceleration of gravity.

Rohsenow's definition of the Reynolds number, $Re^* = qB/\lambda C_{p\ell}$, leads to the correlating equation

$$Re^* = m_6 \left[\frac{C_{p\ell}\Delta T}{\lambda (Pr^{*1.7})} \right]^3 \tag{2-7}$$

where the subscript ℓ refers to the saturated liquid.

The primary path of heat flow in this mechanism was assumed to be: surface → liquid → bubble. The controlling resistance was at the liquid-bubble interface.

In 1959, Forster and Greif [24] advanced the theory

that "vapor-liquid exchange," or the displacement of heated liquid from the surface by a growing bubble, could account for much of the heat transfer. The equation they obtained is:

$$q = 0.0012 \frac{k_\ell T_{sat}}{J\lambda\rho_v\sqrt{\sigma}} \left[\frac{C_{p\ell} T_{sat} g_c \sqrt{\alpha_\ell}}{J(\rho_v \lambda)^2} \right]^{1/4} \left(\frac{\rho_\ell}{\mu_\ell} \right)^{5/8} (Pr_\ell^*)^{1/3} (\Delta P)^2 \tag{2-8}$$

where α is thermal diffusivity $(k/\rho C_p)$, J is the mechanical equivalent of heat, T_{sat} is an absolute saturation temperature, and ΔP is the difference in pressure between the saturated fluid at the wall temperature T_w and the saturation temperature T_{sat}.

Forster and Greif recommend evaluating liquid properties at T_w and vapor properties at T_{sat}. The statistical analysis of Hughmark [40] also pointed up the fact that liquid properties evaluated at T_w are more significant than those evaluated at T_{sat}.

The excess pressure ΔP can be developed into a power series in superheat

$$\Delta P = \left(\frac{dP}{dT} \right)\Big|_{T_{sat}} \Delta T + \frac{1}{2} \left(\frac{d^2 P}{dT^2} \right)\Big|_{T_{sat}} (\Delta T)^2 + \ldots \tag{2-9}$$

which was truncated by Forster and Greif after the first term and evaluated from the Clausius-Clapeyron equation for dP/dT:

$$\Delta P \approx \frac{J\lambda\rho_\ell\rho_v}{T_{sat}(\rho_\ell - \rho_v)} \Delta T \tag{2-10}$$

Other equations of the general kind (2-4) have been presented; Seader et al. [80] have presented seven others besides (2-7) and (2-8). This reference also lists the nine equations in a common Stanton number form, but caution should be exercised in using that table because of their simplifying assumptions that $\rho_\ell >> \rho_v$ and that (2-10) holds. These assumptions would give very misleading comparisons at elevated pressures and possibly also at high ΔT's.

Comparisons of available data on cryogenic boiling with these theories were made recently by Brentari and Smith [11,12] and Seader et al. [80]. The conclusions were:

1. Most of the theories fall within the spread of the data at atmospheric pressure.

2. Disadvantages are that the nature, geometry and orientation of the heater surface are neglected.

3. The equations do not work well at elevated pressures, although the trends are correctly predicted.

Incorporation of Surface Properties

A number of attempts [43,44,61,83,87] have been made to account for surface characteristics with equations of the form (2-11), where N is the number of active sites per unit area.

$$q = m_7 N^{m_8} (\Delta T)^{m_9} \qquad (2\text{-}11)$$

Zuber [89] predicted $m_8 = 1/3$ and $m_9 = 5/3$. He explained that there were actually two areas in the nucleate boiling regime which should be treated separately: the "region of

isolated bubbles" and the "region of interference." He concluded that the mechanism leading to (2-11) dominates in the region of isolated bubbles, and that in the region of interference latent heat transport mechanism (described below) predominates.

An example of an equation of the type (2-11) is that derived by Lienhard [44]:

$$q = mk_\ell (Pr_\ell^*)^{1/3} (\Delta T)^{5/4} N^{1/3} \left[\frac{\sqrt{\frac{\sigma g(\rho_\ell - \rho_v)}{\rho_\ell^2}}}{\left(\sqrt{\frac{\sigma g(\rho_\ell - \rho_v)}{\rho_\ell^2}} \right)_{\text{reference}}} \right] \qquad (2\text{-}12)$$

where m is a constant with units $(ft)^{-1/3} \cdot (F^\circ)^{-1/4}$. The reference fluid Lienhard used was water, and fluid properties were evaluated at saturation temperature. The last term accounts for the varying "pumping capacity" of bubble columns in various fluids.

The active site distribution is very difficult to obtain, especially at high fluxes. At low fluxes, if visual observations can be made, the bubble columns can be photographed and counted, as was done by Rallis and coworkers [71,72]. A method useful at high fluxes is the "electroplated-replica technique" of Gaertner and Westwater [28,29] as analyzed by Gaertner [27], who concluded that the distribution of active sites on the surface is described by the Poisson equation. Gaertner also found that the active site

population was exponentially proportional to the cube of the wall temperature,

$$N = N_o e^{-K/T_w^3} \qquad (2\text{-}13)$$

as expected from classical nucleation theory.

Theories Based on Latent Heat Transport

The equations described above are all derived from the idea that convection, not latent heat transport, is the primary mechanism for heat transfer in boiling. Bankoff [3] discussed an accumulation of evidence indicating that simultaneous vaporization at the bottom of the bubble and condensation at the top was an important mechanism at high fluxes. Moore and Mesler [57] measured rapid local surface temperature fluctuations which could best be explained by the vaporization of a microlayer of liquid in the bubble base. Rogers and Mesler [74] substantiated this hypothesis by proving that growing bubbles cool the surface and that there is no cooling without a bubble. Rallis and Jawurek [71] concluded that latent heat transport is always an important mechanism, becoming more important at high fluxes. The findings of Roll and Myers [79], who investigated the effect of surface tension on boiling heat transfer, supported the microlayer vaporization concept of heat removal.

Hospeti and Mesler [37] measured the deposits formed by boiling radioactive calcium sulfate solutions and were able to calculate the microlayer thickness by the deposit

left by about 7,000 bubbles. (The thickness varied in the range 19-103 μinch.)

Any theory of boiling based on latent heat transport is especially sensitive to the product $f \cdot D$, where f is the frequency of bubbles from a site and D is the bubble diameter at the instant of leaving the surface. At high fluxes, the population becomes so dense that individual bubble columns are indistinguishable. Jacob [41] thought that $f \cdot D =$ constant. Zuber [88] proposed that $f \cdot D = 0.59(\sigma g[\rho_\ell - \rho_v]/\rho_\ell^2)^{\frac{1}{4}}$ which is equivalent to Jacob's expression at a constant pressure. McFadden and Grassmann [51], working with liquid nitrogen, obtained the equation $f \cdot \sqrt{D} = 0.56 \sqrt{g(\rho_\ell - \rho_v)/\rho_\ell}$. Rallis and Jawurek [71] found that the product $f \cdot V$ (V is volume of the bubble at departure) is about the same for each bubble source at a given flux, and that the product increases with flux. All of these results, however, are obtained with relatively low fluxes.

In summary, the latent heat transport mechanism is undoubtedly important, especially at high fluxes. The microlayer vaporization theory of Moore and Mesler [57] is becoming increasingly well-documented. However, difficulties in calculating the site population for any given set of conditions, and in knowing the behavior of $f \cdot D$ at high fluxes and high pressures, have prevented these theories from being satisfactorily quantified.

The Theory of Madejski

A very recent effort at formulating a nucleate boiling theory was that of Madejski [52], published in 1965. Madejski's theory was extremely interesting, as it considered both latent heat transport and convective heat transfer. Even more important, it apparently offered a way to characterize boiling surfaces from the ordinary q vs. ΔT boiling data.

Madejski considered the boiling heat flux to be caused primarily by latent heat transport and bubble-induced turbulence, which were treated as parallel mechanisms. Three constants had to be determined by experiment.

The theory of Madejski was quite complicated, but since it appeared to offer some advantages it was thoroughly compared with the data taken in this work. Since it proved to be no more effective than some of the simpler correlations described above, it will not be developed here.

The First Critical Point

The first critical, or "burnout point," has probably received more attention than any other aspect of boiling heat transfer. There are at least a dozen reasonably well-known correlations; and a survey by Gambill [31] turned up more than thirty others. In spite of this, "considerable disagreement between the various theories exists over the entire pressure range" [80]. However, Seader et al. [80] go on to say that for cryogenic fluids, "the equations of Rohsenow and Griffith, Zuber and Tribus, Kutateladze, Borishanskii,

Noyes, Chang and Snyder, and Moissis and Berenson fall within, or in the near vicinity of the data scatter, except at high pressures."

All of the theories seek to predict the first critical heat flux q_{1c}, with the idea that surface effects influence the critical ΔT but have no effect on q_{1c}. For example, Berenson [4] concluded that "the maximum nucleate-boiling burnout heat flux is essentially independent of surface material, roughness and cleanliness." The predictions of q_{1c} also ignore geometry and orientation of the heater surface.

In the first extensive investigation of boiling fluids under pressure, Cichelli and Bonilla [22] discovered that q_{1c} could be correlated with reduced pressure Pr:

$$\frac{q_{1c}}{P_c} = f(Pr) \qquad (2\text{-}14)$$

Lienhard and Shrock [45] were able to show mathematically that for corresponding states fluids, either the first or second critical fluxes could be correlated in this manner:

$$\frac{q_c}{g^{1/4} P_c \frac{\varphi}{M} \left(\frac{8MP_c}{3RT_c} \right)} = f(Pr, \text{geometry}) = \frac{q_c}{\xi} \qquad (2\text{-}15)$$

where P_c and T_c are critical pressure and temperature, M is molecular weight, and φ is the parachor. The parachor is very nearly independent of temperature (or Pr) but is actually defined by equation (2-16) [36]. It can be estimated, if necessary, from molecular configuration.

$$\varphi = \frac{M\sigma^{1/4}}{(\rho_\ell - \rho_v)} \tag{2-16}$$

Recently Lienhard and Watanabe [46] extended this idea and concluded that the geometric terms and pressure terms could always be separated:

$$\frac{q_c}{\xi} = f_1(\text{geometry}) \cdot f_2(\text{Pr}) \tag{2-17}$$

They speculated that $f_2(\text{Pr})$ might be a general function true for all geometries. Lienhard's analyses are based originally upon the idea that hydrodynamic transactions are dictated by thermodynamic properties and not transport properties.

One of the earlier peak flux correlations was that of Rohsenow and Griffith [78].

$$q_{1c} = 143\lambda\rho_v \left(\frac{\rho_\ell - \rho_v}{\rho_v} \right)^{0.6} \tag{2-18}$$

This correlation, like almost all of the others listed below, predicts a maximum in q_{1c} at about Pr = 1/3 and $q_{1c} = 0$ at Pr = 0 and Pr = 1. This behavior is in accordance with the data of Cichelli and Bonilla [22] and others.

Most of the recent correlations involve the group $\mathcal{L}$ which incorporates the surface tension:

$$\mathcal{L} \equiv \lambda\rho_v \left[\frac{g g_c \sigma(\rho_\ell - \rho_v)}{\rho_v^2} \right]^{1/4} \left(\frac{a}{g} \right)^{1/4} \tag{2-19}$$

$\mathcal{L}$ has units of flux, e.g., Btu per square foot per hour. The ratio of acceleration to gravitational acceleration is

usually unity. Merte and Clark [54] arranged several correlations in a form involving $\mathfrak{L}$, which allows easy comparison. Many of these correlations give similar results at one atmosphere but vary markedly at higher reduced pressures.

Chang [19] suggested that $q_{lc} = K\mathfrak{L}$, with K = 0.098 for vertical surfaces and K = 0.13 for horizontal surfaces. Zuber, in the discussion of Berenson's article [5], suggested that $0.12\mathfrak{L} \leq q_{lc} \leq 0.157\mathfrak{L}$. Kutateladze's correlation, as simplified by Bragg and Smith [9] is $0.13\mathfrak{L} \leq q_{lc} < 0.19\mathfrak{L}$.

Zuber and Tribus [90], Chang and Snyder [21], and Moissis and Berenson [56] modified $\mathfrak{L}$ with some combination of the liquid and vapor densities. The equation of Moissis and Berenson is:

$$q_{lc} = 0.18\mathfrak{L}\left[\frac{\sqrt{\frac{\rho_l + \rho_v}{\rho_l}}}{1 + 2\sqrt{\frac{\rho_v}{\rho_l}} + \frac{\rho_v}{\rho_l}}\right] \qquad (2\text{-}20)$$

At low pressures, $\rho_v << \rho_l$ so that the last term approaches unity. At the critical pressure, $\rho_l = \rho_v$ so that the last term is $\sqrt{2}/4$, making the overall multiple 0.0636. Thus, while the Moissis-Berenson equation is similar to the others at normal atmospheric pressures, it deviates at high pressure. It predicts a maximum in the peak flux at a reduced pressure of about 0.18. Moissis and Berenson emphasize the need for data near P_c.

Other equations use the transport properties. Among

these are those of Addoms [1], Griffith [34], Noyes [62], Borishanskii [8], and Caswell and Balzhiser [18]. The two references [62] and [18] were concerned with boiling liquid metals. Prandtl numbers of liquid metals are very low (a factor of 1000 less than many organic liquids), and the equations developed primarily for organic materials and water did not work well. It was thought that inclusion of the Prandtl number would make the results more general. Noyes' [62] equation was

$$q_{lc} = 0.144\mathfrak{L}\left[\frac{\rho_l - \rho_v}{\rho_l}\right]^{1/4}(Pr_l^*)^{-0.245} \qquad (2\text{-}21)$$

Noyes suggested an alternate equation which does not contain a surface tension term [63]:

$$q_{lc} = 1.19\lambda\rho_v(g\alpha)^{1/3}\left(\frac{\rho_l - \rho_v}{\rho_v}\right)^{0.56}(Pr_l^*)^{1/12} \qquad (2\text{-}22)$$

The correlation of Caswell and Balzhiser [18] passes through its maximum at a very high reduced pressure and gives peculiar results very near Pr = 1, so it is apparently valid only for liquid metals.

Figure 2 shows several peak flux predictions for methane. It can be easily seen in this figure that some of the correlations are quite similar at atmospheric pressure but differ greatly at high pressures. The physical and transport properties used in evaluating the equations are listed in Appendix A.

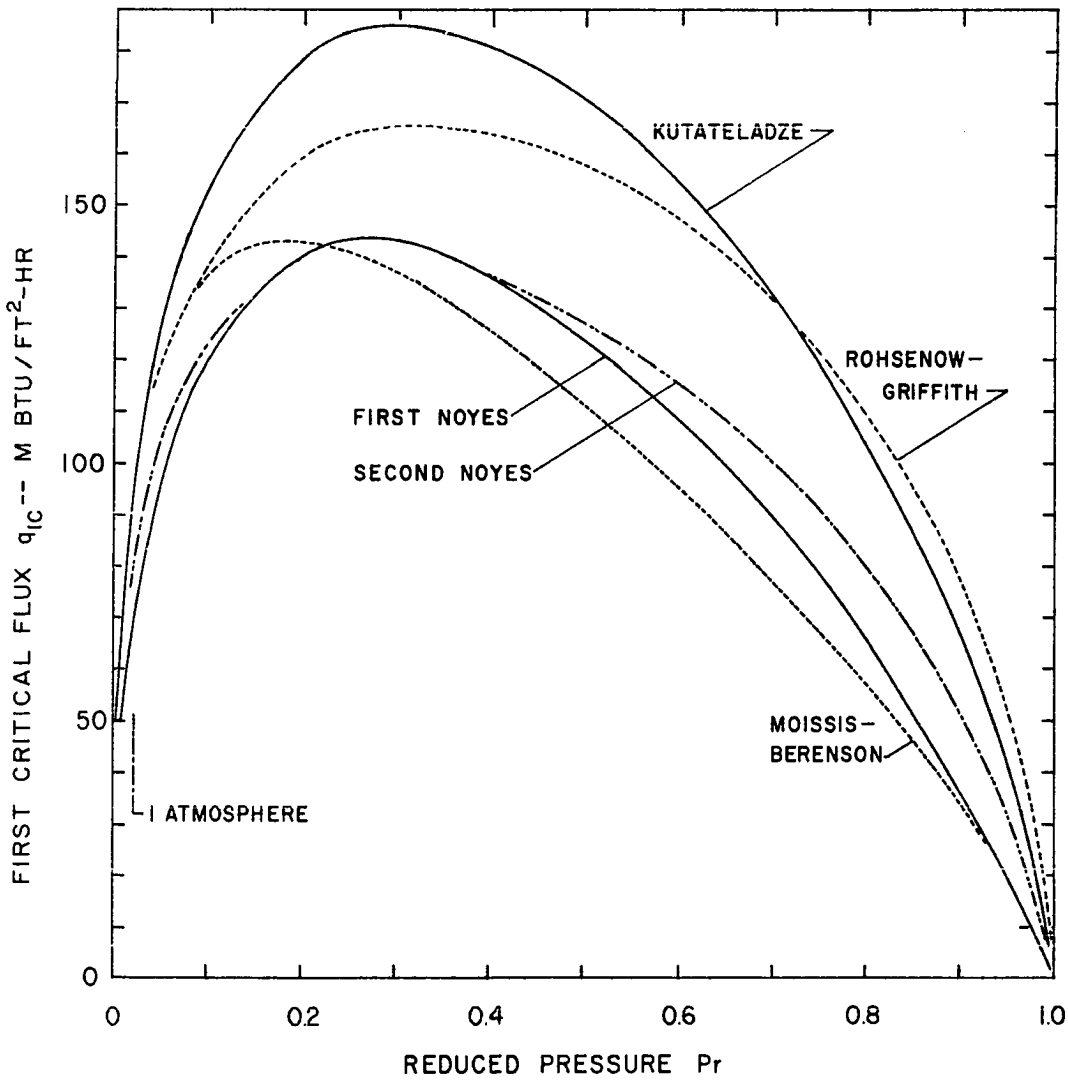

Fig. 2.--Plot of Peak Flux Predictions for Methane

Unresolved Issues in Peak Flux Prediction

As mentioned before, all theories which have led to definite predictions of the first critical heat flux have ignored the effect of geometry or surface conditions.

It is now conceded by most that the critical flux is affected by heater geometry. Carne [15] has described some of the work in this area. Morozov [59], for example, presented data showing that critical fluxes were 30-40% higher on wires than on flat plates.

It is interesting to note, however, that critical fluxes on cylinders are often reported to be lower than those obtained on flat plates. For example, Huber and Hoehne [39] reported fluxes only half as high as those obtained by Cichelli and Bonilla [22] for benzene. Park [66] reported much lower fluxes than those obtained by Lyon, Kosky and Harman [49] for nitrogen. The principal difference in each case was the cylindrical vs. flat plate geometry.

The effect of surface condition on the first critical flux is also open to question. Carne [16] found a definite effect while Berenson [4] found none. Carne and Charlesworth [17] have shown that for thin surfaces of thickness t and conductivity k_m, the burnout flux can be correlated with the product $(k_m t)$.

Zuber and Tribus [90] have predicted a ±14% uncertainty in the critical heat flux, based on hydrodynamic instability. Gambill [30] has experimentally supported this idea. Carne [16] defines the critical flux as the minimum flux at which

instability can lead to burnout; he limits the uncertainty to the time that will elapse between the establishment of a flux $q \geq q_{lc}$ and the actual occurrence of burnout. In either event, the scatter of much data is explained: the apparatus will ordinarily be run at steady state for only a short time before the flux is increased, particularly when an expensive coolant like nitrogen is used.

Previous Experimental Work on Nucleate Boiling of Liquefied Hydrocarbon Gases

Experimental work on boiling light hydrocarbons is not plentiful in the published literature. The earliest study was that of Giauque, Stout, Barieau and Eagan [32] in 1942. Liquefied methane and ethane were boiled at one atmosphere pressure outside a 2.75-inch diameter copper cylinder. Burnout was not achieved because of the very low flux produced by the heater (less than 30,000 Btu/ft^2-hr). To the author's knowledge, [32] is the only published work on boiling ethane.

The first study of a liquefied hydrocarbon gas boiling under pressure was made by Cichelli and Bonilla [22] in 1945. Propane was boiled at reduced pressures between 0.27 and 0.77. The 99%-pure propane was boiled on a 7.88-inch diameter circular chromium-plated copper plate, facing upward. Fluxes ranged up to 84,000 Btu/ft^2-hr.

Myers and Katz [60] boiled propane and n-butane at temperatures between 35°F and 70°F outside four 0.75-inch diameter tubes, each 36 inches long, placed in a vertical

row. Propane and butane differed in behavior from the other substances they tested (Freon 12, methyl chloride, sulfur dioxide).

Park [65,66], in a recent study at this university, boiled methane outside an 0.80-inch diameter gold plated copper cylinder, 2.03 inches long. The condensing capacity of Park's apparatus was not great enough to obtain methane burnout data (his primary purpose was to study boiling nitrogen) but nucleate boiling data were reported.

CHAPTER III

FILM BOILING AND THE SECOND CRITICAL POINT

Film boiling has been described [86] as the "slowest, most orderly, and best defined of the three main types of boiling." There are several theories extant, although recently attention has centered on application of Taylor instability and wave theory. At atmospheric pressure, data agree reasonably well with the theory; however, contradictory results are observed at elevated pressures [12].

In all of the equations to follow, the subscripts "v" and "ℓ" will refer to the saturated vapor and liquid at the saturated fluid temperature T_{sat}. The subscript "f" refers to the vapor at the saturation pressure P corresponding to T_{sat}, but at a film temperature T_f which has been arbitrarily selected to be $\frac{1}{2}(T_w + T_{sat})$.

Stable Film Boiling

The original theoretical treatment of film boiling was presented by Bromley [13], who considered the process of boiling on a horizontal tube. Defining the parameter F,

$$F \equiv \left[\frac{k_f^3 \rho_f(\rho_\ell - \rho_v)g\lambda'}{\mu_f \Delta T} \right]^{1/4} \qquad (3\text{-}1)$$

Bromley's equation was, for cylinders of diameter D,

$$h' = 0.62F/D^{1/4} \tag{3-2}$$

The constant 0.62 is the average of the theoretical extremes 0.512 (stagnant liquid surrounding vapor) and 0.724 (liquid moving with the velocity of the vapor).

The parameter λ' is a modified heat of vaporization which may be calculated in several ways. Bromley used

$$\lambda_1' = \lambda + 0.5\, C_{pf}\Delta T \tag{3-3}$$

and later [14] suggested a form similar to the one used by Breen and Westwater [10],

$$\lambda_2' = \lambda \left(1 + 0.34 \frac{C_{pf}\Delta T}{\lambda} \right)^2 \tag{3-4}$$

Sparrow [81] states that vapor inertia forces and superheating can be taken into account by using

$$\lambda_3' = \lambda \left(1 + 0.84 \frac{k_f \Delta T}{\lambda \mu_f} \right) \tag{3-5}$$

Equation (3-2) holds neither at very small diameters nor very large ones; Breen and Westwater [10] state that (3-2) appears to describe film boiling adequately for diameters from 1/4 to 3/4 inch.

Banchero, Barker and Boll [2] found that equation (3-6) represented their data, which was taken over a range of pressures and diameters.

$$h' = c_1 \left(\frac{1}{D} + c_2 \right) F \tag{3-6}$$

The principal disadvantage here is that c_2 is not a general constant; it varies with the fluid.

Bromley also suggested that (3-2) should describe boiling on vertical tubes if D is replaced by tube length L, and a different constant is used. Hsu and Westwater [38] predict this constant will be in the range 0.667 (stagnant liquid) to 0.943.

Chang [20] applied wave theory to derive an equation describing film boiling on flat plates. At that time very little data of that type were available; subsequent work has shown poor agreement with their equation [12,73].

Berenson [5] applied Taylor-Helmholtz instability theory to describe film boiling on a horizontal flat plate facing upward. If the wavelength Γ_c of the shortest unstable disturbance is

$$\Gamma_c = 2\pi B \tag{3-7}$$

where B is the Laplace reference length defined by equation (2-6), Berenson's result can be expressed by equation (3-8).

$$h' = 0.672 \frac{F}{\Gamma_c^{1/4}} \tag{3-8}$$

Equation (3-8) is very similar to Bromley's equation (3-2); the tube diameter D has been replaced by the critical wavelength Γ_c, which is proportional to bubble diameter. Berenson emphasized that equation (3-8) should hold near the minimum film boiling heat flux q'_{2c} but theorized that it could apply for some fluids to a ΔT as high as 1,000 F°.

Breen and Westwater [10] suggested that equation (3-9) can be used for cylinders over a very wide range of diameters (their data covered the range 0.00022 inch to 1.895 inches).

$$h' = \left(0.59 + 0.069 \frac{\Gamma_c}{D} \right) \frac{F}{\Gamma_c^{1/4}} \qquad (3\text{-}9)$$

At large diameters equation (3-9) approaches 88% of the values predicted by Berenson for flat plates. Their data indicated a minimum h' occurring when D equalled the "most dangerous wavelength" $\Gamma_D = \sqrt{3}\,\Gamma_c$, but equation (3-9) does not reflect this minimum.

Pomerantz [68], in investigating the effect of increased gravity on film boiling, modified Bromley's result, (3-2), by incorporating another term:

$$h' = 0.62 \left(\frac{D}{\Gamma_c} \right)^{0.172} \frac{F}{D^{1/4}} \qquad (3\text{-}10)$$

This expression, in the range $1.0 < D/\Gamma_c < 3.0$, gives values for h' between those of (3-2) and (3-9).

Frederking, Wu, and Clement [25] presented an interesting analysis of film boiling, describing four models in terms of the Laplace reference length B, the Rayleigh number Ra* and the Nusselt number Nu*.

$$Ra^* = \frac{B^3 g \rho_f (\rho_\ell - \rho_f) Pr_f^*}{\mu_f^2} \qquad (3\text{-}11)$$

$$Nu^* = \frac{qB}{k_f \Delta T} \tag{3-12}$$

For convenience, another dimensionless number is defined by (3-13)

$$\theta' = \frac{\lambda'}{C_{pf} \Delta T} \tag{3-13}$$

The models are as follows:

I. Regular cellular two-phase flow and laminar vapor flow. This is Berenson's model, and equation (3-14) is equivalent to (3-8).

$$Nu^* = m(Ra^* \theta')^{1/4} \tag{3-14}$$

II. Regular cellular two-phase flow and vapor flow dominated by inertial forces, after Kistemaker [42]:

$$Nu^* = m[Ra^* Pr_f^* \theta'^2]^{1/4} \tag{3-15}$$

III. Vapor removal at random and laminar vapor flow, after Chang [20], who used m = 0.294:

$$Nu^* = m(Ra^* \theta')^{1/3} \tag{3-16}$$

IV. Vapor removal at random and vapor flow dominated by inertial effects:

$$Nu^* = m[Ra^* Pr_f^* \theta'^2]^{1/3} \tag{3-17}$$

Effect of Radiation

Because film boiling occurs at relatively high surfact temperatures T_w, radiation may become an important

parallel mechanism of heat transfer. It is customary to divide the total flux q into a radiative contribution q_r and a convective contribution q'. Values of h are given similar subscripts. The radiation contribution is

$$q_r = h_r(T_w - T_{sat}) = h_r \Delta T \tag{3-18}$$

and if the emissivity of the liquid surface is unity,

$$h_r = \frac{\varepsilon \sigma^*}{\Delta T} \left[T_w^4 - T_{sat}^4 \right] \tag{3-19}$$

where T_w and T_{sat} are in degrees Rankine, $\sigma^* = 0.1713 \times 10^{-8}$ $Btu/(ft^2)(hr)(F^\circ)^4$ and ε is the emissivity of the metal surface.

Bromley [13] devised a method for calculating h from h' and h_r, which a recent, more complicated analysis by Sparrow [81] has shown to give remarkably good results. Bromley presented equation (3-20), which is implicit in h, and suggested using equation (3-21) if $(h_r/h') < 10$.

$$h = h' \left(\frac{h'}{h} \right)^{1/3} + h_r \tag{3-20}$$

$$h = h' + h_r \left[0.75 + 0.25 \frac{h_r}{h'} \left(\frac{1}{2.62 + (h_r/h')} \right) \right] \tag{3-21}$$

Minimum Film Boiling (Second Critical) Flux

Berenson [6] modified the equation of Zuber and Tribus [89,90] to obtain

$$q_{2c} = 0.09 \rho_f \lambda \sqrt{\frac{gB(\rho_\ell - \rho_v)}{(\rho_\ell + \rho_v)}} \tag{3-22}$$

Berenson [5] then combined equation (3-8), which applies near the minimum flux, with (3-22) to obtain an expression for ΔT_{2c}:

$$\Delta T_{2c} = 0.127 \frac{\rho_f \lambda B}{k_f} \left[\frac{g(\rho_\ell - \rho_v)}{\rho_\ell + \rho_v} \right]^{2/3} \left[\frac{\mu_f}{g(\rho_\ell - \rho_v)} \right]^{1/3} \quad (3\text{-}23)$$

These equations were derived for flat plates but also should apply to cylinders with diameters greater than one cm. In order to predict minimum film boiling on small-diameter cylinders, the reader is referred to the development of Lienhard and Wong [47].

An attempt to translate equation (3-22) into a corresponding states correlation was made by Lienhard and Shrock [45] and amplified by Lienhard and Watanabe [46]. Their technique was to express all fluid properties in terms of reduced pressure Pr. Their result was explained in Chapter II. In his review of [45], however, Owens pointed out that the divisor of q'_{2c} divided by the critical pressure P_c was almost constant for all substances used in checking the correlation.

A number of workers have pointed out that (q'_{2c}/q_{1c}) does not change much with pressure. Morozov [58] presents data illustrating this fact.

Spiegler and coworkers [82] assumed that the wall temperature at which film boiling begins is the "foam limit," or the maximum temperature to which the liquid can be

superheated. They further assume that the foam limit can be calculated satisfactorily from Van der Waals' equation of state. At low pressures this assumption leads to the prediction of a reduced wall temperature of 27/32 at the foam limit. Agreement with data is surprisingly good, considering that Van der Waals' equation gives predictions of maximum superheats which are considerably different from those predicted by equations of state which better describe the liquid state, such as the Benedict-Webb-Rubin equation.

Supercritical "Boiling"

Because of the rapidly changing thermodynamic properties near the critical pressure, a "boiling-like" phenomenon may occur even though only one phase is present. Bonilla and Sigel [7] obtained equation (3-24) based on the liquid density ρ_w at T_w and the liquid density ρ_∞ at T_∞.

$$h' = 0.1722 \left(\frac{\rho_f^2 \, k_f \, C_{pf}}{\mu_f} \, g \, \ln \frac{\rho_\infty}{\rho_w} \right) \qquad (3\text{-}24)$$

They found that once the ratio (hL^*/k_f) reaches 1300, where L^* is the chamber diameter, equation (3-24) is no longer valid and instead becomes

$$h' = \frac{1300 \, k_f}{L^*} \qquad (3\text{-}25)$$

Fritsch and Grosh [26] observe that the "boiling-like" phenomenon probably occurs only at relatively large temperature differences. However, it has been observed that

the transition boiling region disappears as $P \rightarrow P_c$, and the temperature differences in that region are usually quite small for nucleate boiling.

Previous Experimental Work on Film Boiling

To the author's knowledge there have been no film boiling data published on any of the components used in this study except Park's [65,66] work on methane at this university.

Banchero, Barker and Boll [2] boiled oxygen at several pressures, outside horizontal tubes and wires of various diameters.

A good deal of miscellaneous film boiling data has been taken at atmospheric pressure. There is very little data of any kind on the minimum film boiling flux.

CHAPTER IV

THE HEAT TRANSFER ELEMENT

Introduction

Boiling took place outside a gold-plated cylinder, 0.811 inch (2.06 cm) in diameter and four inches long, mounted horizontally. The heater was suspended in the vessel by its electrical leads and was located so that the center was directly between the sight glasses.

Design Considerations

In the study of boiling heat transfer, the heater is of course the critical piece of apparatus. When both nucleate and film boiling are studied, the heater experiences an enormous range of conditions: in this work surface temperatures varied from -260°F to 1100°F, and surface fluxes exceeding 150,000 Btu/ft^2-hr were encountered. The corresponding flux at the surface of the heating element exceeded 1,800,000 Btu/ft^2-hr.

As explained in Chapter I, pool boiling heat transfer data consist of the surface heat flux q, the surface temperature T_w, and the saturation temperature and pressure (T_{sat}, P_{sat}).

Ordinarily the flux at the surface of an electric

heater is calculated from the current and potential drop across the heating element. It is unusual for any independent check on this flux to be made. Westwater [85] states that "probably nine-tenths of the published data on boiling involve no heat balances whatever." The problem is to find an alternate method whose accuracy is comparable to that of the electrical measurements.

It was decided to measure the radial temperature gradient in a metal cylinder separating the heating element and the boiling surface. Fluxes have been calculated this way with flat plate geometry, for example, by Marcus and Dropkin [53]. Jacob [41] describes a method of determining thermal conductivity which uses the technique with a cylindrical geometry; but this was done, of course, at very low fluxes. To the author's knowledge the technique has never been used with cylindrical geometry in boiling heat transfer.

Calculation of Flux and Surface Temperature from Radial Temperature Distribution

It is assumed that the thermal conductivity k of the metal can be represented by equation (4-1),

$$k = \alpha T + \beta \qquad (4\text{-}1)$$

where T is the temperature in degrees F and α and β are constants.

Fourier's law for steady state radial conduction through a homogeneous cylinder is

$$\dot{Q} = -2\pi L(\alpha T + \beta)r \frac{dT}{dr} = \text{constant} \qquad (4\text{-}2)$$

where $\dot{Q}$ is heat flow in Btu/hr, L is the cylinder length in feet, and r is the radius in feet.

Integrating from (T_1,D_1) to (T_2,D_2), where D is diameter, gives

$$\dot{Q} = \frac{2\pi L}{\ln (D_2/D_1)} \left[\frac{\alpha}{2} (T_1^2 - T_2^2) + \beta(T_1 - T_2) \right] \qquad (4\text{-}3)$$

The heat flux $q_i = \dot{Q}/(\pi D_i L)$ can be calculated at any diameter from (4-3). To calculate the surface temperature (T_w,D) from an internal measurement (T_i,D_i), define

$$\gamma \equiv \frac{2\beta}{\alpha} \qquad (4\text{-}4)$$

and

$$\varphi \equiv \frac{qD \ln (D/D_i)}{\alpha} - T_i^2 - \gamma T_i \qquad (4\text{-}5)$$

where q is the surface flux $\dot{Q}/(\pi DL)$. Then

$$T_w = \frac{-\gamma - \sqrt{\gamma^2 - 4\varphi}}{2} \qquad (4\text{-}6)$$

Effect of the Requirement for Radial Temperature Measurements on Heater Design

The two radii at which the temperatures are measured must be as far apart as possible so that the temperatures will differ substantially at low fluxes. For the same reason, the thermal conductivity of the metal should not be too low.

On the other hand, the overall diameter must be kept as small as possible and still be greater than one centimeter. Breen and Westwater [10] report that the diameter effects in film boiling are negligible if D > 1 cm, and it was desired to put the data taken in the present work on the same basis as that taken from flat plates, if possible. The diameter should be kept small for two reasons. First, nitrogen is an expensive coolant and it was desired to use as little as possible. Second, the diameter of a standard one-gallon autoclave is five inches, which limits heater length L, and end effects are reduced if the ratio L/D is large.

The material selected for the heater body was ARMCO iron. Its thermal conductivity follows equation (4-1) very closely from 0°F to about 1000°F, with $\alpha = -0.02$ and $\beta = 43.8$ when T is °F and k is Btu/ft-hr-F° [33,69,70]. Figure 3 compares equation (4-1) with the reported values. ARMCO iron can be used as a thermal conductivity standard since k is accurately known and because the material is readily available.

The final O.D. selected was 0.811 inch. It was decided to use a graphite rod as the heating element, rather than a wound wire, to conserve space. The thermal gradient through the cylinder was so severe, however, that serious doubt existed as to whether a single cylinder would suffice. A multiplex cylinder, however, proved to be impracticable because of the machining problems involved (the cylinders would have to be shrink-fitted and they were too small and

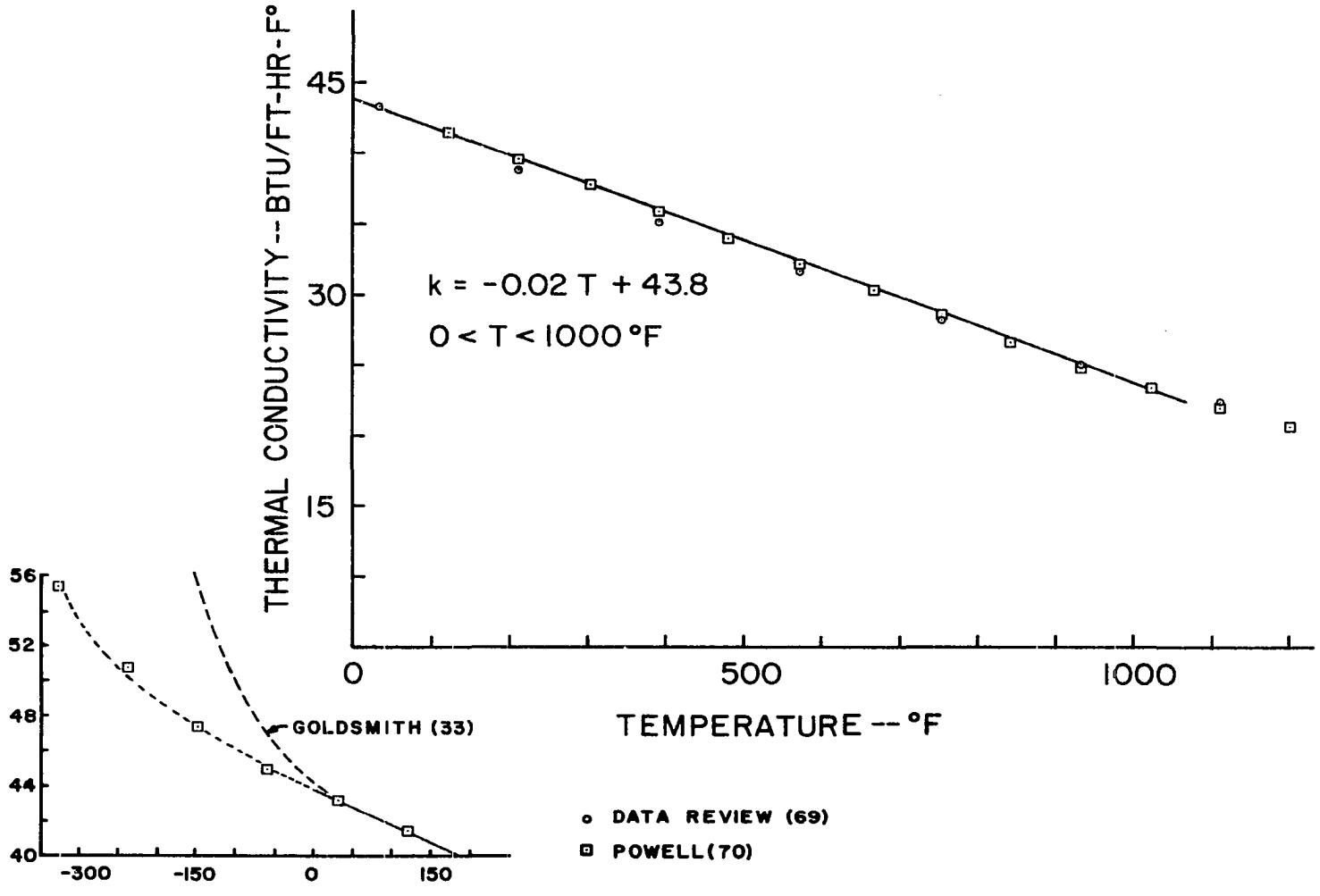

Figure 3. Graph Showing Thermal Conductivity of ARMCO Iron

too long). It turned out that a monoblock (single-cylinder) construction worked anyway, but the theory of thermal stresses in a single thick-walled cylinder is outlined below.

Thermal Stresses

Timoshenko [84] has presented equations for stresses caused by thermal gradients in thick-walled cylinders with unconstrained ends:

$$\sigma_r = \frac{-\alpha E}{r^2(1 - \nu)} \int_a^r Tr\, dr + \frac{E}{1 + \nu}\left(\frac{c_1}{1 - 2\nu} - \frac{c_2}{r^2}\right) \qquad (4\text{-}7)$$

$$\sigma_\theta = \frac{\alpha E}{r^2(1 - \nu)} \int_a^r Tr\, dr - \frac{\alpha E T}{1 - \nu} + \frac{E}{1 + \nu}\left(\frac{c_1}{1 - 2\nu} + \frac{c_2}{r^2}\right) \qquad (4\text{-}8)$$

σ_r radial stress

σ_θ tangential stress

E modulus of elasticity (28×10^6 psi for iron)

α coefficient of thermal expansion ($7 \times 10^{-6}/F^\circ$ at 212°)

ν Poisson's ratio (0.28)

T temperature, °F

r radius, feet

a inner radius, feet

The constants c_1 and c_2 are determined so that $\sigma_r = 0$ at both the inner radius, a, and the outer radius, b:

$$c_1 = \frac{\alpha(1 + \nu)(1 - 2\nu)}{(1 - \nu)(b^2 - a^2)} \int_a^b Tr\, dr \qquad (4\text{-}9)$$

$$c_2 = \frac{1 + \nu}{1 - \nu} \frac{a^2}{b^2 - a^2} \int_a^b Tr \, dr \qquad (4\text{-}10)$$

If the thermal conductivity is constant,

$$Tr = \frac{T_a - T_b}{\ln (b/a)} \ln \frac{b}{r} \qquad (4\text{-}11)$$

Lott [48] has discussed the criteria for design based on the maximum shearing stress. The shearing stress τ is given by (4-12):

$$\tau = \frac{1}{2} (\sigma_\theta - \sigma_r) \qquad (4\text{-}12)$$

Equations (4-7), (4-8), (4-9), (4-10), (4-11) and (4-12) can be combined to give

$$\tau = \frac{\alpha E(T_a - T_b)}{4(1 - \nu) \ln (b/a)} \left[1 - \frac{1}{r^2} \left(\frac{2 a^2 b^2 \ln (b/a)}{b^2 - a^2} \right) \right] \qquad (4\text{-}13)$$

The maximum τ_{max} occurs at r = a. If the ratio (b/a) is denoted by K,

$$\tau_{max} = \frac{\alpha E(T_a - T_b)}{4(1 - \nu) \ln K} \left[1 - \frac{2K^2 \ln K}{K^2 - 1} \right] \qquad (4\text{-}14)$$

The maximum <u>permissible</u> design stress is taken to be

$$\tau_{max} = \frac{\sigma_y}{\sqrt{3}} \qquad (4\text{-}15)$$

where σ_y is the yield strength in simple tension (11,400 psi for iron).

The single-cylinder design was tried in this work with some trepidation, and only after several failures had been encountered in fabricating a shrunk-fit triplex cylinder. Note that equation (4-14) gives a value of $\tau_{max} \approx 100(T_a - T_b)$. At a surface flux of 150,000 Btu/ft^2-hr, τ_{max} becomes about 25,000 psi, almost a factor of four higher than the value $11{,}400/\sqrt{3}$ indicated by (4-15). A triplex cylinder would have reduced the thermal stresses to reasonable levels, but the single cylinder apparently worked. After completion of the work, the heater was cut apart and examined, and no observable defects were found.

Final Design of the Heater

To increase accuracy, the thermocouples were installed in pins made of ARMCO iron, the pins being 5/64 inch in diameter and 1.5 inches long. Figure 4 shows the dimensions of the iron heater body, which was 4.00 inches long. The pins were rotated so that the thermocouple beads were on the line of centers of the pin holes, which minimized the disturbance of flux on the temperature measurements.

Figure 5 shows in detail the installation of the thermocouple pins, graphite heating element, and boron nitride insulator in the heater body. The graphite element was Ultra Carbon Corp. grade UF4S, selected primarily because of its resistance and the available power supplies.

Figure 6 shows in detail the transite end plates and copper electrical lead parts. The heater was suspended in

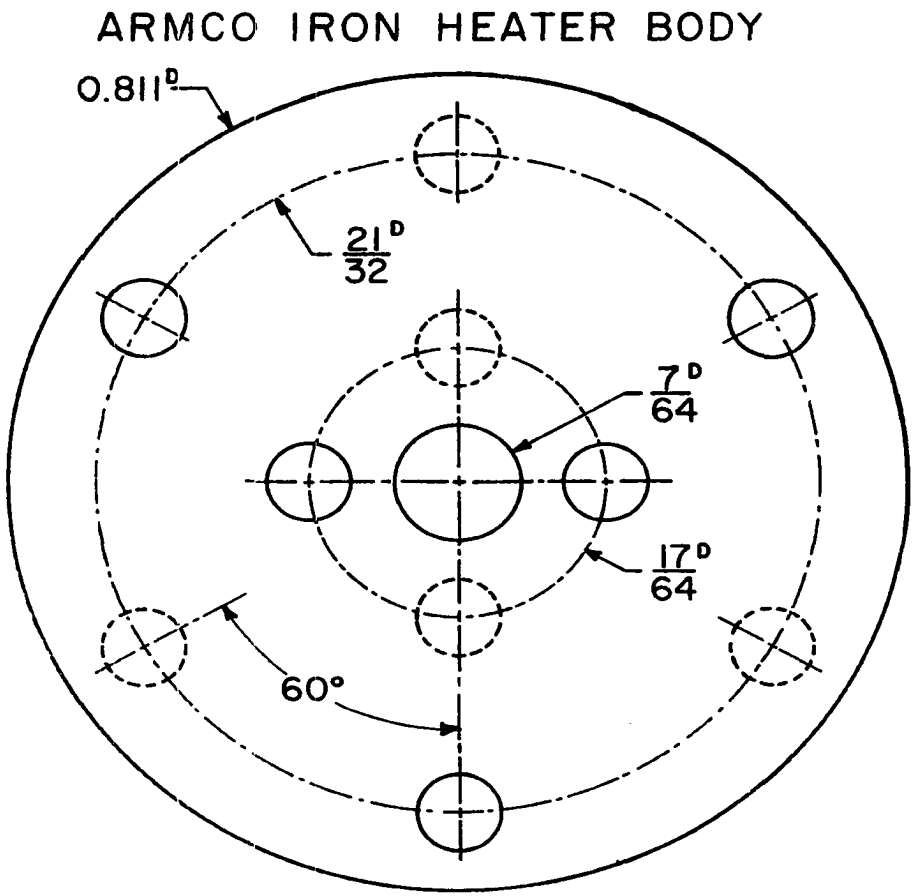

HOLES FOR THERMOCOUPLE PINS ARE $\frac{5^D}{64}$, DRILLED $1\frac{1}{2}$" DEEP.
DASHED LINES INDICATE DRILLING FROM OTHER END OF 4" CYLINDER.

Figure 4. Heater Body Showing Location of Thermocouple Pins

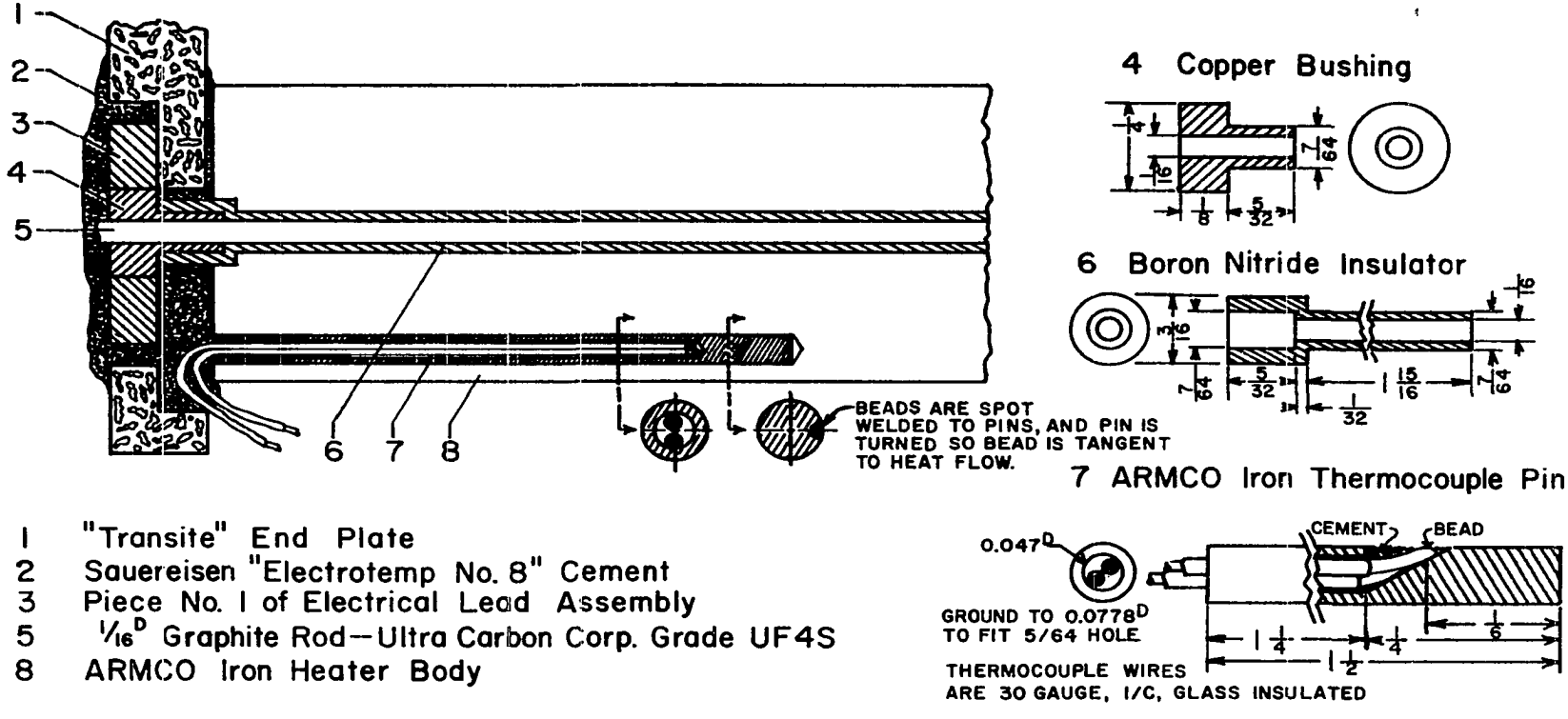

1 "Transite" End Plate
2 Sauereisen "Electrotemp No. 8" Cement
3 Piece No. 1 of Electrical Lead Assembly
5 1/16D Graphite Rod—Ultra Carbon Corp. Grade UF4S
8 ARMCO Iron Heater Body

Figure 5. Detail of Heater and Thermocouple Installation

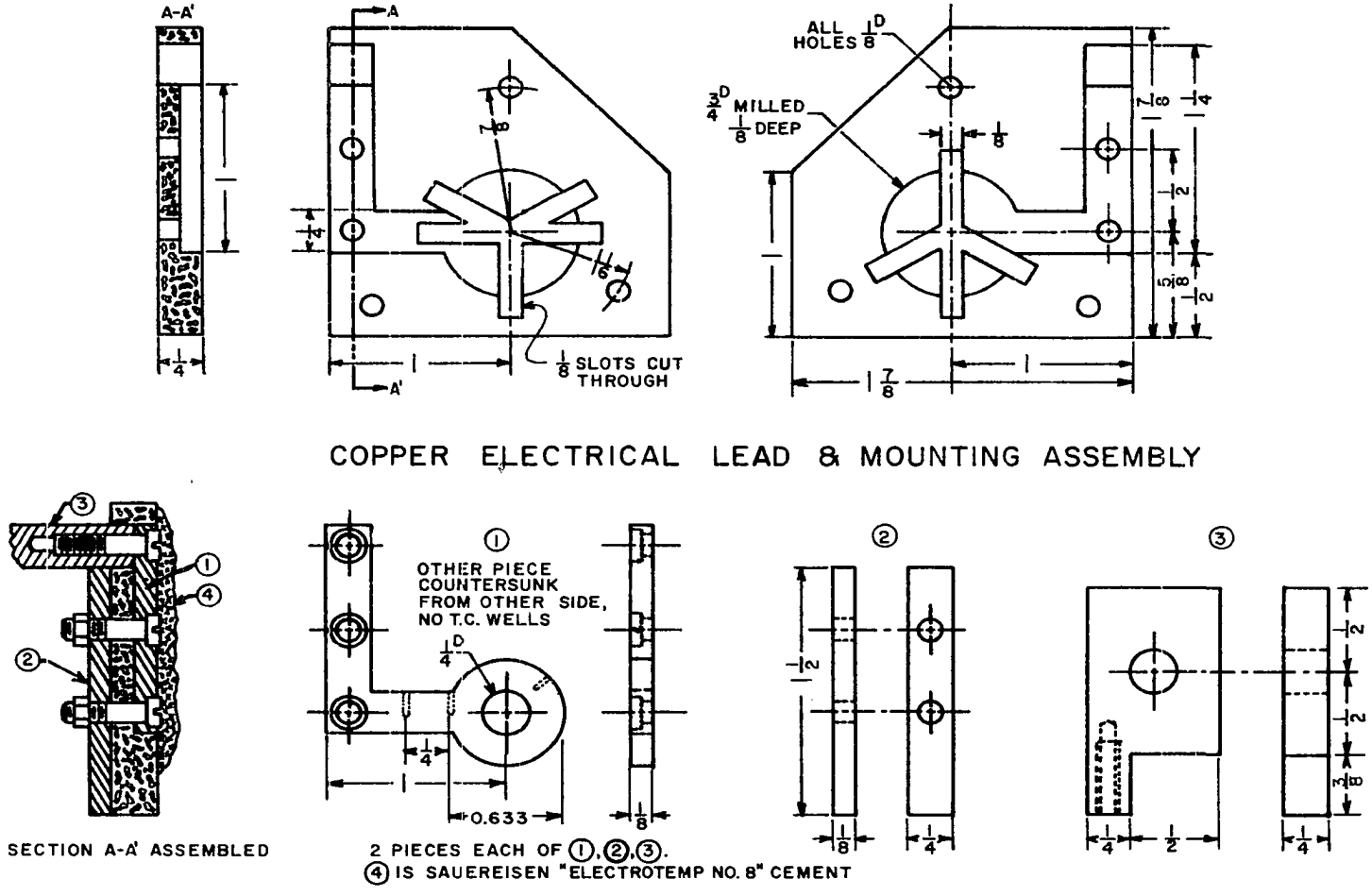

Figure 6. Detail of End Plates and Electrical Leads

the pressure vessel by its electrical leads.

The purpose of the copper bushing (Part 4, Figure 5) was to remove all strain from the graphite rod during assembly.

Ten temperatures were measured inside the heater: six at 60° angles around a 21/32 inch diameter, and four at 90° angles around a 17/64 inch diameter. Five of the pins were inserted from each end (Figure 4).

The surface of the heater was first copper plated and then gold plated. Its finish was approximately 16 microinch RMS.

Figure 7 is a drawing of the assembled heater before insulating cement was applied. The springs helped support the heater, although the transite plates were also cemented to the heater with Sauereisen "Electrotemp No. 8" cement. Only one pair of thermocouple wires has been shown, for simplicity.

Figure 8 shows the installed heater after the nucleate boiling data were taken. The surface was dulled somewhat on one end, but was in no sense fouled. The foreshortening effect of the closeup photographs makes the thermocouple wires and condenser appear to be closer to the heating surface than they actually were.

End Losses

End losses were measured, as described in Appendix B. As outlined in that appendix, the effect of the losses (which

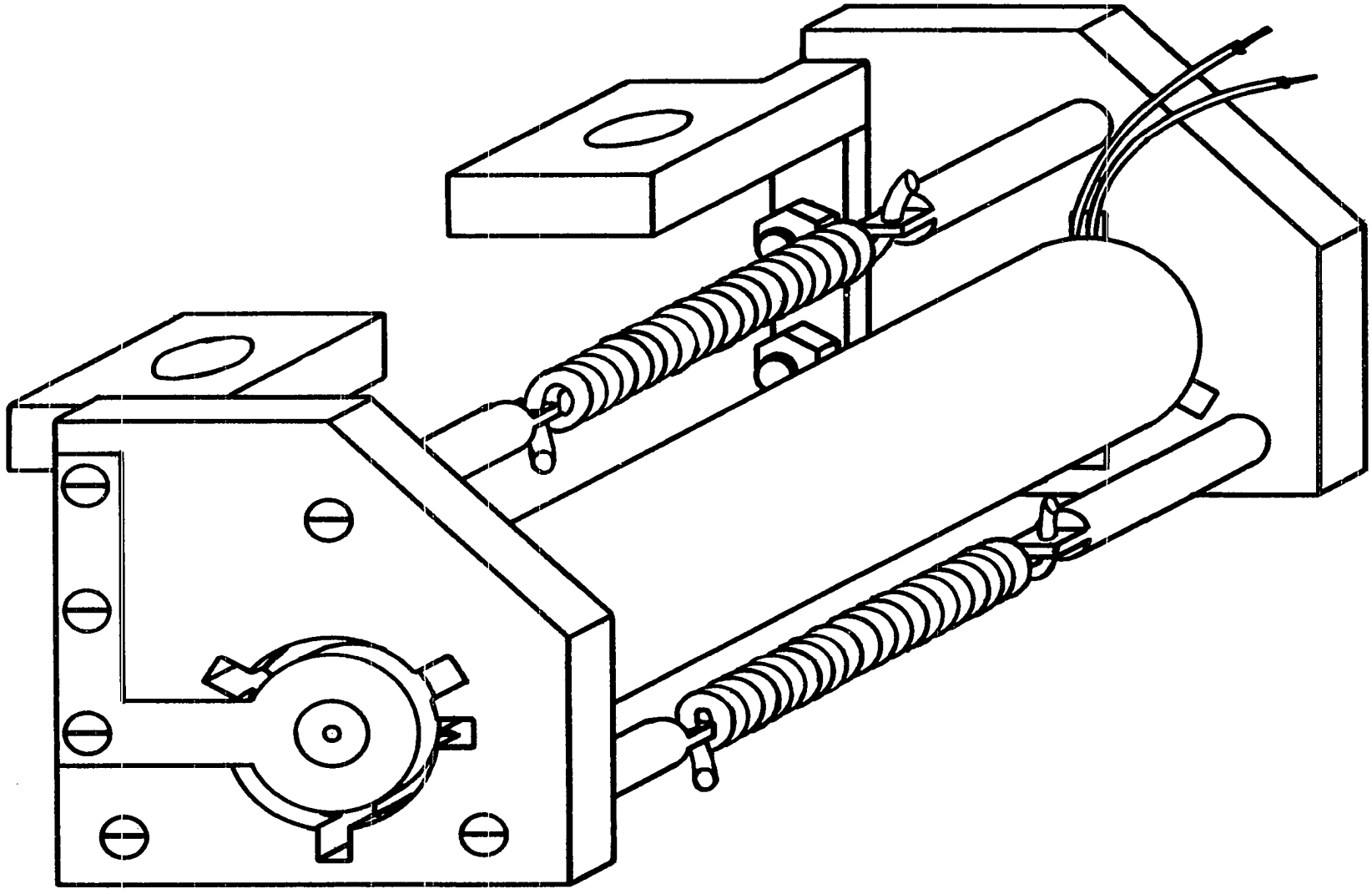

Figure 7. Assembled Heater before Cementing over the Outside of the End Plates

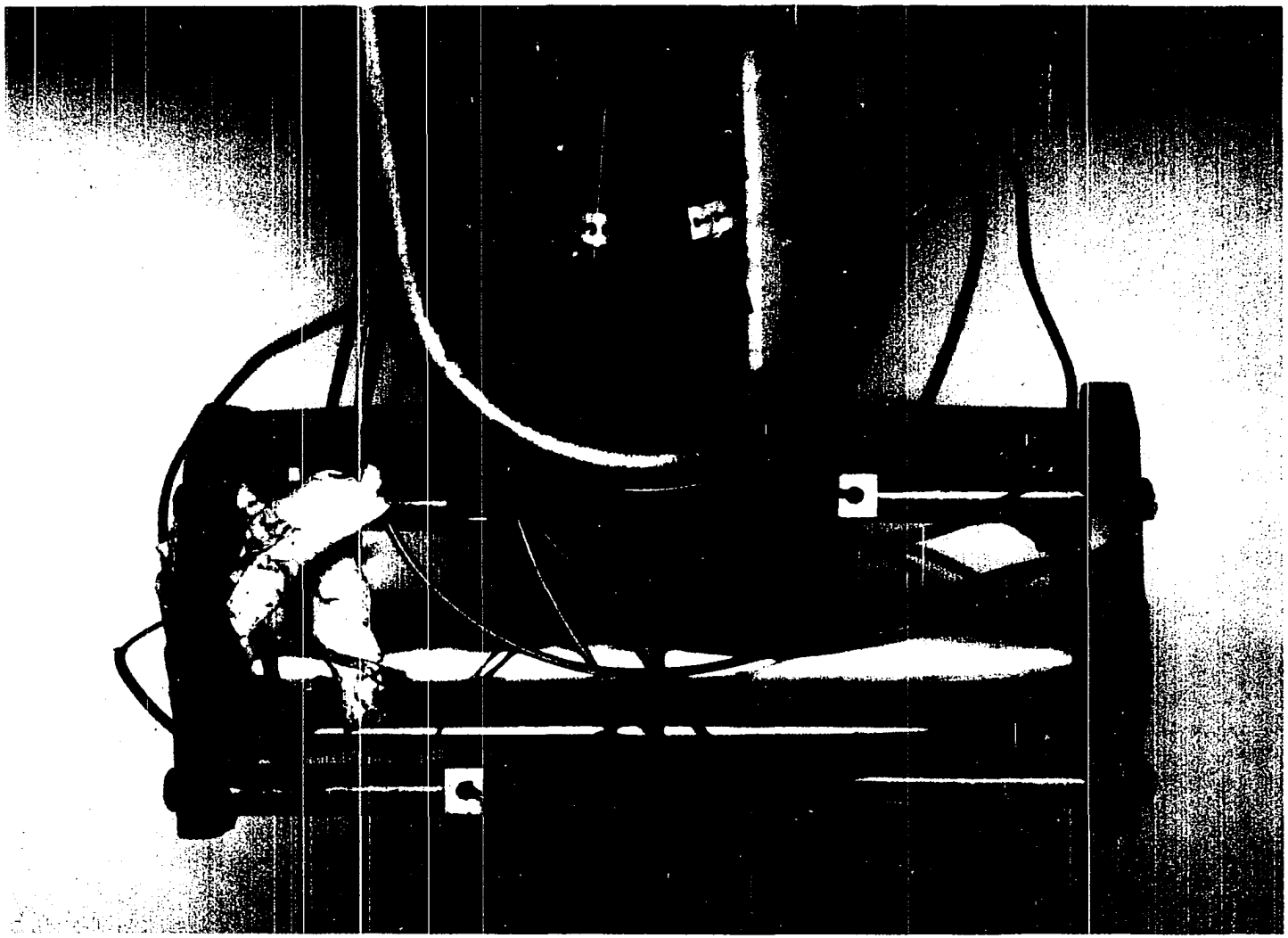

Figure 8. Installed Heater after Completion of Nucleate Boiling Work

averaged about six percent) was negligible in the region where the temperatures were measured. For this reason, no corrections were applied to the data for end effects.

Exact Location of Thermocouple Beads

A disadvantage of installing thermocouples in blind holes is that the holes are seldom exactly straight. Also, the pins can rotate slightly when they are inserted in the heater block.

After completion of the work, the heater was cut apart and enlarged photographs were made to locate the beads. An example is shown in Figure 9. Table 4-1 shows the location of the beads determined visually.

TABLE 4-1

BEAD LOCATIONS DETERMINED VISUALLY

Thermocouple Location Clock Position	Observed Radius inches
Outer Ring	
12	0.325
2	0.321
4	0.330
6	0.326
8	0.324
10	not located
Inner Ring	
12	not located
3	0.135
6	0.147
9	0.144

Corrections for these were applied to the measurements in the following way.

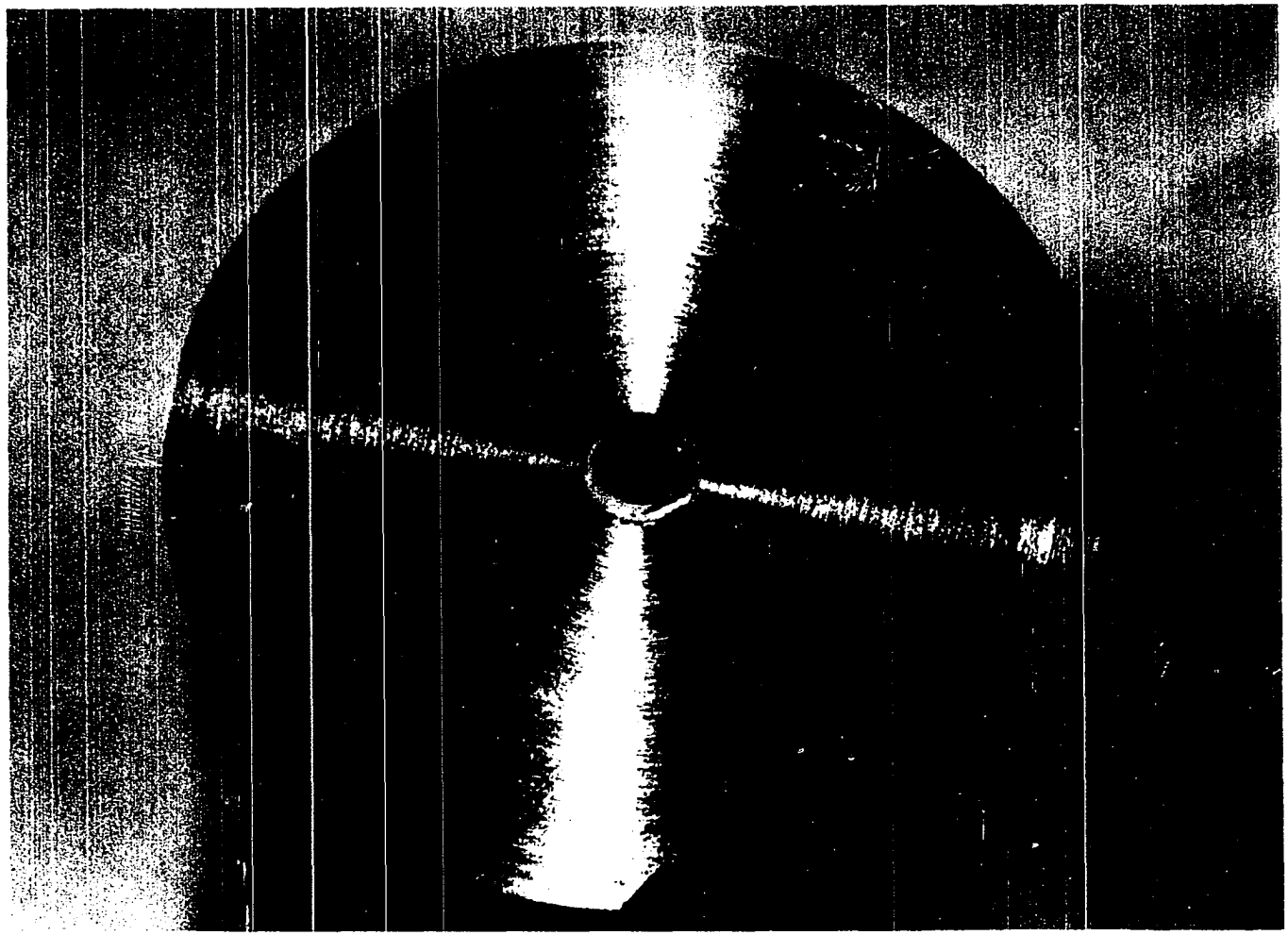

Figure 9. Photograph of Heater Cross-Section Used to Locate Thermocouple Beads. The notch was cut so that the photographs could not be misoriented.

If the thermal conductivity is constant, as it will be over a very small distance, equation (4-2) becomes

$$\int_{r}^{r^*} \frac{dr}{r} = - \frac{2\pi kL}{\dot{Q}} \int_{T}^{T^*} dT \qquad (4\text{-}16)$$

where (r^*,T^*) is the observed point and (r,T) is the "correct" point. Integration gives

$$T - T^* = \frac{\dot{Q}}{2\pi kL} \ln \frac{r^*}{r} \qquad (4\text{-}17)$$

A variation of (4-17) will be used later for another purpose. For $x \sim 1$, $\ln x \sim (x - 1)$. Then for small displacements, $\ln (r/r^*)$ can be approximated by $(r^* - r)/r$. Equation (4-17) gives

$$T = T^* + \frac{\dot{Q}}{2\pi kL} \left(\frac{r^* - r}{r} \right) \qquad (4\text{-}18)$$

Suppose r^* is not known, but an estimate of T (the correct temperature) is available. Then

$$(T^* - T_i) = (r_i - r^*) \left[\frac{q(D/D_i)}{k} \right] \qquad (4\text{-}19)$$

where q is the flux at the surface (D). A plot of $(T^* - T_i)$ vs. $q(D/D_i)/k$ should have a slope of $(r_i - r^*)$.

CHAPTER V

EXPERIMENTAL EQUIPMENT

The heater was described in Chapter IV. The remainder of the apparatus is most conveniently divided into four groups for further discussion: (1) the pressure and condensing system, (2) the electrical system, (3) the temperature measuring system, and (4) auxiliary equipment.

Pressure and Condensing System

The heater was suspended inside the one-gallon autoclave shown in Figure 10. This vessel, manufactured by Autoclave Engineers, Inc., was of the standard one-gallon size: five-inch I.D. and 12-inch depth. It was provided with two 1-1/4 inch diameter quartz sight glasses spaced at 180°. An unusual feature of this vessel was that the cover was fixed in place while the autoclave body could be raised or lowered pneumatically. This feature allowed the heater to be inspected and cleaned without disconnecting any thermocouples or electrical connections.

The vessel was designed for service between -320°F and +400°F, which can be increased to 800°F by replacing the "Teflon" and "Kel-F" packing. It was designed for pressures up to 3,000 pounds per square inch.

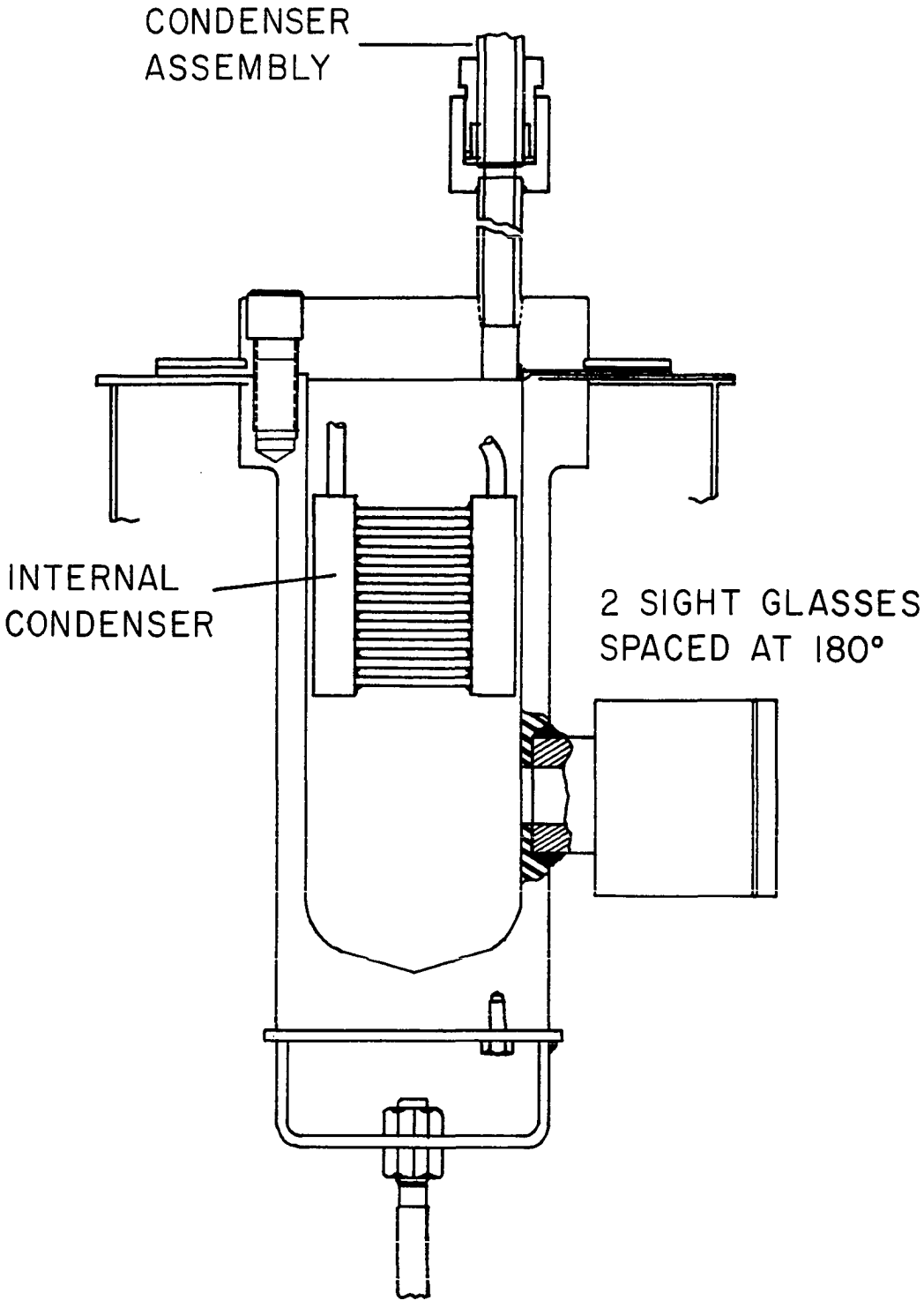

Figure 10. Pressure Vessel Showing Location of Condensers

The bulk of the cooling was done by an external reflux condenser which was a 3/4-inch Schedule 80 stainless steel pipe surrounded by an 1-1/2 inch Schedule 40 insulated jacket, 48 inches long. It contained approximately 0.78 sq ft of condensing surface.

The system pressure was maintained constant by adjusting the flow rate of coolant (liquid nitrogen or water) through the shell side of the condenser. Fine control was achieved with the aid of an internal condenser, shown in Figure 10; one configuration was shaped to fit around 120° of the autoclave wall. A different coil, used for part of the data, was simply a double loop. The bottom of that is shown in Figure 8 in Chapter IV. As little cooling as possible was done with the internal condenser in order to avoid subcooling the liquid.

Liquid nitrogen was supplied at 200 psi in Linde LS-110 dewars. When water was used, it was introduced directly from the building line.

Pressures below 150 psia were measured to ± 0.1 psia with a Wallace and Tiernan gauge, and pressures above 150 psia were measured to ± 1 psi with a Heise gauge. Both gauges were of the Bourdon-tube type, and both had 16-inch dial faces.

The pressure and condensing system layout is shown in Figure 11.

Metering of the nitrogen was done after it had vaporized. It was found that this gave steadier pressure than could be achieved by metering the liquid. Flow through

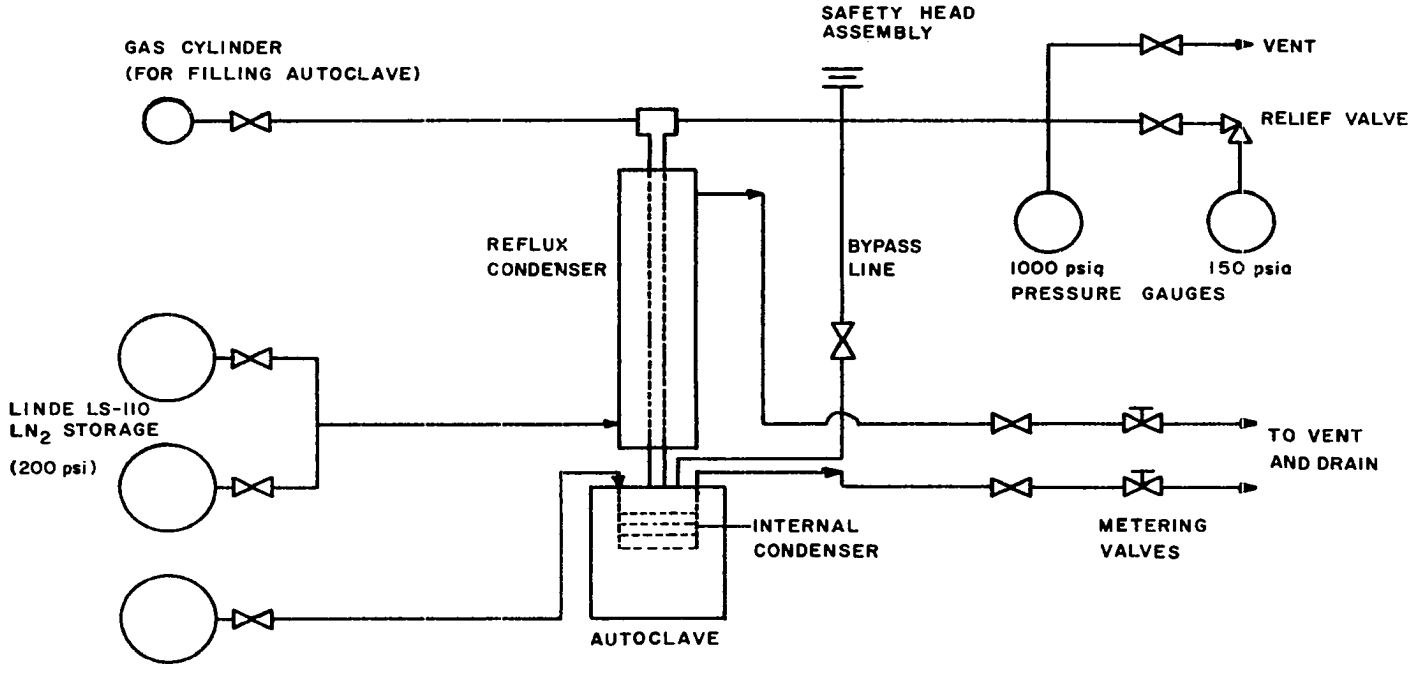

FOR HIGH TEMPERATURE WORK, THE LS-110's WERE REPLACED BY A 1/2-INCH WATER LINE.

Figure 11. Layout of Pressure System

the internal and external condensers was metered separately.

The bypass line shown in Figure 11 was found to be necessary for the external condenser to function properly.

The system was protected by a Universal Safety Head Assembly. The low-pressure gauge was protected with a relief valve, and could be cut off from the rest of the system at high pressure.

The autoclave was filled by connecting the gas cylinder to the line from the top of the reflux condenser.

Stainless steel tubing was used on the high pressure line, with Ermeto fittings. The liquid nitrogen and water lines were copper tubing and schedule 40 iron pipe. Metering valves were standard brass 20-turn (No. 4RB281) Hoke valves.

Electrical System

D.C. power was provided by two Sorensen "Nobatron" MA28-125 power sources connected in series. These could be controlled between 36 and 72 volts and were capable of a maximum current of 125 amperes. A stepwise-variable, air-cooled resistor made of threaded Inconel rods was used so that the effective voltage drop across the heating element could be reduced below nine volts.

Voltage drop across the heating element was measured to about 1/2% with a Simpson model 1700 D.C. voltmeter. Current in the circuit was measured to about 1/2% with a Simpson model 1704 D.C. millivoltmeter connected across a Leeds & Northrup No. 4363, 0.001-ohm standard resistor.

These instruments were both calibrated against a Hewlitt-Packard model 3440A digital voltmeter and found to be more accurate than their rated 1/2% of full scale. The total error in power measurement is estimated to not exceed 1%.

The heater was protected while investigating burnout by connecting one of the internal thermocouples to an Assembly Products Corp. No. 603L indicating pyrometer with No. 905A control module. When the heater temperature passed the high set point, the power was turned off and had to be manually reset.

The heater was mounted inside the vessel by attaching the mounting bracket of the heater to two brass straps. These passed up through the coil and were bolted to the 1/2-inch copper rods sealed into the autoclave cover. The brass straps were modified by soldering copper wire along them to reduce the resistance, and the straps were then wrapped with "Teflon" tape.

Temperature Measuring System

In all, sixteen temperatures were measured: ten internal measurements arranged as shown in Figures 3 and 4; three fluid temperature measurements inside the vessel; and three measurements in the electrical lead and end so that end losses could be calculated. Thirty-gauge iron/constantan, glass-insulated thermocouples were used. The leads from the heater were connected to a screw-post terminal board located inside the vessel. From the terminal board the thermocouple

wires passed out of the vessel through a Conax MHM-062-A16-T gland, with "Teflon" sealant. These leads were Conax mineral-insulated thermocouple stock, which had been supplied with bare wire ends instead of a junction. Bare wires were covered with "Teflon" spaghetti tubing. The fluid temperature thermocouples were standard Conax grounded-tip insulated thermocouples. Outside the autoclave, the thermocouple extensions were joined with a Leeds & Northrup rotary thermocouple switch to a Joseph Kaye and Company electronic reference junction, which is accurate to ± 0.05°F.

Originally it was planned to measure temperatures with a potentiometer. However, the balancing of that instrument was so time-consuming that the steady state could not be maintained without two operators. A Hewlitt-Packard model 3440A digital voltmeter was substituted for the potentiometer. The accuracy limitation on this instrument was about ± 0.5°F, which was insignificant in film boiling but potentially important in nucleate boiling, particularly at high pressures. This limitation represents the major inaccuracy in this work, except for the change in surface properties between runs which seemed to be reflected by a temperature change of about ± 1°F.

Auxiliary Equipment

When operating above room temperature, eight strip heaters ("Chromalox," 500 watt) were fastened around the outside of the autoclave to keep the fluid at the desired temperature without use of the internal heater. When studying

liquid methane, nitrogen was circulated through a copper coil which was wound around the vessel to assist in cooldown. In either case, the autoclave was enclosed in a metal box filled with Perlite insulation. The auxiliary heaters were maintained in an on-off cycle with a "Sim-ply-trol" controller.

Figure 12 shows the assembled apparatus.

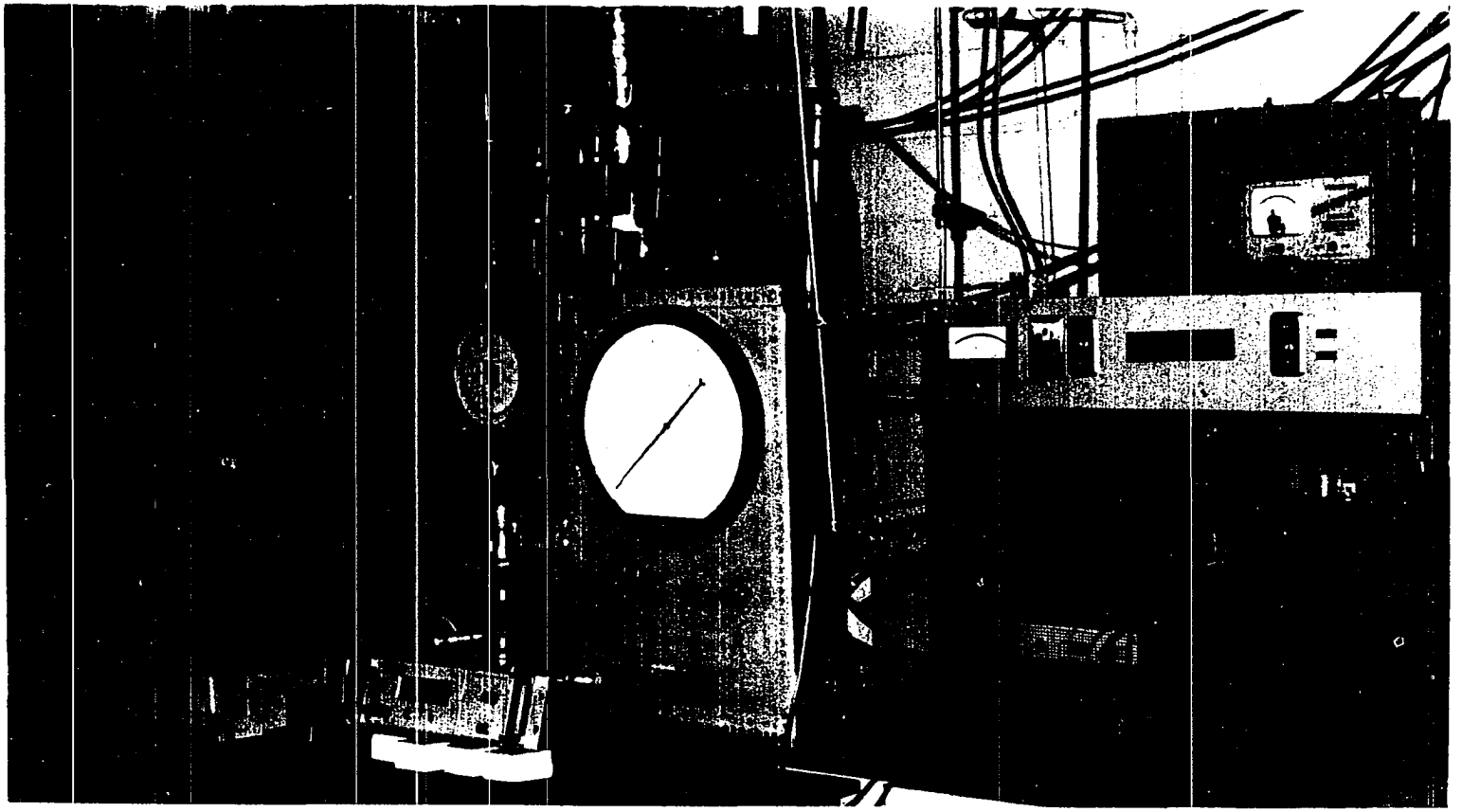

Figure 12. Photograph of Apparatus

CHAPTER VI

EXPERIMENTAL PROCEDURE AND DISCUSSION OF ERRORS

General

Before filling, the system was flushed with vapor. Methane and ethane were condensed into the system, but propane and butane were charged directly as liquids. The liquid level was determined in the following way: the rise of the liquid level to cover the sight glass was timed, and the system was allowed to continue filling for three times that length of time. Since the sight glass had a diameter of 1.25 inches, this meant that the heater would be covered approximately four inches.

Liquid level is not supposed to have much effect on boiling heat transfer unless the heater is practically uncovered [85], a condition which could be readily observed in the sight glass. However, the variation in liquid level as the pressure is changed from the filling condition can be readily calculated from a mass balance. If the volume of the condenser and tubing is combined with the autoclave volume, the total can be considered to be a cylinder of five-inch diameter and height H (about 13.5 inches). If h_l is the liquid depth at any pressure, and h_l° is the depth at

filling conditions,

$$h_{\ell} = \frac{h^{\circ}_{\ell} (\rho^{\circ}_{\ell} - \rho^{\circ}_{v}) + H(\rho^{\circ}_{v} - \rho_{v})}{\rho_{\ell} - \rho_{v}} \qquad (6\text{-}1)$$

where ρ_{ℓ} and ρ_{v} are the liquid and vapor densities, respectively. This equation is primarily of interest when the vessel is filled at high pressure, as was done with ethane.

The materials used were of the following purity: (1) methane, furnished in liquid form by Continental Oil Company, not less than 99.7% pure; (2) ethane, Phillips Petroleum Company, 99.0% pure; (3,4) propane and butane, Phillips Petroleum Company Instrument Grade, 99.5% pure.

The recorded data were: pressure, voltage drop across the heater, current through the heater, three fluid temperatures and thirteen heater temperatures.

Nucleate Boiling

Nucleate boiling data on all substances were taken first; that is, before any film boiling data were taken. Runs 1-5 were primarily for checkout of the equipment, and after run five two inner-ring thermocouples were replaced. After that, the heater was never removed from the system until all nucleate boiling data had been taken.

For saturation temperatures above 90°, external heaters were used around the autoclave to maintain the system pressure. Supplying additional heat in this manner was important at low heater fluxes.

After filling the vessel, the heater was turned on

and allowed to boil for about one hour at 500 watts to condition the surface. Surface changes were minimized between runs by leaving the heater immersed whenever possible. Liquid methane could not be left in the system, of course, because room temperature is above methane's critical temperature.

Nucleate boiling data were always taken with increasing power, so that the hysteresis effects would be identical in every run. The only exceptions to this were Runs 38 and 39 (see Chapter VII).

Periodically, the heater would be turned off and the system allowed to stabilize, so that the thermocouples could be compared with one another (see Appendix C for thermocouple calibration).

The pressure of the system oscillated sharply at high fluxes (greater than 10^5 Btu/ft^2-hr). This oscillation was of such a high frequency that it did not affect the surface temperature appreciably, but it made the pressure hard to read.

Film Boiling

Film boiling data were taken with power increasing or decreasing, whichever was convenient. About ten minutes were required for the surface temperature to stabilize after the power setting was changed, as opposed to nucleate boiling where only about two minutes were required. Small pressure fluctuations were not reflected in the surface temperature in film boiling, as contrasted to nucleate boiling where

there was almost instantaneous change.

Some difficulty was encountered in film boiling because the graphite heating element tended to break. Failure usually occurred when the heater dropped into nucleate boiling and was never definitely connected with the passage from nucleate to film boiling. The element had to be replaced four times during the film boiling runs, but since temperature differences are so much higher in film boiling and surface has a negligible effect, it is assumed that no appreciable loss in accuracy resulted.

The surface temperature was not always uniform in film boiling, but these differences were a small percentage of the ΔT.

First Critical Flux

The burnout (first critical) flux was determined for each material at a number of pressures. It was found that setting the power at a constant value and allowing the pressure to drift slowly gave much more consistent values for the burnout flux than did changing the flux at constant pressure. When the burnout point was reached, the pressure gauge dropped almost instantaneously and very sharply. This reaction was followed by a rise in the heater body temperature. Temperatures at the burnout point could not be manually recorded because the attention of the operator was required elsewhere and the change was very fast. Accurate automatic recording equipment was not available, so burnout temperature

differences were determined by extrapolation of the stable nucleate boiling curves to the experimental burnout flux.

The reaction of the pressure gauge was considerably more sluggish near the critical pressure, principally because the burnout fluxes were so low.

Second Critical Point

No minimum film boiling data taken at elevated pressures were found in the literature: experimental techniques for determining this had to be developed and were not uniform throughout this study. A very effective method was developed, however, after a peculiar effect was observed.

Nucleate and film boiling commonly exist simultaneously on wires, as Farber and Scorah [23] observed. It was surprising to find that this effect could also be observed on the 0.811 inch diameter heater used in this work. On several occasions it was clearly seen in the sight glass that one end of the heater was in film boiling and the other end in nucleate boiling, with an almost perfect demarcation line in the center of the heater. The first time two boiling regimes were established simultaneously, it was thought that the heater was broken, since the two ends were at radically different temperatures. It was observed, too, that the same end of the heater almost always dropped into film boiling first.

The last effect provided the key to getting accurate minimum film boiling points. The digital voltmeter was set to display one of the outer-ring temperatures on the end

which usually went into nucleate boiling first. The power was decreased in increments, and the temperature was watched very carefully while its rate of descent (the surface temperature was dropping, of course, with decreasing flux) became slower and slower, then suddenly increased. With a little practice, the surface temperature could be made to level off just before the transition into nucleate boiling caused it to drop sharply.

The great advantages of this technique were:

(1) The minimum film boiling temperature difference could be closely approximated, as well as the flux.

(2) The power could be increased again before the heater went entirely into film boiling, which would reestablish film boiling over the entire surface. This procedure seemed to prevent breakage of the graphite element.

(3) Trying to locate the second critical flux accurately by small power changes is extremely time-consuming, because of the ten minutes required to stabilize after a power change. The technique described above is effective with relatively large power changes, provided the operator knows approximately where the transition will occur.

Since this method was not evolved until nearly all of the data had been taken, not very many second critical point temperature differences were recorded. There are virtually no data of this type in the literature.

Errors

As already mentioned in Chapter V, it is believed that power was measured to within 1%. Although end losses averaged about 6%, as will be seen in Appendix B these end effects were negligible because losses of this magnitude do not affect the flux near the center of the heater where the temperatures were measured (see Appendix B). These losses were not from the insulated end of the iron body but rather down the electrical lead which acted as a fin protruding into the liquid. Film boiling fluxes were not corrected for radiation because of the smallness of this correction and difficulty in accurately determining the emissivity of the surface.

Temperature differences were measured to within about $\pm$ 0.5°F, with an additional scatter of as much as $\pm$ 1.5°F coming from other factors such as surface changes. The thermocouples were calibrated in place (Appendix C).

During film boiling, errors in temperature differences, ΔT_s, were negligible, but in the nucleate boiling regime an error of $\pm$ 2°F meant errors in ΔT from 8% to more than 100%.

The surface temperatures were calculated using the average of the temperatures measured around the outer ring of thermocouples. The smoothing effect of averaging five or six temperatures (usually one thermocouple was used as a burnout monitor and could not be read on the digital voltmeter) helped hold the variations down. Because of duplication of runs, it is believed that the average error in ΔT at

any given pressure is less than 15% except at high reduced pressures (above 0.6).

Several other effects of small magnitude were neglected. For example:

(1) change in heater surface area with temperature,

(2) potential drop through the 1/2-inch diameter by 12 inch long copper electrodes sealed into the reactor, and through the copper and brass mounting bracket, and

(3) rapid pressure fluctuations of as much as $\pm$ 3 psi at high fluxes, which made selection of the correct pressure difficult.

Errors in Individual Temperature Readings Caused by High Fluxes

Heat fluxes across the outer thermocouple ring ranged up to 190,000 Btu/ft^2-hr, and those across the inner thermocouple ring went as high as 500,000 Btu/ft^2-hr. For a typical thermal conductivity of 40 Btu/ft-hr-F°, a flux of 500,000 Btu/ft^2-hr would result in a temperature drop of more than one F° for each thousandth of an inch across the inner ring. The thermocouple wires were about 0.010 inch in diameter, so it is apparent that small errors in bead location or very tiny obstructions or gaps near the thermocouple bead can cause large errors in the temperature measurement.

In Chapter IV, the precautions which were taken to minimize this kind of error were described. Also, the procedure was described whereby bead locations of all but two thermocouples were determined by cutting apart the heater.

Still, readings of individual thermocouples were found to deviate from the average by several degrees at high fluxes. A procedure used to correct for this error is described in Appendix G.

These thermocouple corrections were applied only to the nucleate boiling data. The correction to the average surface temperature was only about two degrees at the highest fluxes, which is negligible in film boiling. The correction tends to make the nucleate boiling lines on a log q vs. log ΔT plot slightly steeper.

In Chapter IX, the advantages and disadvantages of measuring ΔT's directly by differential thermocouples are discussed.

CHAPTER VII

RESULTS AND DISCUSSION

First Critical Flux

The data obtained on the burnout (first critical) heat flux are listed in Appendix E. All of the predictive equations mentioned in Chapter II were compared with these data. The equation of Noyes [62],

$$q_{1c} = 0.144\mathfrak{L}\left[\frac{\rho_\ell - \rho_v}{\rho_\ell}\right]^{1/4}\left(\frac{\mu_\ell C_{p\ell}}{k_\ell}\right)^{-0.245} \qquad (2\text{-}21)$$

where $\mathfrak{L}$ is the group defined by (2-19), gave the best results over the pressure range from one atmosphere to the critical pressure. The equation of Moissis and Berenson [56],

$$q_{1c} = 0.18\mathfrak{L}\left[\frac{\sqrt{\frac{\rho_\ell + \rho_v}{\rho_\ell}}}{1 + 2\sqrt{\frac{\rho_v}{\rho_\ell} + \frac{\rho_v}{\rho_\ell}}}\right] \qquad (2\text{-}20)$$

gave somewhat better results at high pressures (above a reduced pressure Pr of 0.4) but was inaccurate at low pressures.

Figures 13, 14, 15 and 16 compare the data taken in this work with equation (2-21), and at high pressures with

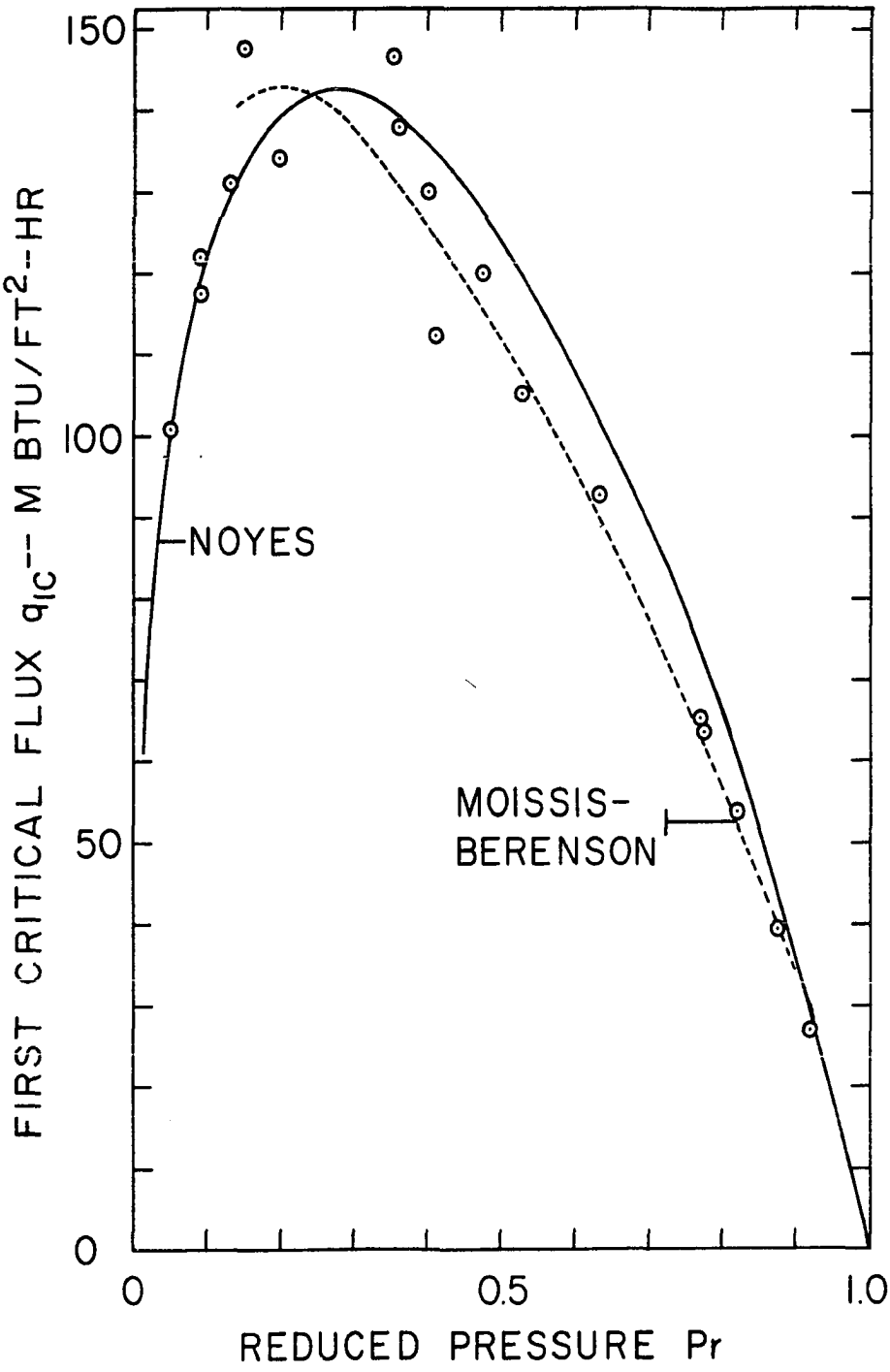

Figure 13. Methane Burnout Heat Flux Compared with the Equations of Noyes and of Moissis and Berenson

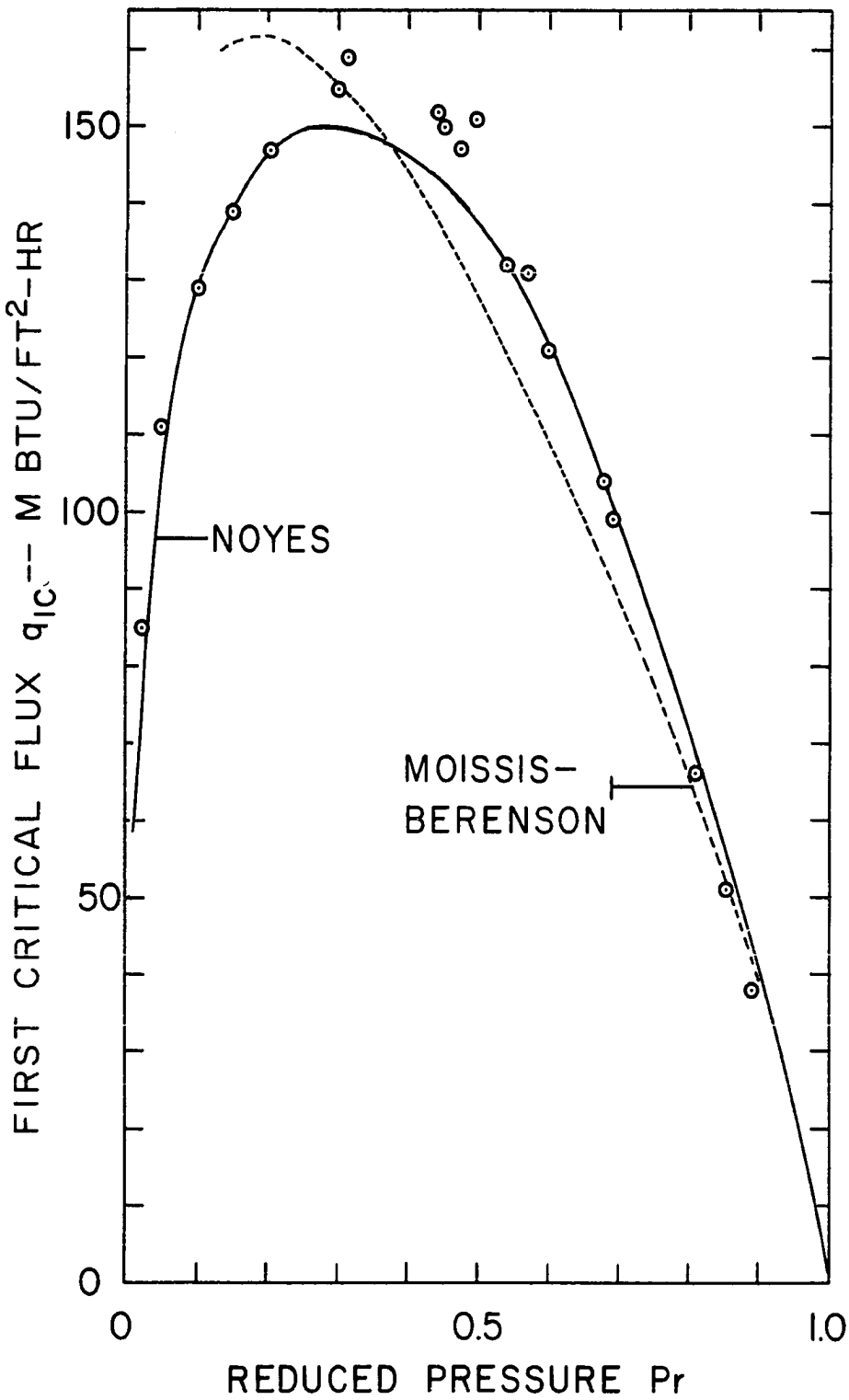

Figure 14. Ethane Burnout Heat Flux Compared with the Equations of Noyes and of Moissis and Berenson

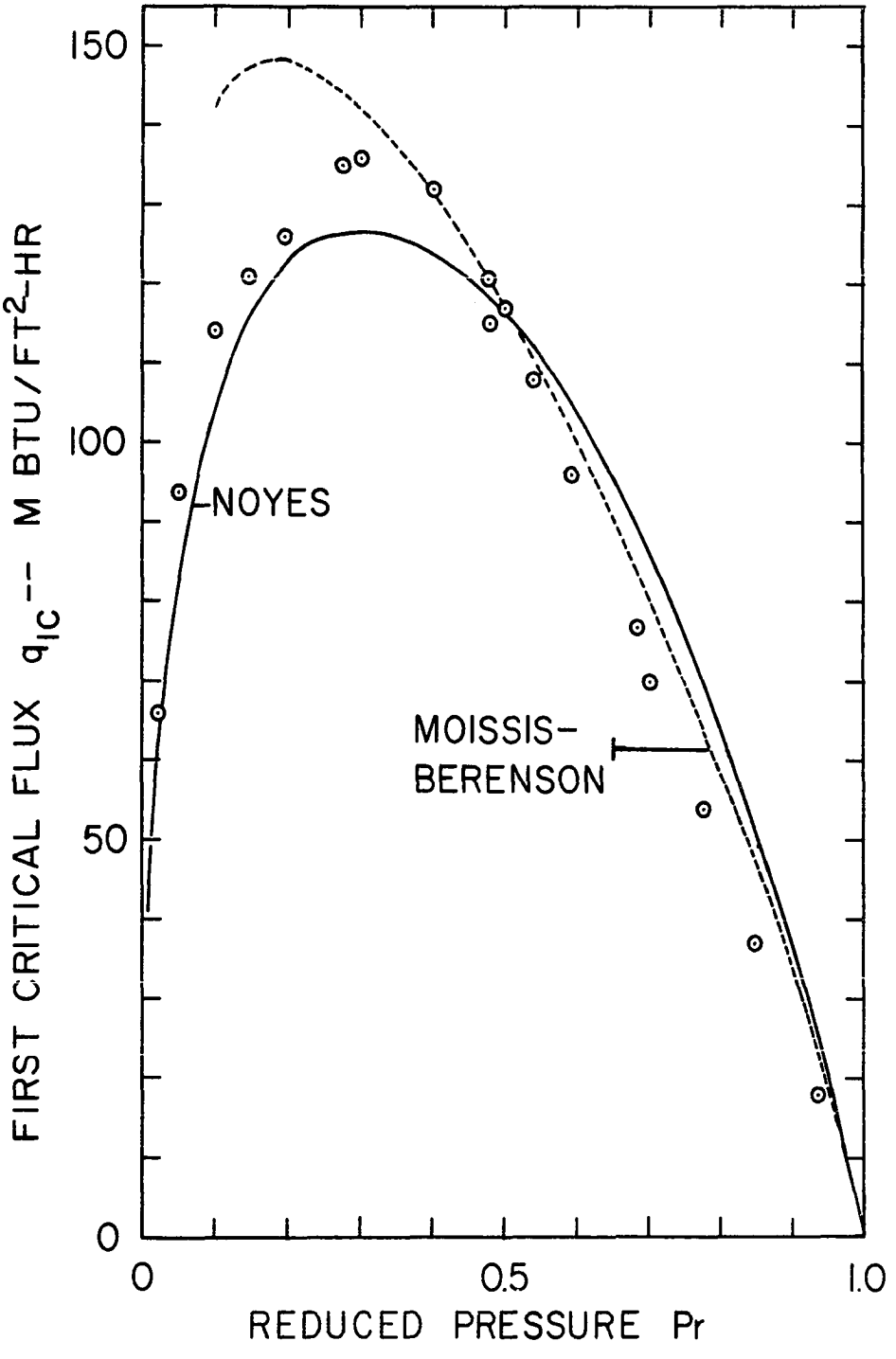

Figure 15. Propane Burnout Heat Flux Compared with the Equations of Noyes and of Moissis and Berenson

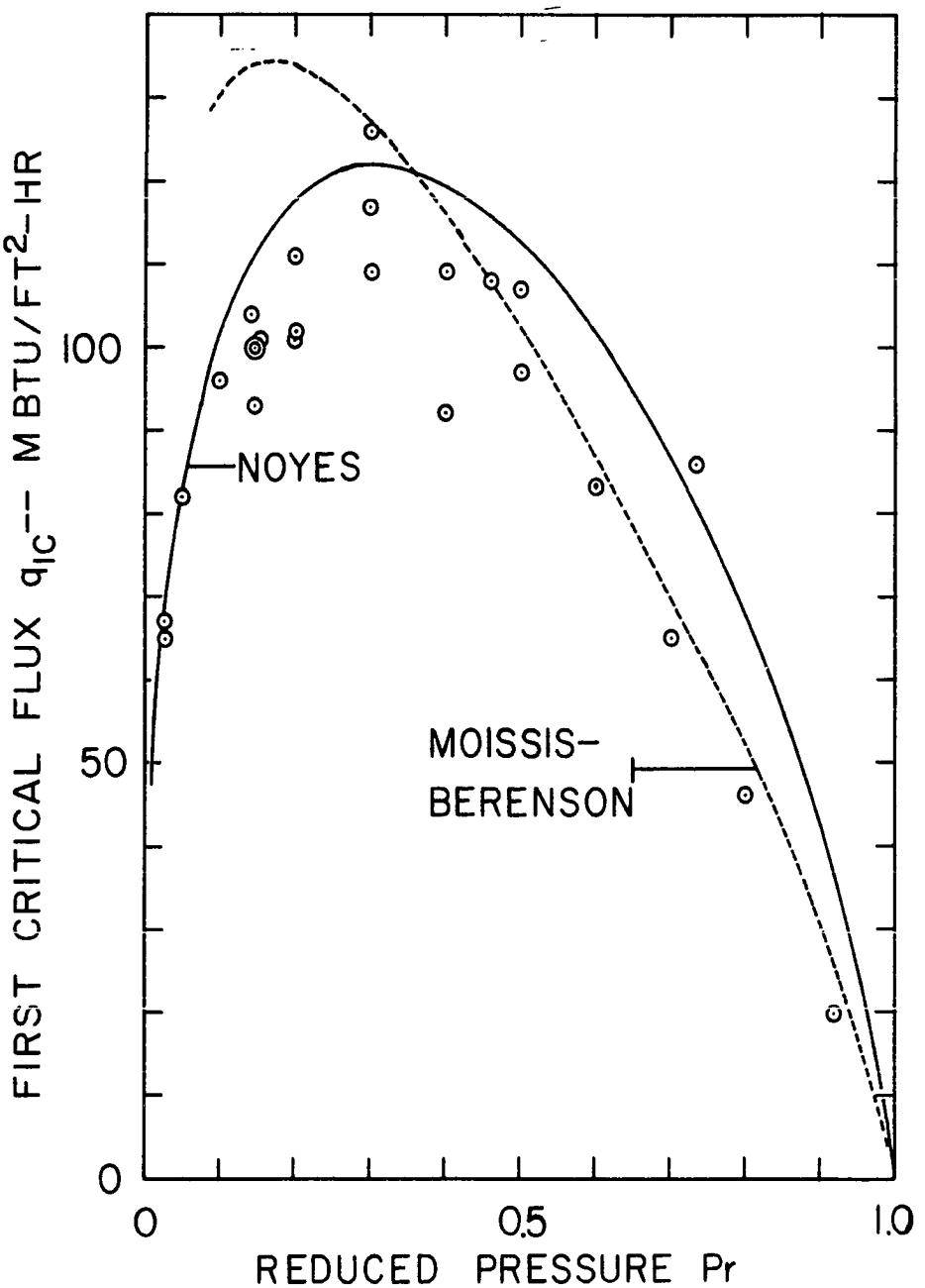

Figure 16. Butane Burnout Heat Flux Compared with the Equations of Noyes and of Moissis and Berenson

(2-20).

Agreement of the data with the Noyes equation was so good that it was not considered appropriate to add another burnout equation to the more than 50 already in the literature.

Nucleate and Film Boiling Data

Forty experimental runs were made. Their dates, with comments and general information, are listed in Appendix D.

Data obtained in the nucleate boiling regime are listed in Appendix H. Data taken in the stable film boiling regime are listed in Appendix I.

Figures 17, 18, 19, and 20 show these data in the conventional log q vs. log ΔT form, with lines of constant reduced pressure. Data are not shown if the measured $\Delta T < 1F^{\circ}$, because the error can exceed 100% for these very small ΔT's (see the discussion of errors in Chapter VI).

Correlation of Film Boiling Data

Equations (3-11) through (3-17) presented some correlating equations for film boiling in the form used by Frederking, Wu and Clement [25]. The pertinent groups are the Prandtl Number $Pr^* \equiv \mu C_p/k$, the group $\theta' \equiv (\lambda + 0.5C_{pf}\Delta T)/(C_{pf}\Delta T)$, the Nusselt Number $Nu^* \equiv qB/k_f\Delta T$ (B is the Laplace Reference length, equation (2-6)), and the Rayleigh Number,

$$Ra^* \equiv B^3 g\rho_f(\rho_\ell - \rho_f)C_{pf}/\mu_f k_f \qquad (3\text{-}11)$$

where the film properties are evaluated at $\frac{1}{2}(T_w + T_{sat})$.

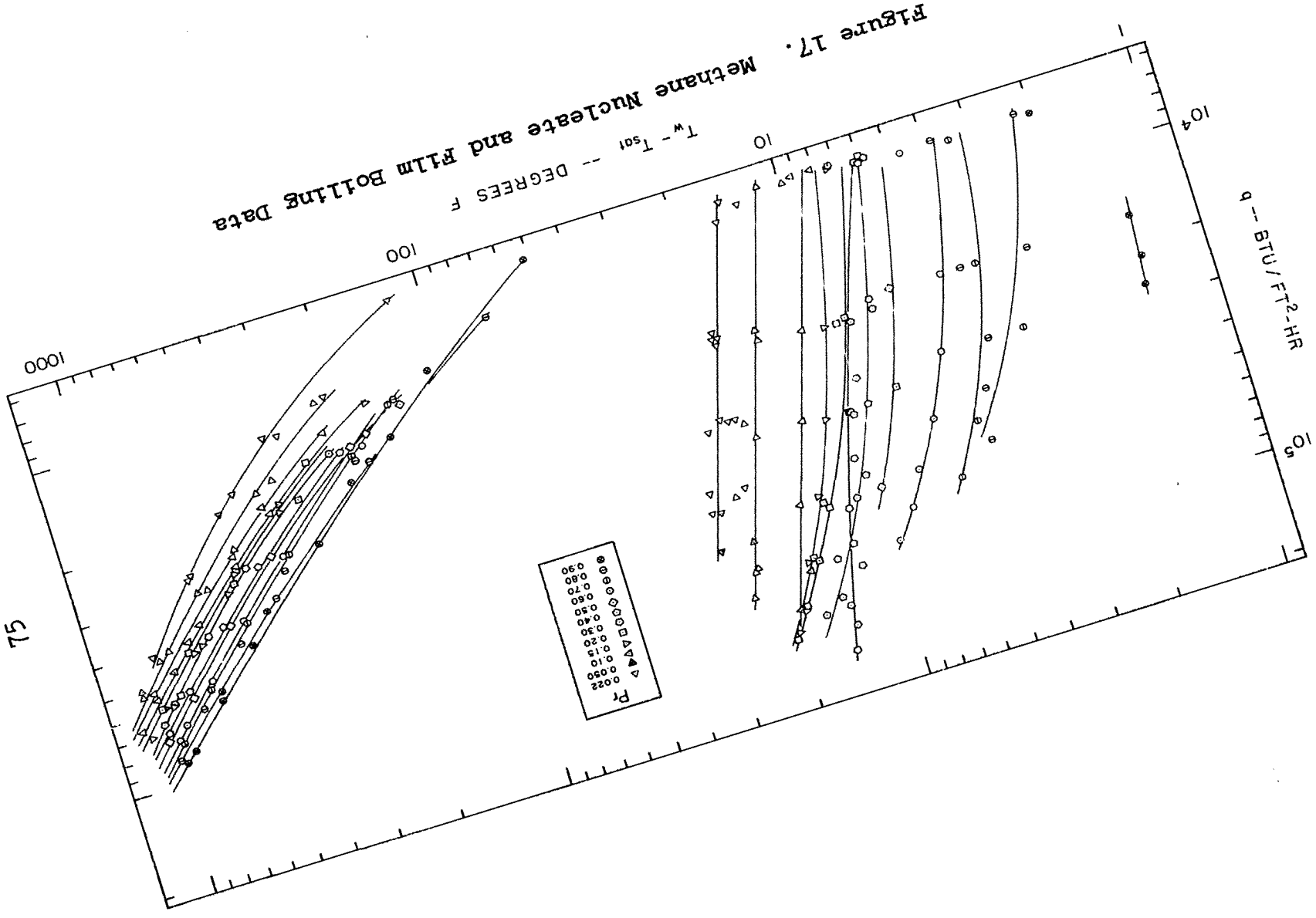

Figure 17. Methane Nucleate and Film Boiling Data

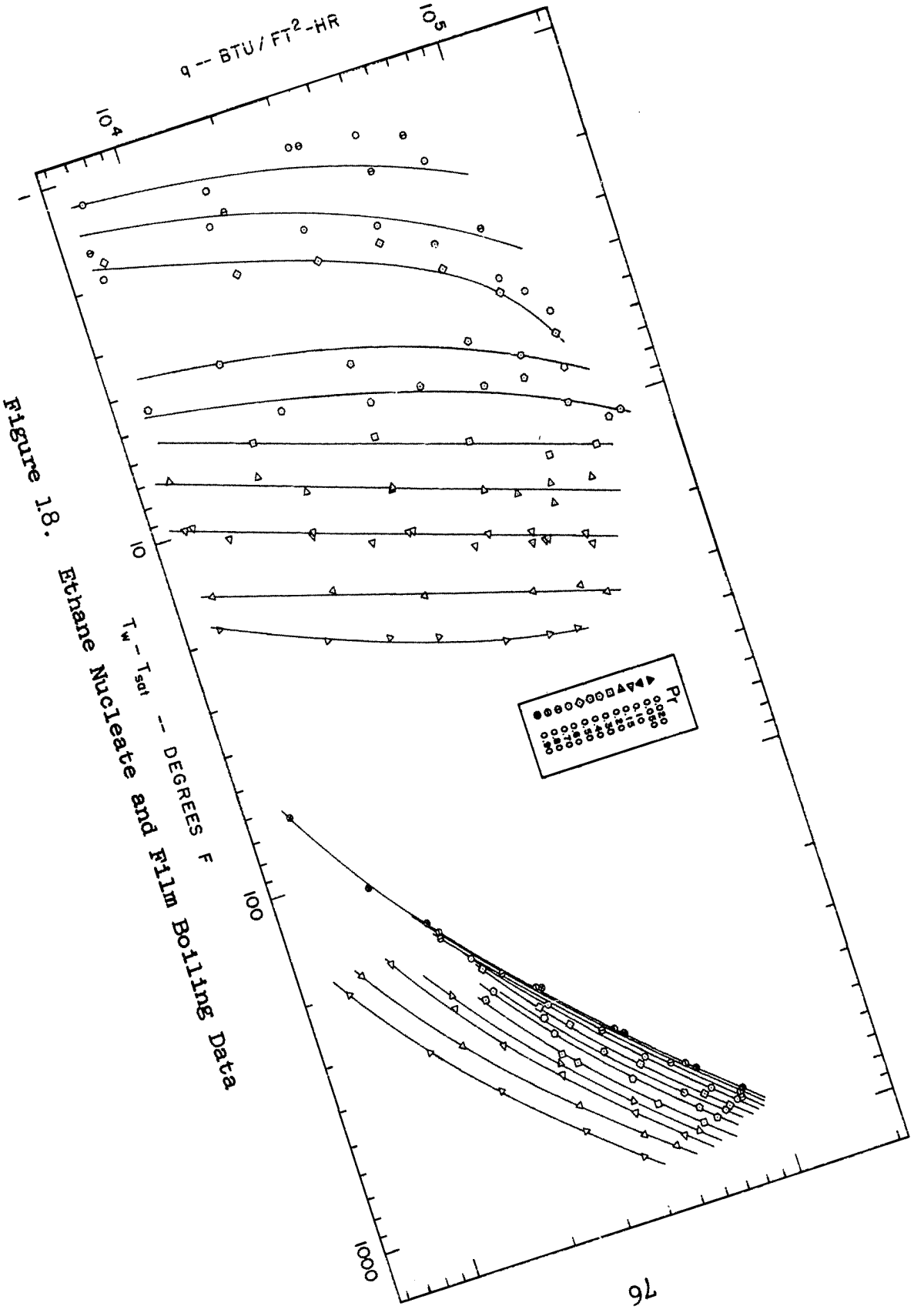

Figure 18. Ethane Nucleate and Film Boiling Data

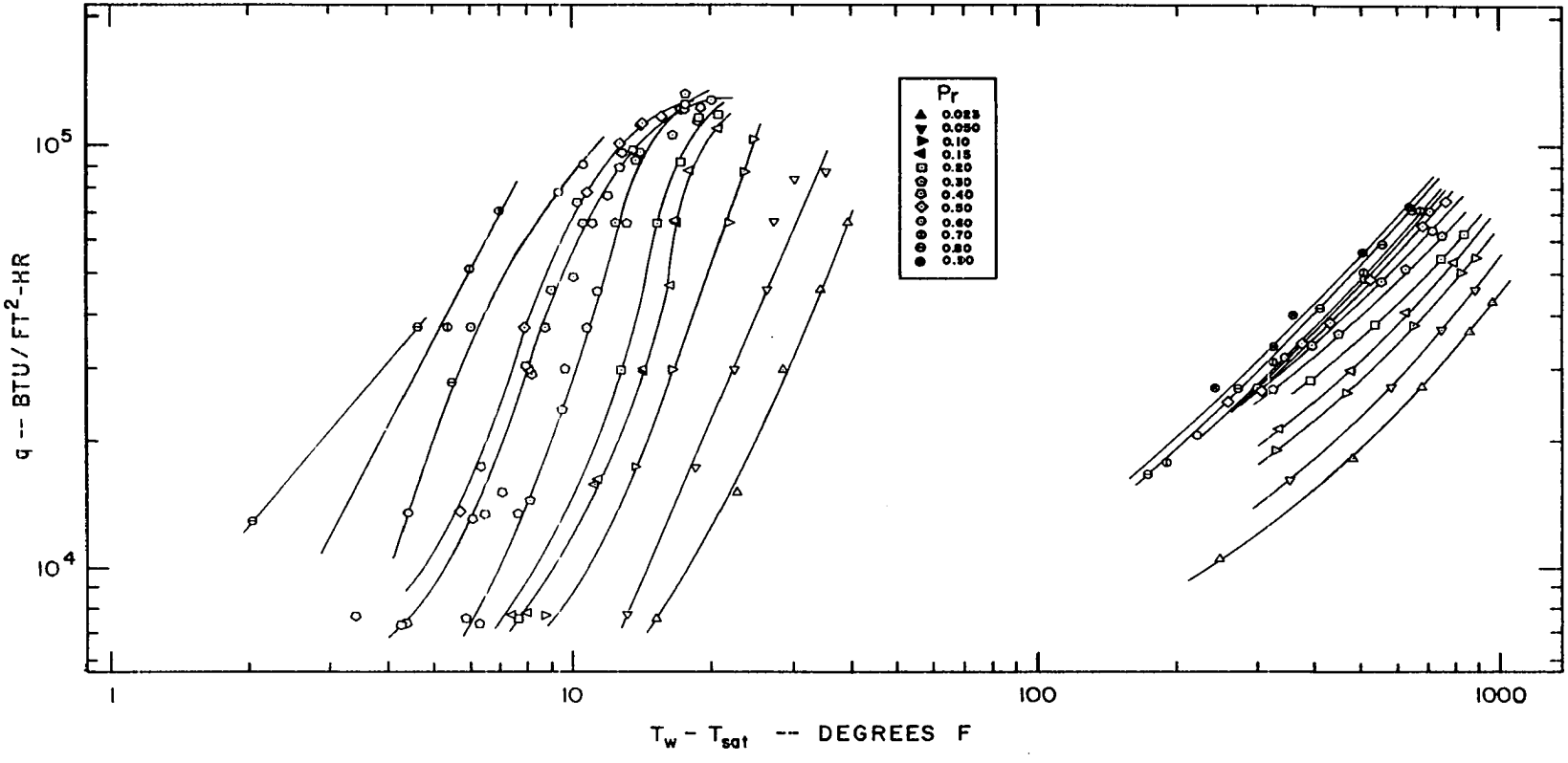

Figure 19. Propane Nucleate and Film Boiling Data

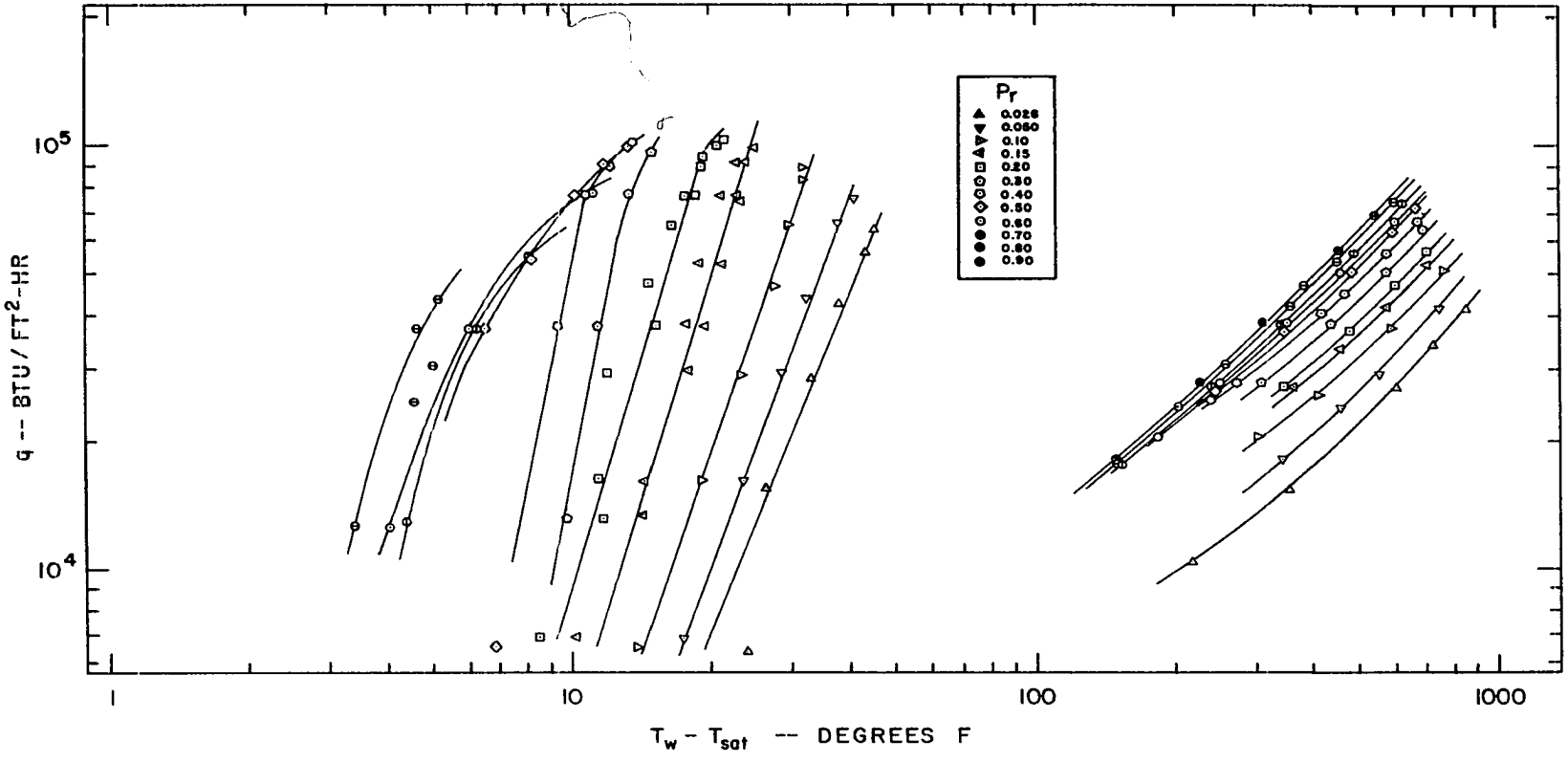

Figure 20. Butane Nucleate and Film Boiling Data

For each of the correlations, the data are plotted as log Nu^* vs. log x, where $x = Ra^*\theta'$ for models assuming laminar vapor flow and $x = Ra^*Pr_f^*\theta'^2$ for models assuming vapor flow dominated by inertial forces.

The models predict that $Nu^* = mx^{1/3}$ if the vapor is removed from the surface at random, and that $Nu^* = mx^{1/4}$ if the vapor is removed from the surface with regular cellular flow.

It was found that the data taken in this work, when plotted as log Nu^* vs. log $(Ra^*\theta')$ or as log Nu^* vs. log $(Ra^*Pr_f\theta'^2)$, had a slope between 1/3 and 1/4, but showed a substantial drift with pressure. It was further found that dividing either term on the abscissa by the square of the reduced temperature eliminated this drift.

Table VII-1 summarizes the results when the data were fitted by each method. It is apparent that division by Tr^2 reduced the scatter in every case, no matter which model is assumed. The recommended equation is

$$\frac{qB}{k_f\Delta T} = 0.369 \left[\frac{B^3 g\rho_f(\rho_\ell - \rho_f)}{\mu_f k_f Tr^2 \Delta T} \right]^{0.267} \qquad (7\text{-}1)$$

The data are compared with (7-1) in Figures 21, 22, 23 and 24. For reference, the equation which best fits that particular component is also shown as a dashed line. In every case, log Nu^* vs. log $(Ra^*\theta'/Tr^2)$ was the best correlating form.

Equation (7-1) seems to represent the data very well.

TABLE VII-1

COMPARISON OF FILM BOILING DATA WITH CORRELATING EQUATIONS

Substance	y = log Nu^* vs. x =	Slope of Best Fit Line	Standard Deviation of Log Nu^*
Methane (96 points)	log $(Ra^*\theta')$	0.297	0.0556
	log $(Ra^*\theta'/Tr^2)$	0.276	0.0273
	log $(Ra^*Pr_f\theta'^2)$	0.234	0.0576
	log $(Ra^*Pr_f\theta'^2/Tr^2)$	0.224	0.0310
Ethane (62 points)	log $(Ra^*\theta')$	0.308	0.0386
	log $(Ra^*\theta'/Tr^2)$	0.274	0.0210
	log $(Ra^*Pr_f\theta'^2)$	0.237	0.0501
	log $(Ra^*Pr_f\theta'^2/Tr^2)$	0.219	0.0354
Propane (55 points)	log $(Ra^*\theta')$	0.297	0.0304
	log $(Ra^*\theta'/Tr^2)$	0.263	0.0195
	log $(Ra^*Pr_f\theta'^2)$	0.248	0.0359
	log $(Ra^*Pr_f\theta'^2/Tr^2)$	0.227	0.0236
n-Butane (58 points)	log $(Ra^*\theta')$	0.310	0.0236
	log $(Ra^*\theta'/Tr^2)$	0.267	0.0163
	log $(Ra^*Pr_f\theta'^2)$	0.263	0.0332
	log $(Ra^*Pr_f\theta'^2/Tr^2)$	0.234	0.0246
All Together (271 points)	log $(Ra^*\theta')$	0.297	0.0472
	log $(Ra^*\theta'/Tr^2)$	0.267	0.0249
	log $(Ra^*Pr_f\theta'^2)$	0.238	0.0508
	log $(Ra^*Pr_f\theta'^2/Tr^2)$	0.223	0.0329

It would be more appealing on a theoretical basis to break the data into two parts, depending on Rayleigh Number. The film boiling data having laminar and turbulent vapor flow would then be fit separately. However, (7-1) represents the data well enough so that such a division is unnecessary.

The Laplace reference length B was used as a correlating length because it was desired to make these data comparable with that taken from flat plates. Breen and

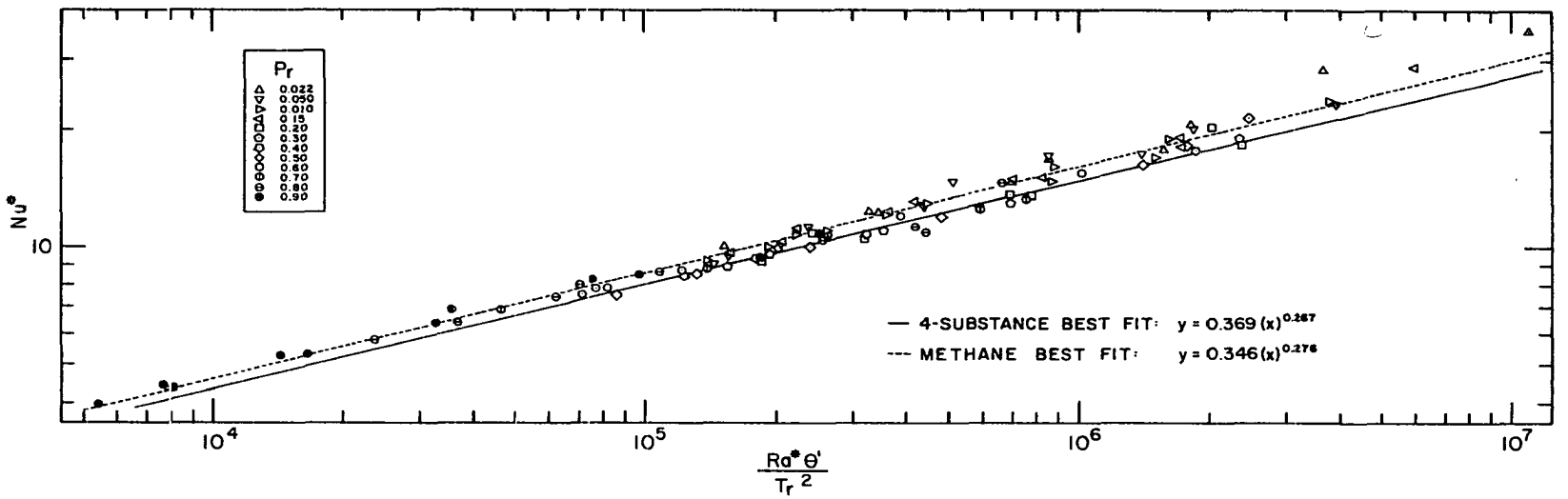

Figure 21. Methane Film Boiling Data Compared with the Proposed Equation

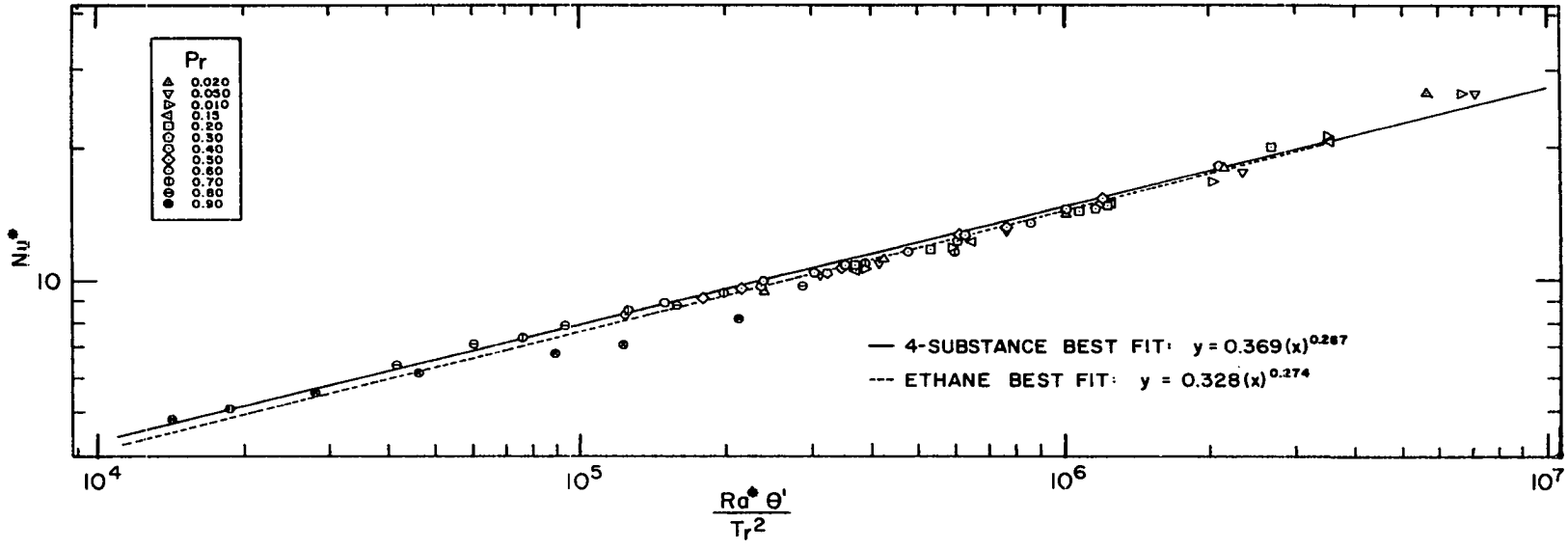

Figure 22. Ethane Film Boiling Data Compared with the Proposed Equation

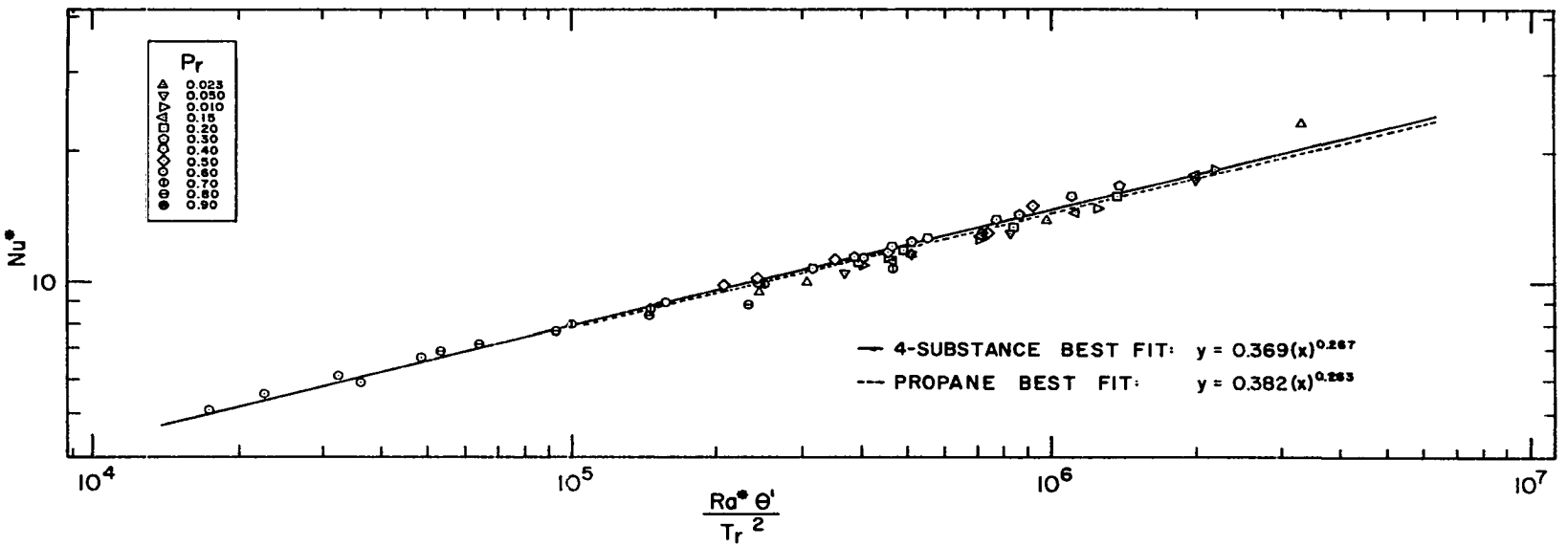

Figure 23. Propane Film Boiling Data Compared with the Proposed Equation

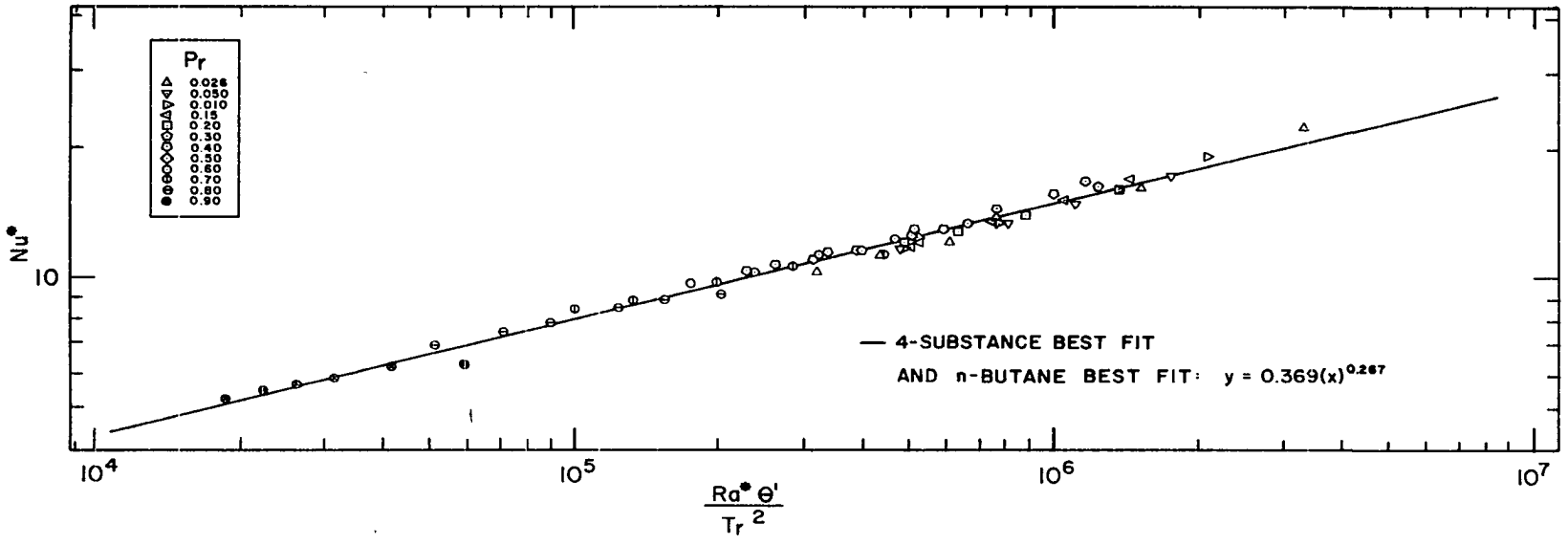

Figure 24. Butane Film Boiling Data Compared with the Proposed Equation

Westwater [10] showed that diameter effects disappear for diameters greater than one cm, and the heater used in this work was 2.06 cm in diameter.

The modified heat of vaporization λ' was considered to be $\lambda + 0.5C_{pf}\Delta T$ (3-3) instead of the alternate forms (3-4) or (3-5) because Frederking et al. [25] used that form. Time did not permit comparing each alternate form in detail.

Correction of Nucleate Boiling Data

Small corrections were applied to the nucleate boiling temperature differences. These are explained in Appendix G, and were mentioned also in Chapter VI.

Correlation of Nucleate Boiling Data

The nucleate boiling data were compared with the correlating equations of Rohsenow [75], Forster and Greif [24], and Madejski [52]. The latter two were unsatisfactory. The Rohsenow equation (2-7) came closest, but the constant c changed with pressure. $Re^* = qB/\lambda C_{p\ell}$.

$$Re^* = c\left[\frac{1}{\theta Pr_\ell^{*1.7}}\right]^3 \qquad (2\text{-}7)$$

It was found that the propane and butane data, and the methane data at reduced pressures less than 0.7, could be correlated reasonably well with the following modification of the Rohsenow equation:

$$Re^* = c\left[\frac{1}{\theta}\left(\frac{Tr}{Pr_\ell^*}\right)^{1.18}\right]^n \qquad (7\text{-}2)$$

For methane data shown in Figure 25, $c = 3.25 \times 10^5$, $n = 2.89$ and the standard deviation on log Re^* (for $Pr < 0.7$) was 0.124.

The propane data are shown in Figure 26. For propane, the fitting technique gave an unrealistic slope, so the line was drawn in as $c = 5.77 \times 10^5$, $n = 2.6$.

The n-butane data are shown in Figure 27. The best fit line was $c = 2.33 \times 10^5$ and $n = 2.84$ for reduced pressures less than 0.7. This is very nearly the same as the best fit for methane.

For propane and butane, (7-2) puts all of the pressures on a common basis, although the fitting was done for $Pr < 0.7$.

For ethane, however, equation (7-2) was completely unsuccessful. n is about 3, but a large drift with pressure was observed. This is perhaps because ethane was the least pure substance (99%) used. Figure 28 shows the ethane data to illustrate the scatter. No correlation was obtained for the ethane nucleate boiling data.

Second Critical Point

The data taken at the minimum film boiling point (second critical point) are listed in Appendix F.

Not very many second critical ΔT's were observed, but Figure 29 shows how Berenson's prediction (equation 3-23) compares with the data. This equation must be evaluated by trial and error because of the film properties. It appears

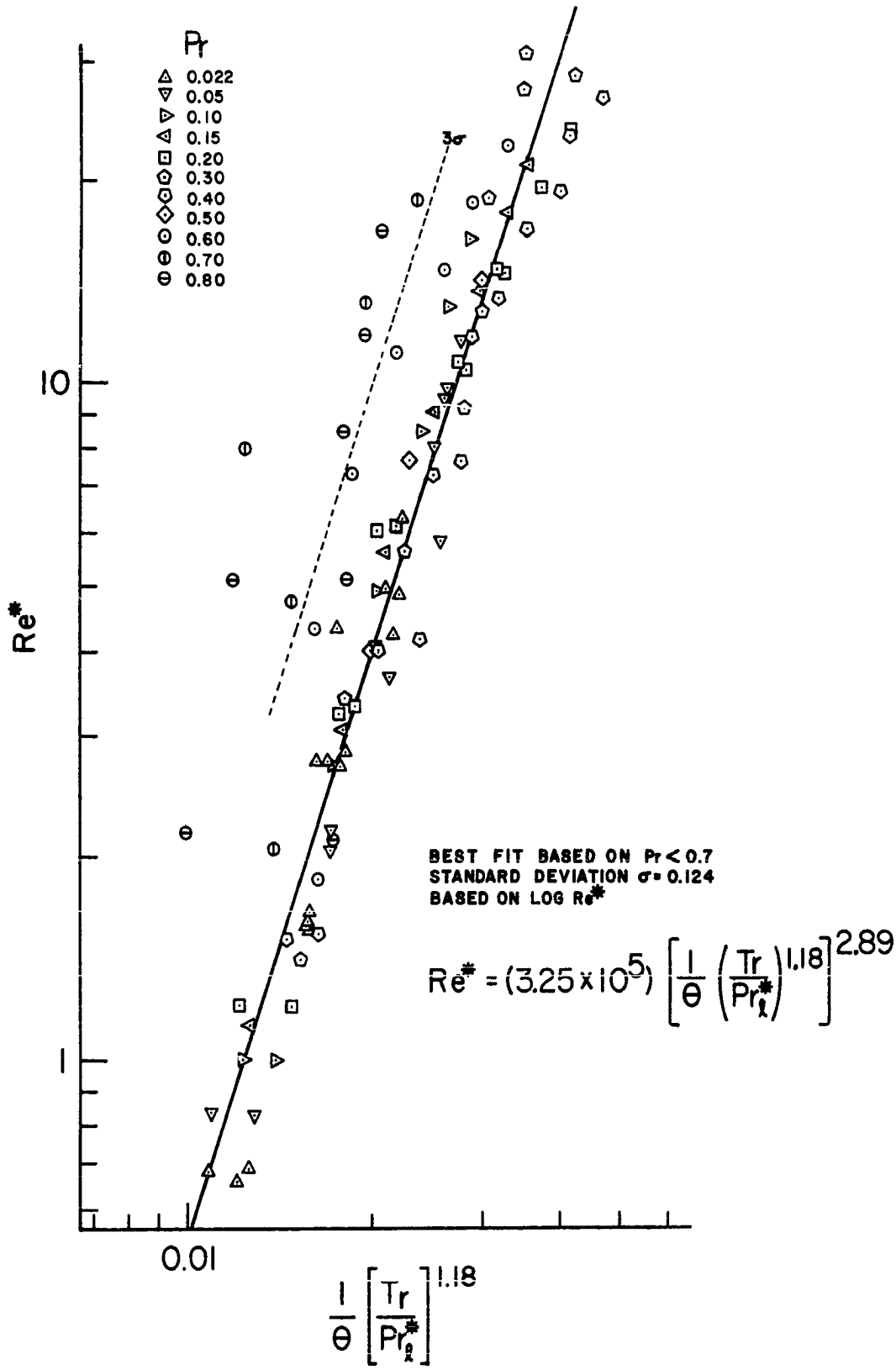

Figure 25. Methane Nucleate Boiling Data Compared with the Proposed Correlation

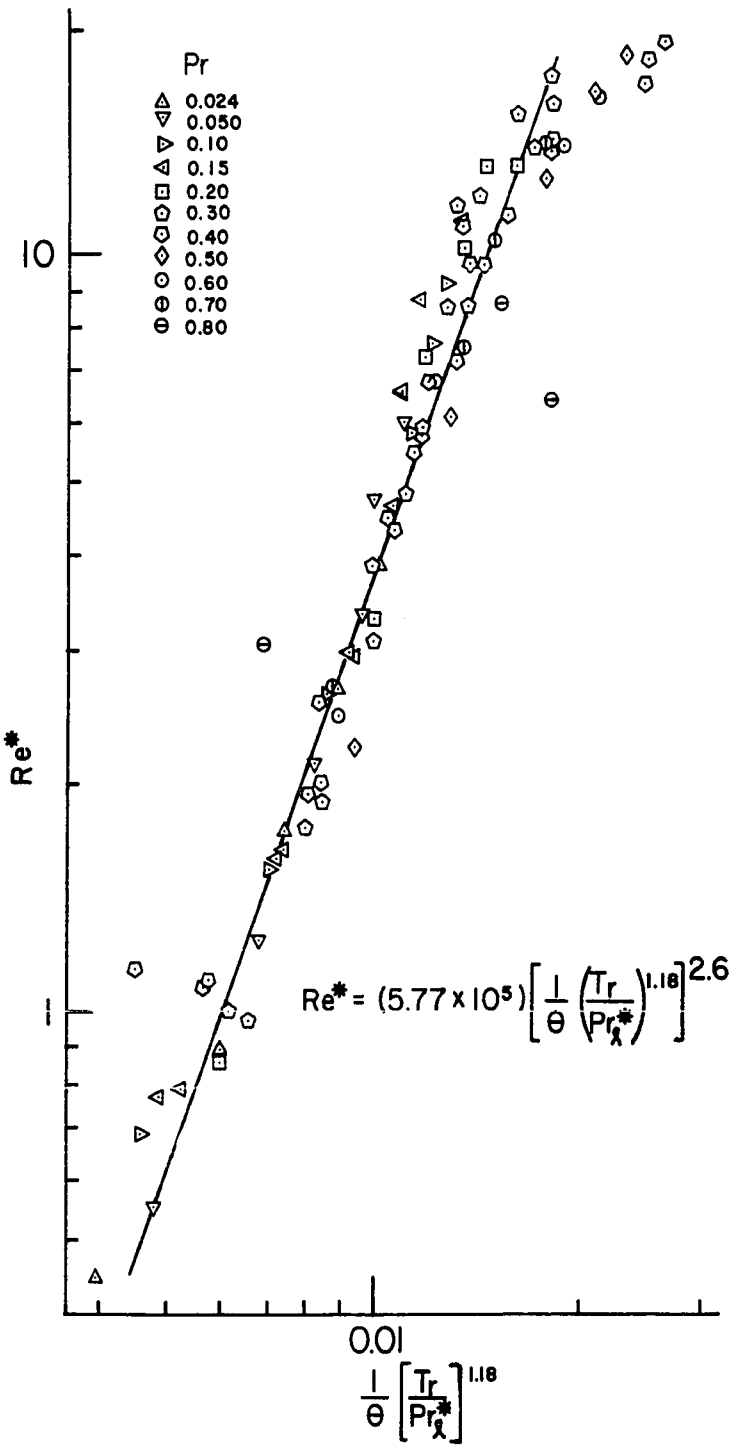

Figure 26. Propane Nucleate Boiling Data Compared with the Proposed Correlation

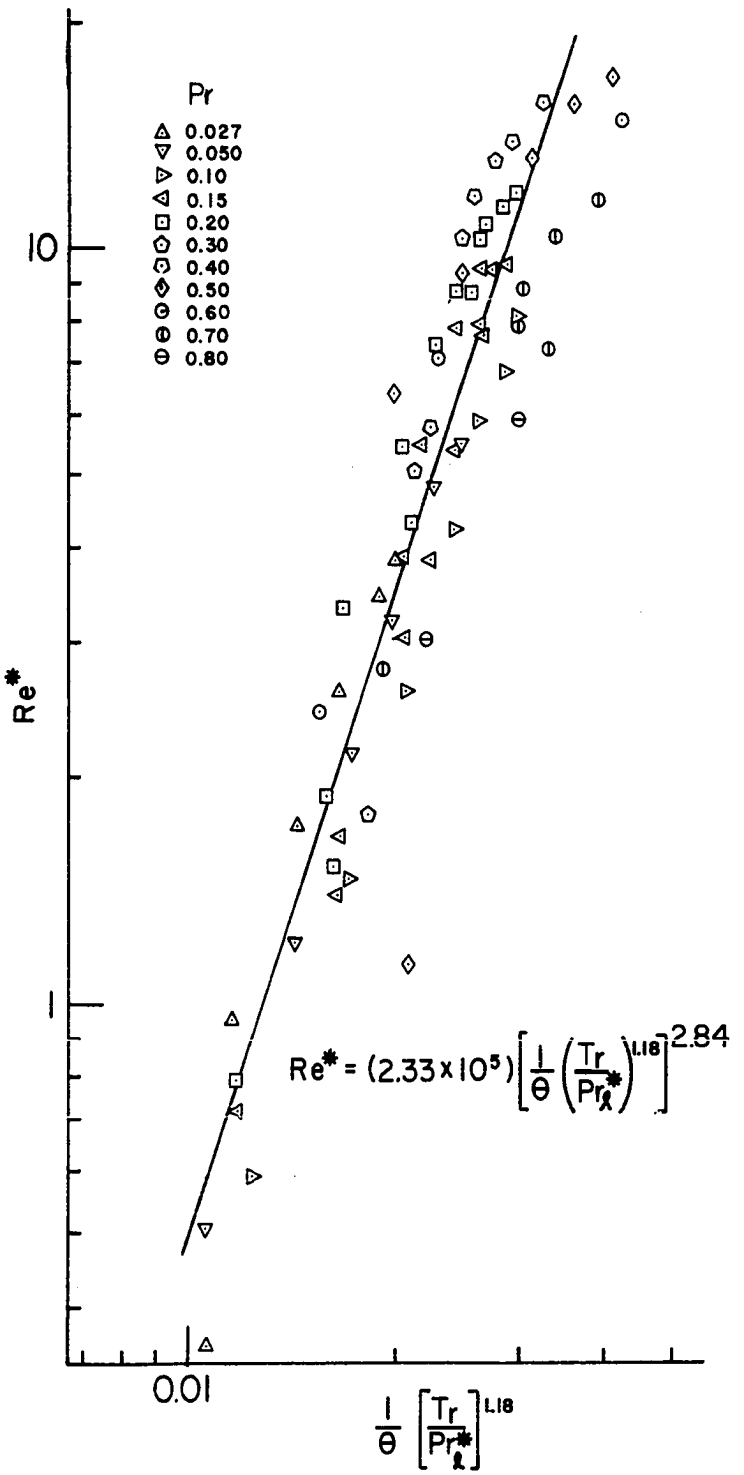

Figure 27. Butane Nucleate Boiling Data Compared with the Proposed Correlation

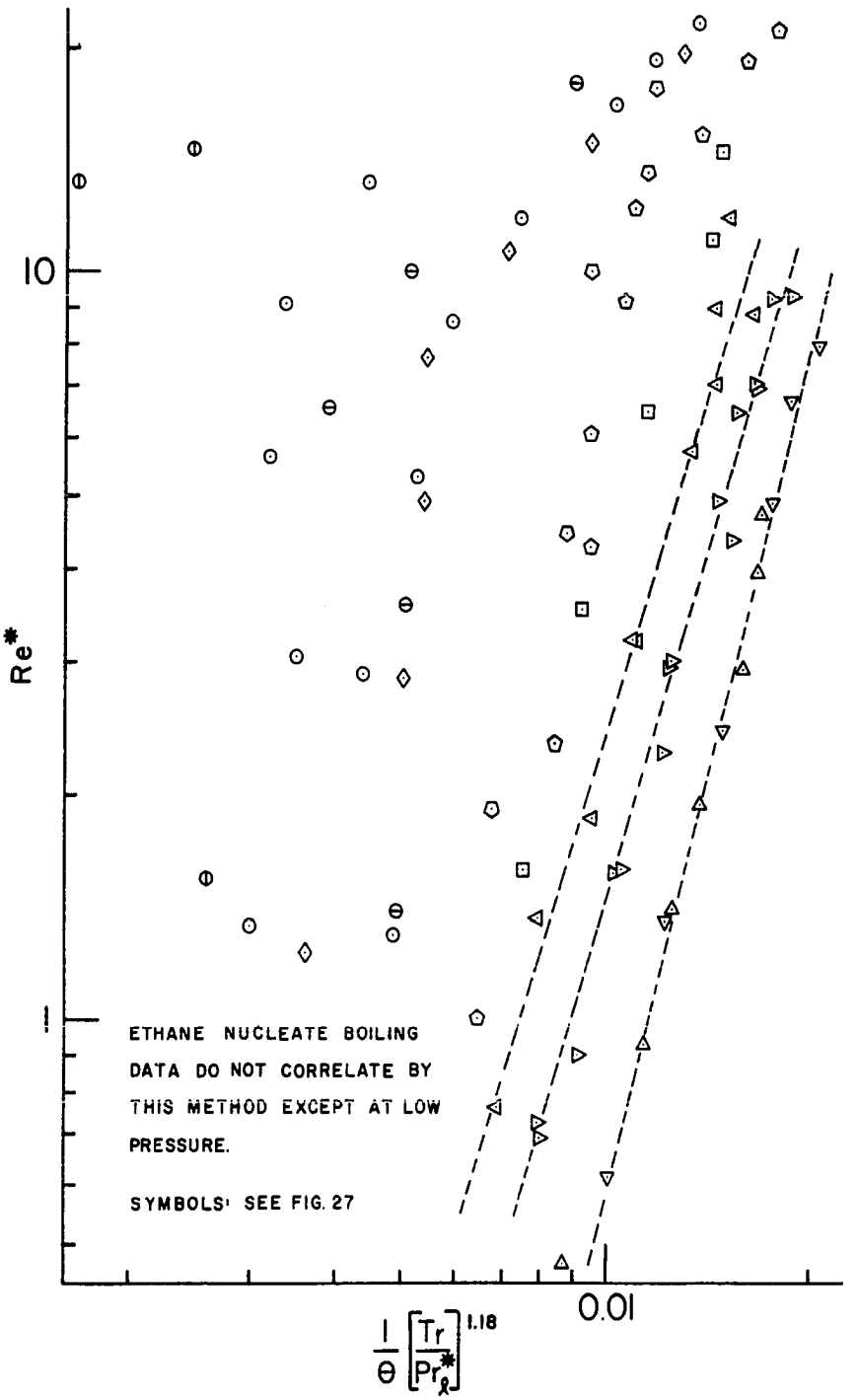

Figure 28. Ethane Nucleate Boiling Data Compared with the Proposed Correlation

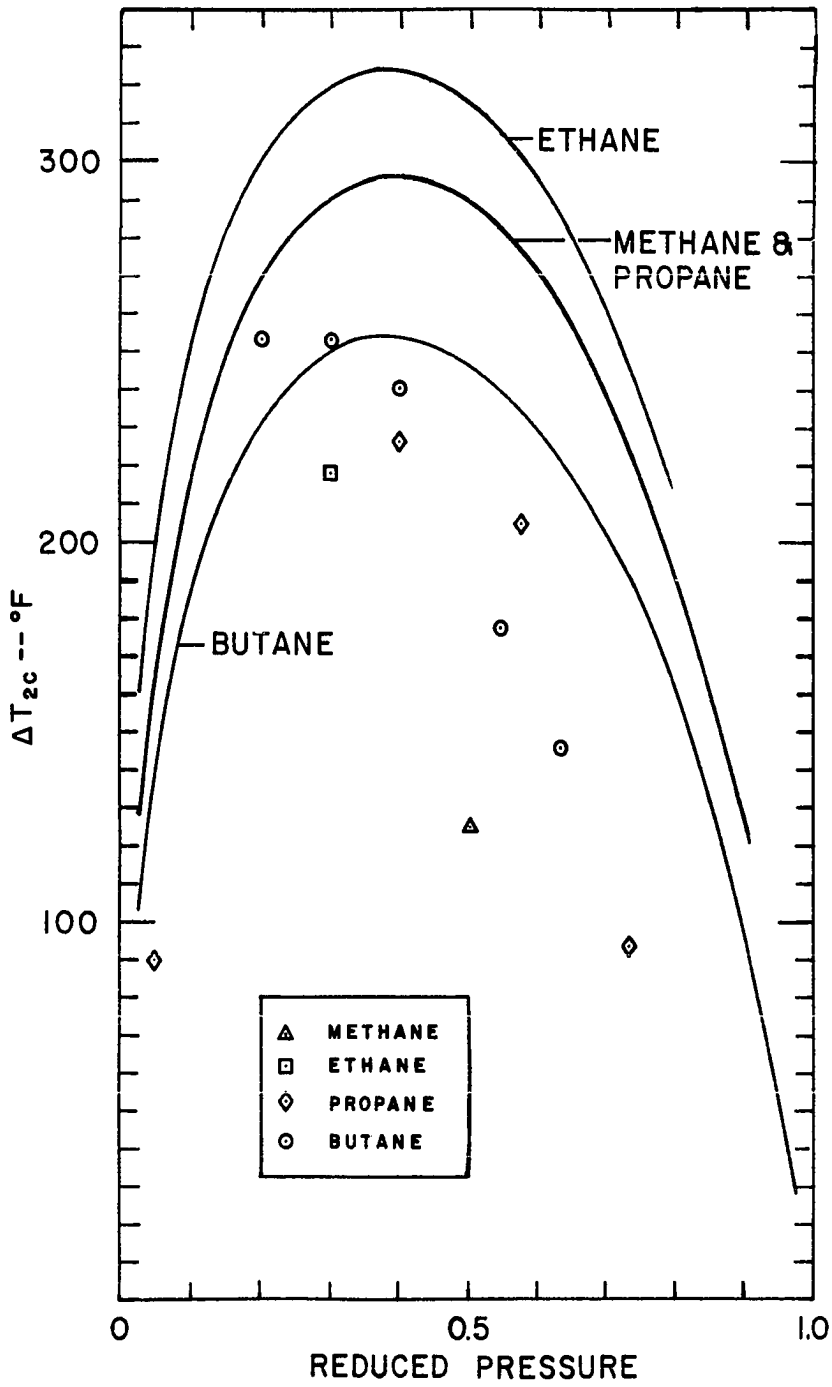

Figure 29. Second Critical ΔT Compared with Berenson's Equation (3-23)

that (3-23) predicts values that are too high, particularly at reduced pressures above 0.4.

Figure 30 compares the second critical flux data with Berenson's version of the Zuber-Tribus equation (3-22).

Miscellaneous

The attempt to check flux measurements by measurement of radial temperature distribution was not entirely successful. It is discussed in detail in Appendix J.

The temperature variation around the circumference of the heater was measured, but was found to be small and relatively patternless. These are discussed in Appendix K.

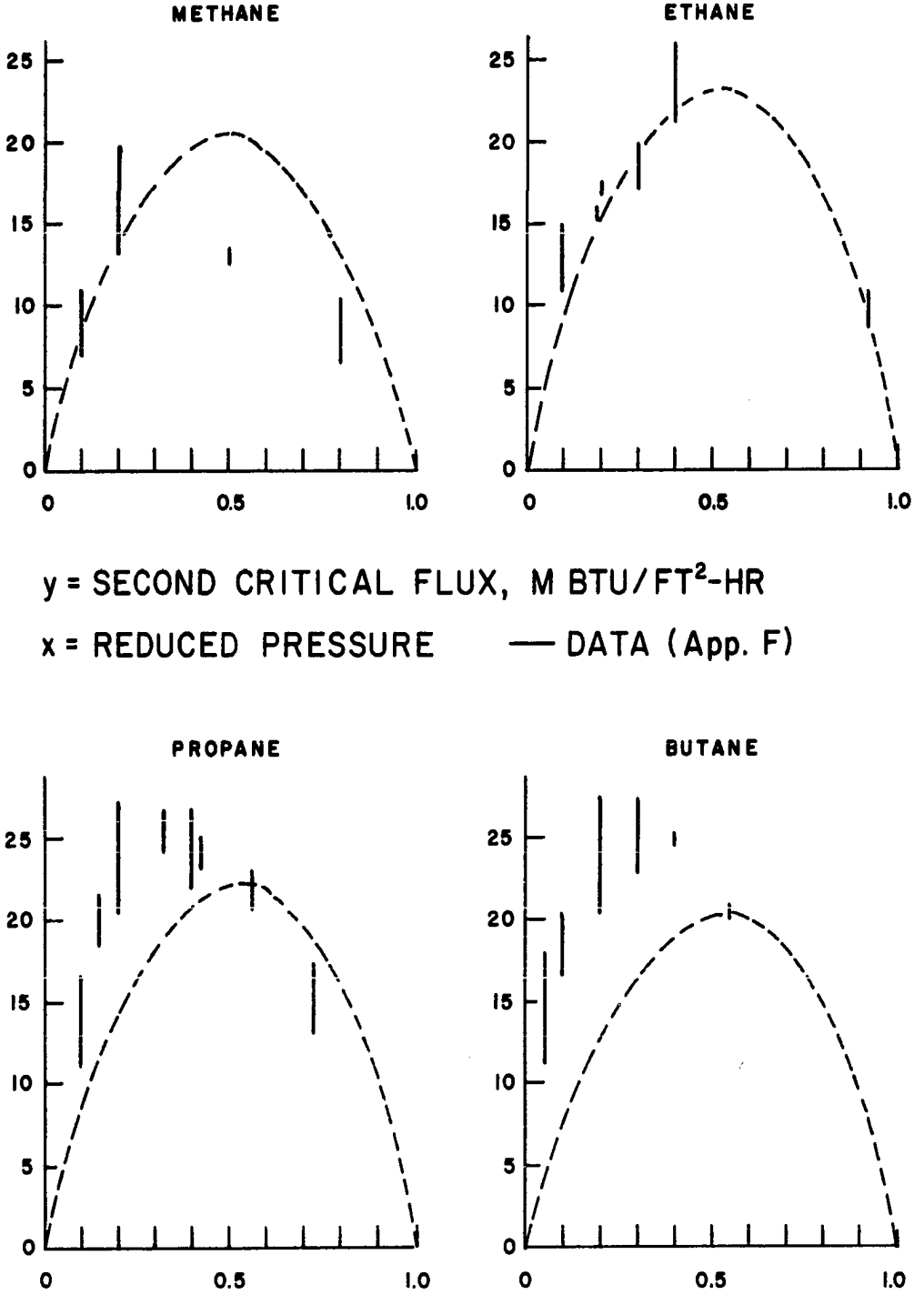

Figure 30. Second Critical Flux Compared with Equation (3-22)

CHAPTER VIII

CONCLUSIONS

1. Nucleate and film saturated pool boiling data were taken for methane, ethane, propane and n-butane at twelve reduced pressures between 0.02 (one atmosphere) and 0.9.

2. Complete burnout flux vs. reduced pressure curves were obtained for each substance. The equation of Noyes [62], equation (2-21), was found to describe these data with reasonable accuracy over the entire pressure range.

3. An empirical modification of the equation of Chang [20] and of Berenson [5] (equation (7-1)) was developed which accurately represented all of the film boiling data.

4. The nucleate boiling data were correlated using a modification (equation (7-2)) of the Rohsenow [75] equation. The propane, butane and methane data were described adequately, particularly for reduced pressures less than 0.7. The ethane nucleate boiling data were not satisfactorily correlated by this method, possibly because the ethane was only 99% pure.

5. Some second critical ΔT's were determined and found to be less than predicted values, especially at reduced pressures above 0.4. Predictions of second critical fluxes are too high at high reduced pressures.

6. The variation in temperature around the circumference of the heater is small and random, although usually consistent within one run.

CHAPTER IX

RECOMMENDATIONS FOR FUTURE WORK

1. Retain the basic heater design, as outlined in Chapter IV, with the following changes:

a. Eliminate the end loss measurements. As shown in Appendix B, they are unnecessary, since the ΔT's near the center of the heater are unaffected by end losses.

b. Eliminate the inner thermocouple ring. The check on flux provided by these measurements was not as reliable as the electrical measurements, as explained in Appendix J.

c. Make the heater body of copper rather than iron. Eliminating the inner ring of thermocouples obviates the need for the large temperature drop given by the iron. The greater thermal conductivity of copper would greatly improve the corrections and extrapolations of temperatures to the surface of the heater. In connection with this, the thermocouple pins should be moved closer to the surface, if possible.

d. Use twelve outer ring thermocouple pins instead of six. The elimination of end loss measurements and inner ring measurements frees seven thermocouples. Six of these should be used to get additional surface temperature measurements.

e. Mount an "inner ring" thermocouple to use only as a burnout monitor. This would use the other thermocouple mentioned in "d" above, making the total number of measured heater temperatures 13, as was done in this study.

f. Make six of the outer ring thermocouples read $\Delta T = T_w - T_{fluid}$ directly. This can be accomplished by locating one reference junction inside the vessel, connected to the thermocouples through a switch. Whether to measure T_w or $\Delta T = (T_w - T_{fluid})$ is an interesting problem, apparently best solved by doing some of each. Measuring ΔT directly is more accurate: since the ΔT's are small, the measuring instrument will give more consistent results (accuracy of a digital voltmeter is $\pm$ 1 digit plus a small percentage of the reading). However, measuring T_w is more reliable because only the sensor is inside the pressure system out of sight, instead of both the sensor and the reference junction. Knowing the pool is really saturated becomes very important if ΔT's are measured directly.

2. Use a digital voltmeter accurate to $\pm$ 1 microvolt instead of the $\pm$ 10 microvolt voltmeter used in this work. Measurement of nucleate boiling ΔT's at high pressures requires that temperatures be measured to at least $\pm$ 0.1 degree.

3. General nature of the investigation:

a. Investigate the boiling of azeotropic mixtures. Since the vapor and liquid are presumably of the same composition, an important factor can be held constant.

b. Investigate the effect of pressure on the second

critical (minimum film boiling) flux and ΔT, using the technique described in Chapter VI.

c. Recheck the nucleate boiling data for ethane, which did not seem to match that of the other substances, and study ethane-ethylene mixture boiling. Ethane and ethylene are similar in behavior, industrially important, and are particularly easy to work with in this apparatus. (It is desirable to have a cryogenic fluid whose critical temperature is above room temperature, so the system can be left filled.)

critical (minimum film boiling) flux and ΔT, using the technique described in Chapter VI.

c. Recheck the nucleate boiling data for ethane, which did not seem to match that of the other substances, and study ethane-ethylene mixture boiling. Ethane and ethylene are similar in behavior, industrially important, and are particularly easy to work with in this apparatus. (It is desirable to have a cryogenic fluid whose critical temperature is above room temperature, so the system can be left filled.)

NOMENCLATURE

Temperatures and Pressures

P	pressure, psia
P_c	critical pressure, psia
Pr	reduced pressure P/P_c, dimensionless
P_{sat}	saturation pressure, psia
ΔP	defined by (2-9), psia
T	temperature, °F (degrees Fahrenheit)
T_c	critical temperature, °F
T_f	film temperature, $\frac{1}{2}(T_w + T_{sat})$, °F
Tr	reduced temperature, $(T + 459.6)/(T_c + 459.6)$, dimensionless
T_{sat}	saturation temperature, °F
T_w	temperature of metal surface on which boiling occurs, °F
T^*	observed temperature (in equation where the correct temperature T is unknown), °F
T_∞	bulk fluid temperature, °F
ΔT	$(T_w - T_{sat})$, F°
ΔT_{2c}	$(T_w - T_{sat})$ at the second critical (minimum film boiling point), F°

Fluid Properties

C_p	heat capacity at constant pressure, Btu/lb_m-F°
k	thermal conductivity, Btu/ft-hr-F°

α thermal diffusivity, $k/\rho C_p$, ft^2/hr

λ heat of vaporization, Btu/lb_m

λ' modified heat of vaporization: see (3-3), (3-4) and (3-5)

μ viscosity, $lb_m/ft\text{-}hr$

ν kinematic viscosity, μ/ρ, ft^2/hr

ρ density, lb_m/ft^3

σ surface tension, lb_f/ft

Subscripts Used with Fluid Properties

f vapor property evaluated at the film temperature $\frac{1}{2}(T_w + T_{sat})$

ℓ saturated liquid property

v saturated vapor property

w evaluated at the metal surface temperature T_w

∞ evaluated at the bulk fluid temperature

Miscellaneous Quantities

a inner cylinder radius, feet, (4-7)ff.; also acceleration, ft/hr^2

b outer cylinder radius, feet, (4-7)ff.

c_i constants

f frequency of bubble departure from an active site

g acceleration of gravity, 4.17×10^8 ft/hr^2

g_c unit conversion factor, 4.17×10^8 $lb_m\text{-}ft/lb_f\text{-}hr^2$

h heat transfer coefficient, $q/\Delta T$, $Btu/ft^2\text{-}hr\text{-}F^\circ$

h_b boiling h defined by (1-1)

h_r radiative contribution to film boiling h (3-19)

h' convective contribution to film boiling h (3-20)

h_ℓ height of liquid in system (6-1)

h_ℓ° initial h_ℓ (6-1)

k thermal conductivity, Btu/ft-hr-F°

k_m thermal conductivity of metal

m_i constants

q heat flux, Btu/ft^2-hr

q_r radiative contribution to film boiling q

q' convective contribution to film boiling q

q_c critical flux, Btu/ft^2-hr

q_{1c} first critical (burnout) flux

q_{2c} second critical (minimum film boiling) flux

q'_{2c} second critical flux without radiative component

r radius, ft

r^* "observed" radius in equations where the "correct" radius r is the thermocouple radius shown in Figure 4

t thickness of metal, ft

B Laplace reference length, ft, (2-6)

D (1) bubble diameter, ft, at departure; or
(2) heater diameter, ft

E modulus of elasticity, psi

F quantity defined by (3-1)

G^* characteristic mass velocity, lb$_m$/ft^2-hr

H height of system, ft, if all volume has 5" diameter, (6-1)

K constant in (2-13)

L heater length, feet

L^* characteristic length, ft

M molecular weight

N	population of active nucleation sites, sites/ft
N_o	constant in (2-13)
Nu^*	Nusselt Number, $qB/k_f\Delta T$ in film boiling, dimensionless
Pr^*	Prandtl Number, $\mu C_p/k$, dimensionless
$\dot{Q}$	heat flow, Btu/hr
Ra^*	Rayleigh Number, $B^3 g\rho_f(\rho_\ell - \rho_f)C_{pf}/\mu_f k_f$ in film boiling, dimensionless
Re^*	Reynolds Number, $qB/\lambda C_{p\ell}$ in nucleate boiling, dimensionless
$\mathfrak{L}$	quantity defined by (2-19), Btu/ft^2-hr
α	constant in (4-1) if not a fluid property
β	constant in (4-1)
γ	$2\beta/\alpha$, (4-4)ff.
ϵ	emissivity of metal surface
ν	Poisson's ratio
ξ	quantity defined in (2-15)
σ^*	Stephan-Boltzmann constant, 0.1713×10^{-8} Btu/ft^2-hr-F$^{\circ 4}$
σ_r	radial stress (4-7)
σ_y	yield strength in simple tension, psi
σ_θ	tangential stress (4-8)
τ	shearing stress
τ_{max}	maximum shearing stress, design limitation defined by (4-15)
φ	(1) parachor (2-16), (2) quantity in (4-5)ff.
Γ_c	critical wavelength, ft, (3-7)
Γ_D	most dangerous wavelength, $\sqrt{3}\,\Gamma_c$
θ	$\lambda/C_{p\ell}\Delta T$, used in nucleate boiling, dimensionless
θ'	$(\lambda + 0.5C_{pf}\Delta T)/C_{pf}\Delta T$, used in film boiling, dimensionless

LITERATURE CITED

1. Addoms, J. N. "Heat Transfer at High Rates to Water Boiling Outside Cylinders." Sc.D. Thesis in Chemical Engineering, Massachusetts Institute of Technology, 1948.

2. Banchero, J. T., G. E. Barker and R. H. Boll. "Stable Film Boiling of Liquid Oxygen Outside Single Horizontal Tubes and Wires." Chemical Engineering Progress Symposium Series, 51, No. 17 (1955), 21.

3. Bankoff, S. G. "A Note on Latent Heat Transport in Nucleate Boiling." A.I.Ch.E. Journal, 8, No. 1 (March, 1962), 63.

4. Berenson, P. J. "Experiments on Pool Boiling Heat Transfer." International Journal of Heat and Mass Transfer, 5, No. 8 (October, 1962), 985.

5. Berenson, P. J. "Film Boiling Heat Transfer from a Horizontal Surface." Journal of Heat Transfer, 83, No. 3 (August, 1961), 351.

6. Berenson, P. J. "Transition Boiling Heat Transfer from a Horizontal Surface." Massachusetts Institute of Technology Heat Transfer Laboratory Technical Report No. 17 (March, 1960).

7. Bonilla, Charles F. and Leon A. Sigel. "High-Intensity Natural-Convection Heat Transfer near the Critical Point." Chemical Engineering Progress Symposium Series, 57, No. 32 (1961), 87.

8. Borishanskii, V. M. "An Equation Generalizing Experimental Data on the Cessation of Bubble Boiling in a Large Volume of Liquid." Zhurnal Teknicheski Fiziki, 25 (1956), 252. See also: Soviet Physics--Technical Physics, 1, American Institute of Physics, New York, p. 438.

9. Bragg, S. L. and I. E. Smith. "Dimensional Analysis of Burnout Heat Transfer." International Journal of Heat and Mass Transfer, 3, No. 3 (1961), 252.

10. Breen, B. P. and J. W. Westwater. "Effect of Diameter of Horizontal Tubes on Film Boiling Heat Transfer." Chemical Engineering Progress, 58, No. 7 (July, 1962), 67.

11. Brentari, E. G., P. J. Giarratano, and R. V. Smith. "Boiling Heat Transfer for Oxygen, Nitrogen, Hydrogen, and Helium," National Bureau of Standards Technical Note No. 317 (September, 1965).

12. Brentari, E. G. and R. V. Smith. "Nucleate and Film Pool Boiling Design Correlations for O_2, N_2, H_2 and He." International Advances in Cryogenic Engineering. Vol. 10, p. 325. New York: Plenum Press, 1965.

13. Bromley, L. A. "Heat Transfer in Stable Film Boiling." Chemical Engineering Progress, 46, No. 5 (May, 1950), 221.

14. Bromley, L. A., R. S. Brodkey and N. Fishman. "Effect of Heat Capacity of Condensate." Industrial and Engineering Chemistry, 44 (1952), 2966. See also: Vol. 45 (1953), p. 2639.

15. Carne, M. "Some Effects of Test Section Geometry in Saturated Pool Boiling on the Critical Heat Flux for Some Organic Fluids and Liquid Mixtures." Paper presented at the Seventh National Heat Transfer Conference, Cleveland, Ohio (August, 1964).

16. Carne, M. "The Critical Heat Flux--Its Inherent Uncertainty and Variation with Surface Conditions." Paper presented at the Fifty-Seventh National Meeting of the American Institute of Chemical Engineers, Boston, Massachusetts (December, 1964).

17. Carne, M. and D. H. Charlesworth. "Thermal Conduction Effects on the Critical Heat Flux in Pool Boiling." Paper presented at the Eighth National Heat Transfer Conference, Los Angeles, California (August, 1965).

18. Caswell, B. F. and R. E. Balzhiser. "The Critical Heat Flux for Boiling Liquid Metal Systems." Paper presented at the Eighth National Heat Transfer Conference, Los Angeles, California (August, 1965).

19. Chang, Y. P. "Some Possible Critical Conditions in Nucleate Boiling." Journal of Heat Transfer, 85, No. 2 (May, 1963), 89.

20. Chang, Y. P. "Wave Theory of Heat Transfer in Film Boiling." Journal of Heat Transfer, 81, No. 1 (February, 1959), 1.

21. Chang, Y. P. and N. W. Snyder. "Heat Transfer in Saturated Boiling." Chemical Engineering Progress Symposium Series, 56, No. 30 (1960), 25.

22. Cichelli, M. T. and C. F. Bonilla. "Heat Transfer to Liquids Boiling under Pressure." Transactions of the American Institute of Chemical Engineers, 41 (1945), 755.

23. Farber, E. A. and R. L. Scorah. "Heat Transfer to Water Boiling under Pressure." Transactions of the American Society of Mechanical Engineers, 70 (May, 1948), 369.

24. Forster, K. and R. Greif. "Heat Transfer to a Boiling Liquid--Mechanism and Correlations." Journal of Heat Transfer, 81, No. 1 (February, 1959), 43.

25. Frederking, T. H. K., Y. C. Wu, and B. W. Clement. "Effects of Interfacial Instability on Film Boiling of Saturated Liquid Helium I above a Horizontal Surface," A.I.Ch.E. Journal, 12, No. 2 (March, 1966), 238.

26. Fritsch, C. A. and R. J. Grosh. "Free Convective Heat Transfer to Supercritical Water Experimental Measurements." Journal of Heat Transfer, 85, No. 4 (November, 1963), 289.

27. Gaertner, R. F. "Distribution of Active Sites in the Nucleate Boiling of Liquids." Chemical Engineering Progress Symposium Series, 59, No. 41 (1963), 52.

28. Gaertner, R. F. and J. W. Westwater. Chemical Engineering Progress Symposium Series, 56, No. 30 (1960), 39.

29. Gaertner, R. F. and J. W. Westwater. "Novel Method for Determining Nucleate Boiling Sites." Chemical Engineering Progress, 55, No. 10 (October, 1959), 58.

30. Gambill, Wallace. "An Experimental Investigation of the Inherent Uncertainty in Pool Boiling Critical Heat Fluxes to Saturated Water." A.I.Ch.E. Journal, 10, No. 4 (July, 1964), 502.

31. Gambill, W. R. "A Survey of Boiling Burnout," British Chemical Engineering, 8, No. 2 (February, 1963), 93.

32. Giauque, W. F., J. W. Stout, R. E. Barieau, and C. J. Eagan. "Report on Cascade Oxygen System." OSRD Report No. 491, Ser. No. 201, Div. B, National Defense Research Committee (March, 1942).

33. Goldsmith, A., T. E. Waterman and H. J. Hirschhorn. Handbook of Thermophysical Properties of Solid Materials, Vol. 1 (Elements). New York: Macmillan Company, 1961.

34. Griffith, P. "The Correlation of Nucleate Boiling Burnout Data." Paper #57-HT-21, ASME-AIChE Heat Transfer Conference, Pennsylvania (August 1957).

35. Gunther, F. C. and F. Kreith. Heat Transfer and Fluid Mechanics Institute. New York: American Society of Mechanical Engineers, May, 1949, p. 113.

36. Hirschfelder, J. O., C. F. Curtiss and R. B. Bird. Molecular Theory of Gases and Liquids. New York: John Wiley and Sons, Inc., 1954.

37. Hospeti, N. B. and R. B. Mesler. "Deposits Formed Beneath Bubbles During Nucleate Boiling of Radioactive Calcium Sulfate Solutions." Paper presented at Eighth National Heat Transfer Conference, Los Angeles, California (August, 1965).

38. Hsu, Y. Y. and J. W. Westwater. "Film Boiling from Vertical Tubes." A.I.Ch.E. Journal, 4, No. 1 (March, 1958), 58.

39. Huber, D. A. and J. C. Hoehne. "Pool Boiling of Benzene, Diphenyl, and Benzene-Diphenyl Mixtures under Pressure," Journal of Heat Transfer, 85, No. 3 (August, 1963), 215.

40. Hughmark, G. A. "A Statistical Analysis of Nucleate Pool Boiling Data." International Journal of Heat and Mass Transfer, 5, No. 5 (July, 1962), 667.

41. Jakob, Max. Heat Transfer, Vol. I. New York: John Wiley and Sons, Inc., 1949.

42. Kistemaker, T. Physica, 29 (1963), 351. (Reference from [25]).

43. Kurihara, H. M. and J. E. Myers. "The Effects of Superheat and Surface Roughness on Boiling Coefficients." A.I.Ch.E. Journal, 6, No. 1 (March, 1960), 83.

44. Lienhard, J. H. "A Semi-Rational Nucleate Boiling Heat Flux Correlation." International Journal of Heat and Mass Transfer, 6 (1963), 215.

45. Lienhard, J. H. and V. E. Schrock. "The Effect of Pressure, Geometry, and Equation of State upon the Peak and Minimum Boiling Heat Flux." Journal of Heat Transfer, 85, No. 3 (August, 1963), 261.

46. Lienhard, J. H. and K. Watanabe. "On Correlating the Peak and Minimum Boiling Heat Fluxes with Pressure and Heater Configuration." Paper presented at the Eighth National Heat Transfer Conference, Los Angeles, California (August, 1965).

47. Lienhard, J. H. and P. T. Y. Wong. "The Dominant Unstable Wavelength and Minimum Heat Flux during Film Boiling on a Horizontal Cylinder." Journal of Heat Transfer, 86, No. 2 (May, 1964), 220.

48. Lott, Jerry L. "The Selective Oxidation of Methane at High Pressures." Ph.D. Thesis, The University of Oklahoma, 1965.

49. Lyon, D. N., P. G. Kosky and B. N. Harman. "Nucleate Boiling Heat Transfer Coefficients and Peak Nucleate Boiling Fluxes for Pure Liquid Nitrogen and Oxygen on Horizontal Platinum Surfaces from below 0.5 Atmosphere to the Critical Pressures." Advances in Cryogenic Engineering, Vol. 9. New York: Plenum Press, 1965, 77.

50. McAdams, W. H. Heat Transmission, Third Ed. New York: McGraw-Hill Book Company, Inc., 1954.

51. McFadden, P. W. and P. Grassmann. "The Relation Between Bubble Frequency and Diameter During Nucleate Pool Boiling." International Journal of Heat and Mass Transfer, 5, No. 2 (March, 1962), 169.

52. Madejski, Jan. "Theory of Nucleate Pool Boiling." International Journal of Heat and Mass Transfer, 8, No. 1 (January, 1965), 155.

53. Marcus, B. D. and D. Dropkin. "The Effect of Surface Configuration on Nucleate Boiling Heat Transfer." International Journal of Heat and Mass Transfer, 6, (1963), 863.

54. Merte, H. Jr. and J. A. Clark. "Boiling Heat Transfer with Cryogenic Fluids at Standard, Fractional, and Near-Zero Gravity." Journal of Heat Transfer, 86, No. 3 (August, 1964), 351.

55. Mickley, H. S., T. K. Sherwood and C. E. Reed. Applied Mathematics in Chemical Engineering. New York: McGraw-Hill Book Company, Inc., 1957.

56. Moissis, R. and P. J. Berenson. "On the Hydrodynamic Transitions in Nucleate Boiling." Journal of Heat Transfer, 85, No. 3 (August, 1963), 221.

57. Moore, F. D. and R. B. Mesler. "The Measurement of Rapid Surface Temperature Fluctuations During Nucleate Boiling of Water." A.I.Ch.E. Journal, 7, No. 4 (December, 1961), 620.

58. Morozov, V. G. "An Experimental Investigation of the Cessation of Film Boiling of a Liquid on a Submerged Heating Surface." International Chemical Engineering, 3, No. 1 (January, 1963), 48.

59. Morozov, V. G. "An Experimental Study of Critical Heat Loads at Boiling of Organic Liquids." International Journal of Heat and Mass Transfer, 2, No. 3 (1961), 252.

60. Myers, J. E. and D. L. Katz. "Boiling Coefficients Outside Horizontal Tubes." Chemical Engineering Progress Symposium Series, 49, No. 5 (1953), 107.

61. Nishikawa, K. and K. Yamagato. "On the Correlation of Nucleate Boiling Heat Transfer." International Journal of Heat and Mass Transfer, 1 (1960), 219.

62. Noyes, R. C. "An Experimental Study of Sodium Pool Boiling Heat Transfer." Journal of Heat Transfer, 85 (May, 1963), 125.

63. Noyes, R. C. and H. Lurie. "Boiling Studies for Sodium Reactor Safety, Part II," A.E.C. R & D Report NAA-SR-9477, October 15, 1964 (Atomics International Div. of North American Aviation, Inc.)

64. Nukiyama, S. Journal of the Society of Mechanical Engineers (Japan), 37, No. 206 (June, 1934), 367. (English Abstract p. S-53).

65. Park, Efton L. Jr. "Nucleate and Film Boiling Heat Transfer to Methane and Nitrogen from Atmospheric Pressure to the Critical Pressure." Ph.D. Thesis, The University of Oklahoma, 1965.

66. Park, Efton L. Jr., C. P. Colver, and C. M. Sliepcevich. "Nucleate and Film Boiling Heat Transfer to Nitrogen and Methane at Elevated Pressures and Large Temperature Differences," Advances in Cryogenic Engineering, 11. New York: Plenum Press, (1966), 516.

67. Peebles, F. and H. Garber. "Studies on the Motion of Gas Bubbles in Liquids." Chemical Engineering Progress, 49 (1953), 88.

68. Pomerantz, M. L. "Film Boiling on a Horizontal Tube in Increased Gravity Fields." Journal of Heat Transfer, 86, No. 2 (May, 1964), 213.

69. Powell, R. W. "Armco Iron as a Thermal Conductivity Standard--Review of Published Data." Progress in International Research on Thermodynamics and Transport Properties, p. 454. New York: Academic Press, 1962.

70. Powell, R. W., M. J. Hickman, R. P. Tye, and M. J. Woodman. "Armco Iron as a Thermal Conductivity Standard--New Determinations at the National Physical Laboratory." Progress in International Research on Thermodynamics and Transport Properties, p. 466. New York: Academic Press, 1962.

71. Rallis, C. J. and H. H. Jawurek. "Latent Heat Transport in Saturated Nucleate Boiling." International Journal of Heat and Mass Transfer, 7, No. 10 (October, 1964), 1051.

72. Rallis, C. J., R. V. Greenland and A. Kok. "Stagnant Pool Nucleate Boiling from Horizontal Wires under Saturated and Sub-cooled Conditions." The South African Mechanical Engineer, 10 (January, 1961), 171.

73. Richards, R. J., W. G. Steward and R. B. Jacobs. "A Survey of the Literature on Heat Transfer from Solid Surfaces to Cryogenic Fluids." National Bureau of Standards Technical Note No. 122, October, 1961.

74. Rogers, T. F. and R. B. Mesler. "An Experimental Study of Surface Cooling by Bubbles During Nucleate Boiling of Water." A.I.Ch.E. Journal, 10, No. 5 (September, 1964), 656.

75. Rohsenow, W. M. "Heat Transfer with Boiling." Transactions of the American Society of Mechanical Engineers, 74 (1952), 969. Reprinted in Modern Developments in Heat Transfer, Warren Ibele, Editor. New York: Academic Press, 1963.

76. Rohsenow, W. M. and H. Y. Choi. Heat, Mass, and Momentum Transfer. Englewood Cliffs, New Jersey: Prentice-Hall, Inc., 1961.

77. Rohsenow, W. M. and J. A. Clark. "A Study of the Mechanism of Boiling Heat Transfer." Transactions of the American Society of Mechanical Engineers, 73 (July, 1951), 609.

78. Rohsenow, W. M. and P. Griffith. "Correlation of Maximum Heat Flux Data for Boiling of Saturated Liquids." Chemical Engineering Progress Symposium Series, 52, No. 18 (1956), 47.

79. Roll, John B. and John E. Myers. "The Effect of Surface Tension on Factors in Boiling Heat Transfer." A.I.Ch.E. Journal, 10, No. 4 (July, 1964), 530.

80. Seader, J. D., W. S. Miller and L. A. Kalvinskas. "Boiling Heat Transfer for Cryogenics." National Aeronautics and Space Administration Contractor Report NASA CR-243, Prepared under contract NAS8-5337 by Rocketdyne (June, 1965).

81. Sparrow, E. M. "The Effect of Radiation on Film-Boiling Heat Transfer." International Journal of Heat and Mass Transfer, 7, No. 2 (February, 1964), 229.

82. Spiegler, P., J. Hopenfeld, M. Silberberg, C. F. Bumpus, Jr., and A. Norman. "Onset of Stable Film Boiling and the Foam Limit." International Journal of Heat and Mass Transfer, 6 (1963), 987.

83. Tien, C. L. "A Hydrodynamic Model for Nucleate Pool Boiling." International Journal of Heat and Mass Transfer, 5, No. 4 (June, 1962), 533. Erratum: 8, No. 6 (June, 1965), 972.

84. Timoshenko, S. and J. N. Goodier. Theory of Elasticity, 2nd Ed. New York: McGraw-Hill Book Company, Inc. (1951).

85. Westwater, J. W. "Boiling of Liquids." Advances in Chemical Engineering, Vol. I. T. B. Drew and J. W. Hoopes, Jr., Editors. New York: Academic Press, Inc., 1956.

86. Westwater, J. W. "Boiling of Liquids." Advances in Chemical Engineering, Vol. II. T. B. Drew and J. W. Hoopes, Jr., Editors. New York: Academic Press, Inc., 1958.

87. Yamagata, K., F. Hirano, K. Nishikawa, and H. Matsuoka. "Nucleate Boiling of Water on a Horizontal Surface." Mem. Faculty Engineering Kyushu University, 15, No. 1 (1955), 97.

88. Zuber, N. "Hydrodynamic Aspects of Boiling Heat Transfer." Atomic Energy Commission Report No. AECU-4439, Physics and Mathematics (June, 1959), 82.

89. Zuber, N. "Nucleate Boiling. The Region of Isolated Bubbles and the Similarity with Natural Convection." International Journal of Heat and Mass Transfer, 6 (1963), 53.

90. Zuber, N. and M. Tribus. "Further Remarks on the Stability of Boiling Heat Transfer." UCLA Report No. 58-5, University of California at Los Angeles (January, 1958).

APPENDIX A

PHYSICAL AND TRANSPORT PROPERTIES OF LIGHT HYDROCARBONS

Introduction

Because of the variety of correlations available for boiling heat transfer data, it was decided to compute all physical and transport properties from equations. These were programmed for the University of Oklahoma "OSAGE" computer using the ALGOL language.

There are two advantages which accrue in addition to the resulting ease in correlating heat transfer data. The precision of the property values used is easily verified and can be refined, if necessary and if data are available, to almost any desired degree. Also, individual calculated points will be consistent with each other, the errors which invariably occur when reading graphs being eliminated.

Properties used in correlating boiling heat transfer data are: vapor pressure, density of the liquid and vapor, heat of vaporization, surface tension, liquid and vapor viscosity, liquid and vapor thermal conductivity, and liquid and vapor isobaric heat capacity. The methods used to calculate these properties are described below.

Tabular or graphical data were not used whenever a reasonable correlation could be found, because correlations were so much easier to handle. The work of Canjar and Manning [31], Din et al. [7] and Jones et al. [15] were bypassed for this reason. Also, information which was published after the programs were checked out and had been used was not incorporated because of the difficulty of putting earlier calculations on the same basis. For example,

Carmichael, Reamer and Sage [32] published data on thermal conductivity of methane in January 1966 which would undoubtedly have been used had it been published six months earlier.

Tables summarizing these calculated properties of methane, ethane, propane, and n-butane along with some common groups are presented.

References, in brackets, are to the list at the end of this appendix. When reported, average deviations are listed. The reader is referred to the article for the maximum deviations and other relevant information.

Vapor Pressure

It is possible to calculate vapor pressures by trial and error from an equation of state. For liquefied hydrocarbon gases, however, a very accurate empirical equation has been presented by Thodos [30]:

$$\log P_s = A + B/T + C/T^2 + D(T/T_d - 1)^n \qquad (A\text{-}1)$$

P_s is the vapor pressure in mm Hg, and T is temperature in degrees K. The last term is applied only if (T/T_d) is greater than unity. Thodos obtained the constants listed in Table A-1.

Thodos reports average deviations covering the range from the triple point to the critical point of only 0.15%, 0.08%, 0.10%, and 0.17%, respectively.

The method of Thodos was used in this work. A

four-constant equation for vapor pressures which would be easier to use in hand calculations is presented by Frost and Kalkwarf [12]. The average deviations of their equation are roughly three times those of Thodos, but are still less than 0.5%.

TABLE A-1

CONSTANTS USED IN VAPOR PRESSURE EQUATION OF THODOS

Substance	T_d	A	B	C	D	n
Methane	118.83	6.18025	-296.1	-8000	0.257	1.32
Ethane	204.74	6.73244	-624.24	-15912	0.1842	1.963
Propane	261.20	6.80064	-785.6	-27800	0.2102	2.236
n-Butane	312.30	6.78880	-902.4	-44493	0.4008	2.40

Density of Saturated Liquid

It is also possible to get the saturated liquid density from an equation of state, but an equation presented by Francis [11] enables calculation of ρ_l over the entire range up to the critical point with an average deviation of about 5×10^{-4}. Francis used one of two equations, depending on proximity to the critical temperature.

$$\rho_l = A - Bt - C/(E - t) \qquad \text{(A-2)}$$

$$\rho_l = \rho_c + [G(t_c - t)]^{1/h} \qquad \text{(A-3)}$$

where t is temperature in degrees C and the density is in

gm/ml. Equation (A-3) is to be used near the critical temperature t_c, and equation (A-2) applies at lower temperatures. The regions in which each equation applies actually overlap considerably, and for the purpose of these calculations an arbitrary dividing point was selected halfway between the upper recommended temperature for (A-2) and the lower value for (A-3). The constants presented by Francis are listed in Table A-2.

TABLE A-2

CONSTANTS USED IN LIQUID DENSITY EQUATION OF FRANCIS

Substance	A	B	C	E	h	G	ρ_c	Break*
Methane	0.3254	0.00094	6	-48	2.5	0.000437	0.162	-115
Ethane	0.4990	0.00099	6	66	2.8	0.000384	0.203	-15
Propane	0.5750	0.00097	6	129	2.7	0.000397	0.220	67
n-Butane	0.6376	0.00087	7	186	2.7	0.000390	0.228	132

*"Break" is the temperature in degrees C below which Equation (A-2) is used and at or above which equation (A-3) is used.

Liquid density values obtained by this method are better than those calculated from the Benedict-Webb-Rubin equation of state [1,2]. For example, Table A-3 compares values for methane calculated by the two methods with the data of Matthews and Hurd as presented by Perry [23].

Surface Tension

Brock and Bird [3] present two predictions for

TABLE A-3

COMPARISON OF CALCULATED METHANE LIQUID DENSITY WITH EXPERIMENTAL DATA

Temperature, °F	Density ρ_ℓ, lb_m/ft^3		
	Calculated		Experimental
	Francis	BWR	
-260	26.55	26.52	26.55
-200	23.25	22.68	23.22
-160	20.29	19.69	20.23
-120	14.09	13.62	14.37

surface tension based on corresponding states theory. The equation which best represents light hydrocarbons is:

$$\sigma^o = P_c^{2/3} T_c^{1/3} \left(-0.951 + \frac{0.432}{Z_c}\right)(1 - T_r)^{11/9} \qquad (A\text{-}4)$$

where P_c is the critical pressure in atmospheres, T_c is the critical temperature in degrees K, Z_c is the critical compressibility factor, and T_r is the reduced temperature. Figure A1 compares Equation (A-4) with data presented by Rossini et al. [25]. It can be seen that the correlation is improved slightly by rotating the curves. This was done by using a small correction factor ε with the equation

$$\sigma = \varepsilon\sigma^o$$

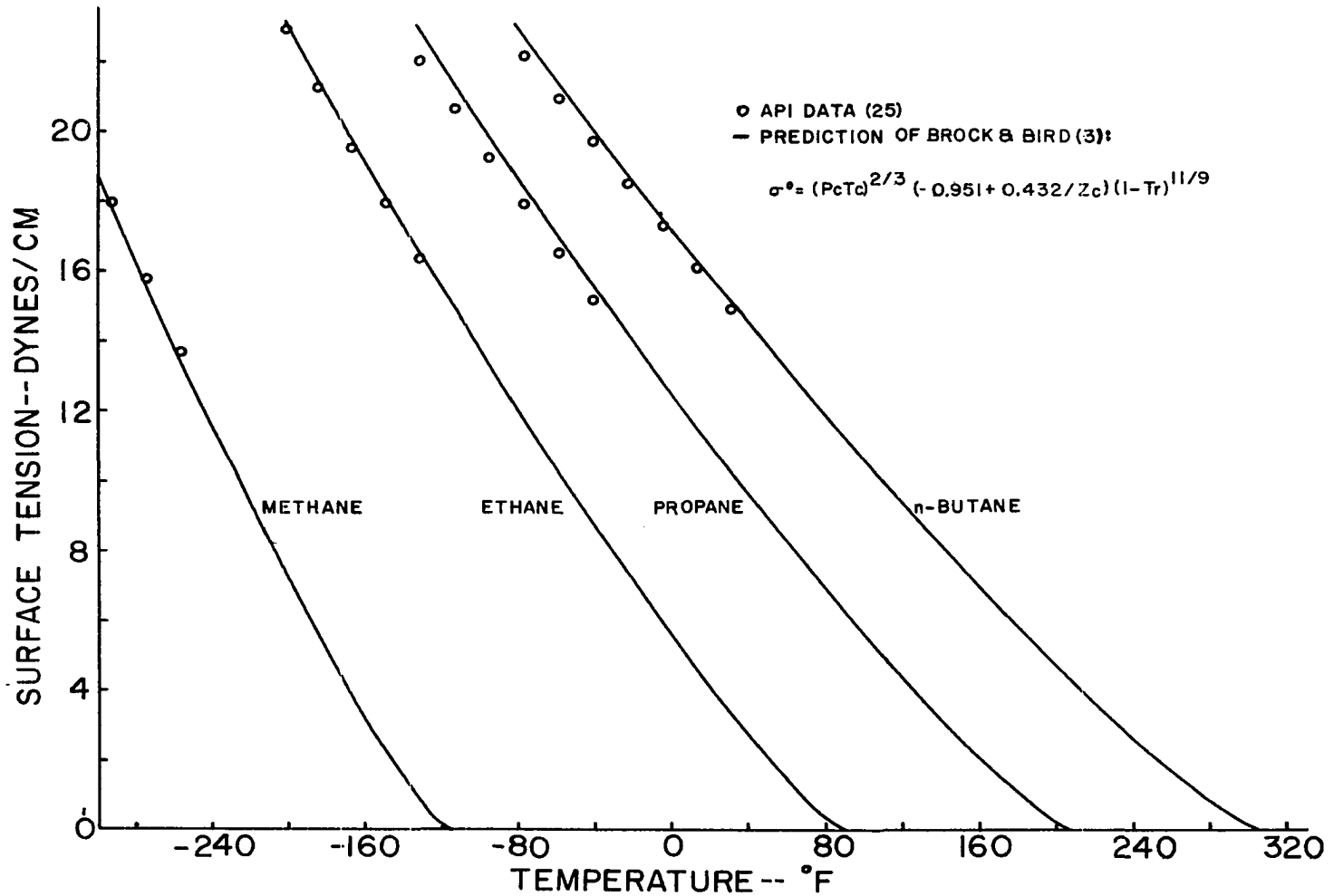

Figure A1
Surface Tension of Saturated Hydrocarbons

The values of ϵ were 1.015, 0.990, 0.971 and 0.978 for methane through butane respectively.

Although the surface tension values calculated by equation (A-5) represent an extrapolation of data taken below one atmosphere pressure, they correspond with the curves presented by Katz et al. [16] which contain some additional data for ethane and propane.

Heat Capacity at Constant Pressure of Saturated Liquid

The heat capacity C_p can be calculated from an equation of state, but values calculated from the Benedict-Webb-Rubin equation for the saturated liquid were found to deviate greatly from data. The data presented in Appendix A of the Pratt and Whitney progress report [24] were fitted by a series of equations, each applying in a limited temperature range. The curve on methane is in reasonable agreement with the experimental data presented by Jones, Mage, Faulkner and Katz [15].

Thermal Conductivity of Saturated Liquid

The residual methods used to correlate vapor and film thermal conductivity were unsatisfactory for high densities. Data from Appendix A of the Pratt and Whitney progress report [24] were fitted in the same way as those for $(C_p)_\ell$.

Viscosity

There are two methods of calculating viscosity which have received attention recently. Carmichael, Berry and

Sage [6] advocate plotting the "residual viscosity" ($\mu - \mu^\circ$) vs. density and fitting this to a cubic polynomial, then obtaining the viscosity at attenuation μ° as a cubic polynomial in temperature. They furnish the necessary constants for ethane, propane and n-butane.

Lee, Starling, Dolan and Ellington [18], and earlier Starling and Ellington [28], use a different approach. They found that the viscosity (in millipoise) of all four of the light hydrocarbons being considered could be represented as a function of molecular weight M, temperature T (degrees R), and density ρ (grams/cc) by Equations (A-6) through (A-9).

$$\mu = K(T,M) \cdot \exp\left[\chi(T,M) \cdot \rho^{Y(T,M)}\right] \qquad \text{(A-6)}$$

$$K(T,M) = \frac{(7.77 + 0.0063M)T^{3/2}}{(122.4 + 12.9M) + T} \qquad \text{(A-7)}$$

$$\chi(T,M) = 2.57 + \frac{1914.5}{T} + 0.0095M \qquad \text{(A-8)}$$

$$Y(T,M) = 1.11 + 0.04\chi(T,M) \qquad \text{(A-9)}$$

It will be noted that (A-7) is a form of the Sutherland equation. The authors report a standard deviation of 1.34% over the entire range for the pure components.

The liquid viscosities calculated from these equations are compared in Figure A2 with the data of Swift, Lorenz and Kurata [29] and Rossini *et al.* [25]. The densities used were calculated from the equation of Francis as explained above. Agreement was good for propane and n-butane, but poor for

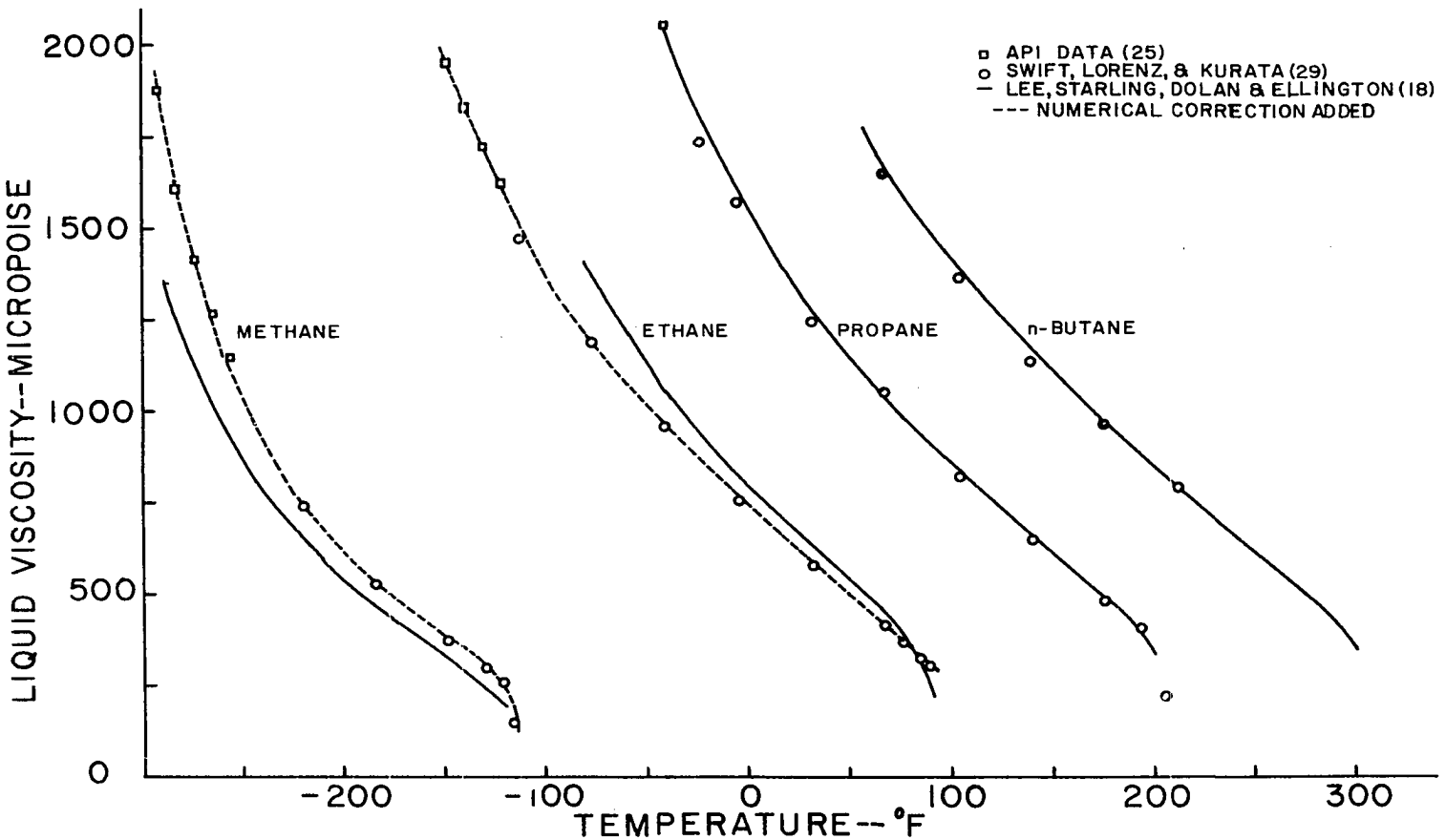

Figure A2
Viscosity of Saturated Liquid Hydrocarbons

methane and ethane. In order to bring the calculated viscosity to within acceptable range of the available data, a correction factor $\Delta\mu$ was added to the value calculated from equation (A-6). The corrected values are also plotted in Figure A2. The corrections used were:

Methane

$$\Delta\mu = 330\left(\frac{-t}{280}\right)^{6.31} \qquad t < -225°F$$

$$\Delta\mu = -0.3125t + 9.375 \qquad -225°F \leq t < -121°F$$

Ethane

$$\Delta\mu = 3.74t + 93.75 \qquad t < -50°F$$

$$\Delta\mu = 0.72t - 57.6 \qquad -50°F \leq t < 80°F$$

Equations (A-6) through (A-9) were satisfactory for viscosity of the saturated vapor and vapor film, although the saturated vapor viscosity of propane predicted by this method was about 10% lower than indicated by the curve presented by Katz *et al.* [16]. The method of Lee *et al.* is used in this work.

A number of papers present viscosity data for these substances. Particularly valuable are those by Swift, Lorenz and Kurata [29], Carmichael, Berry and Sage [6], Carmichael and Sage [4], Eakin, Starling, Dolan and Ellington [10,8], and Starling, Eakin and Ellington [27]. The method of Lee *et al.* was selected because of convenience and because it

can be readily extended to mixtures if desired.

Density of Saturated Vapor and Vapor Film

Equations of state usually describe the vapor state more accurately than that of the liquid. The eight-constant equation of Benedict, Webb and Rubin [1,2] was used in this work:

$$P = RT\rho + (B_oRT - A_o - \frac{C_o}{T^2})\rho^2 + (bRT - a)\rho^3 + a\alpha\rho^6 + \frac{c\rho^3}{T^2}(1 + \gamma\rho^2)e^{-\gamma\rho^2} \qquad \text{(A-10)}$$

Figure A3 illustrates three isotherms generated by the BWR equation for propane. Because the isotherms are continuous throughout the range shown, there are three points on each isotherm which correspond to the correct vapor pressure. The smallest density among the three corresponds to the saturated vapor and the largest to the saturated liquid. The other point has no physical significance. The problem when using the computer to generate saturated vapor densities is to always select the correct solution, preferably without first having to find all three.

Ordinarily, when working with the BWR equation, one generates the vapor pressure curve by finding two densities such that

$$P(\rho_1,T) = P(\rho_2,T) \qquad \text{(A-11)}$$

and

$$RT \ln f_1 = RT \ln f_2 \qquad \text{(A-12)}$$

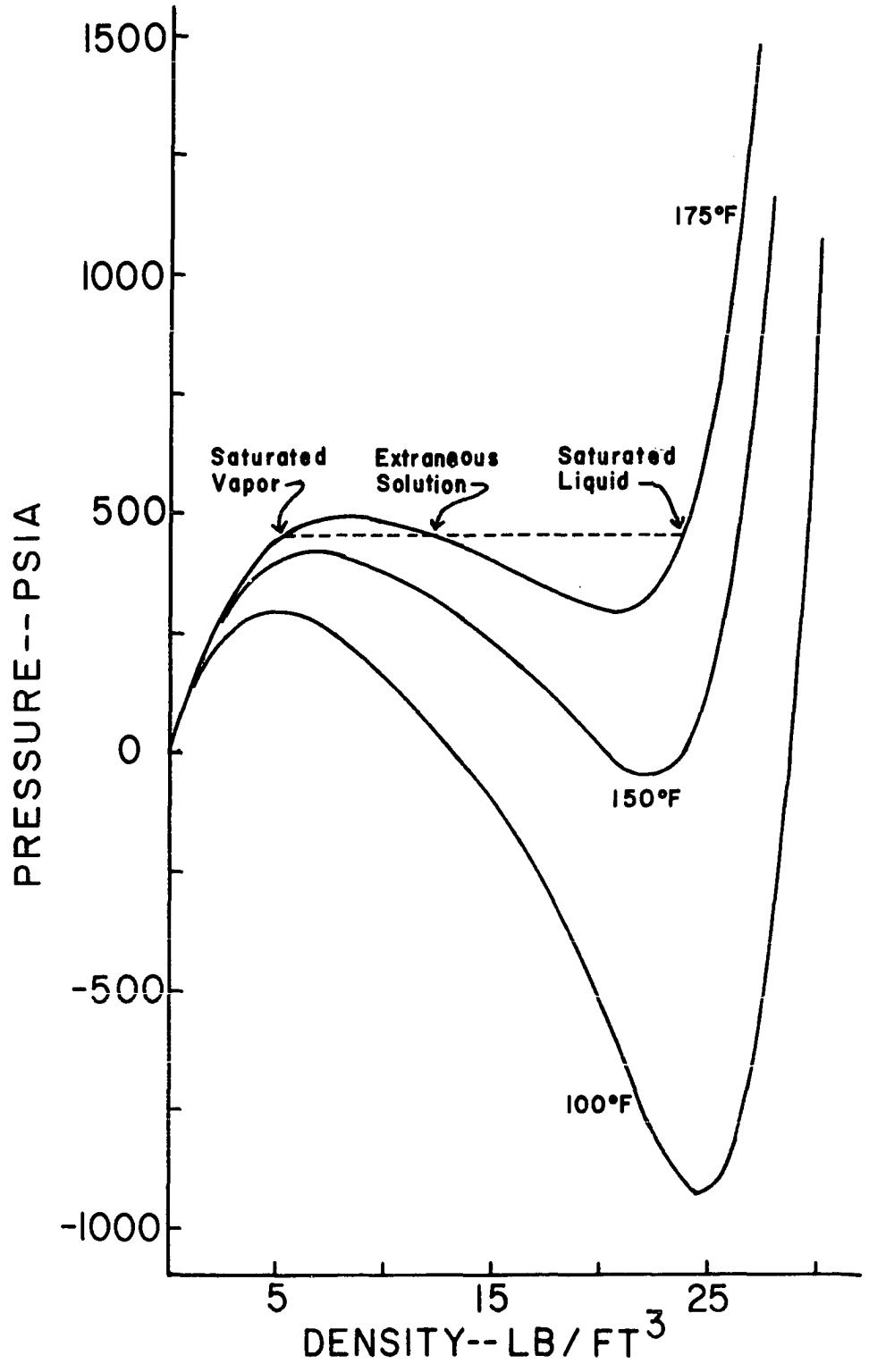

Figure A3
Isotherms for Propane at 100°F, 150°F and 175°F Calculated from the Benedict-Webb-Rubin Equation of State

where f is the fugacity. When both (A-11) and (A-12) are satisfied, ρ_1 and ρ_2 are the saturation densities at the given P and T. The equation for (RT ln f), using the BWR equation of state, is

$$(RT \ln f) = [RT \ln (\rho RT)] + 2(B_o RT - A_o - \frac{C_o}{T^2})\rho + \frac{3}{2}(bRT - a)\rho^2$$

$$+ \frac{6}{5} a\alpha\rho^5 + \frac{c\rho^2}{T^2}\left[\frac{(1 - e^{-\gamma\rho^2})}{\gamma\rho^2} + \frac{1}{2} e^{-\gamma\rho^2} + \gamma\rho^2 e^{-\gamma\rho^2}\right] \quad \text{(A-13)}$$

The equations of Thodos and Francis described above describe the vapor pressure and saturated liquid density more accurately than the BWR equation, so a slightly different procedure was used.

The vapor pressure is assumed to be known exactly. The known liquid density is used as the first estimate in the determination of the BWR liquid density. This trial and error calculation converges rapidly because of the good initial value and because the isotherm is very steep in the liquid region. The initial estimate for calculating saturated vapor density was taken to be that of the ideal gas under the same conditions.

At first, the values of (RT ln f) calculated at each point were compared to insure that the correct roots had been located. However, it turned out that the correct values were always located by this procedure except very near the critical point so the fugacity comparison was eliminated.

The only exceptions to this procedure were made near

the critical pressure for methane and propane. The BWR equation overestimates the critical pressure of methane by 22 psi and that of propane by 6 psi [22]. Almost all of the error occurs within a few degrees of the critical temperature, however, because of the large $(\partial P/\partial T)$. Accordingly, the vapor pressure used in the BWR calculations for methane above -125°F was raised by the quantity 2.0(125 + T) and that of propane above 203°F was raised (6.2/3.26)(206.26 - T), with temperature in degrees F. The corrections were checked by plotting the pressure vs. density isotherms in the critical region.

Accuracy was very good for vapor density. Figure A4 compares calculated and experimental values for n-butane. The constants used are listed in Table A-4; they are those originally published by Benedict et al. [2]. Opfell, Schlinger and Sage [22] point out that the BWR equation is not suitable for extrapolation and must be used in the range for which the constants were fitted. They comment that Benedict's constants fit the saturation region quite well. They present constants which can be used for the homogeneous fluid from 100-460°F and up to 10,000 psi. Douslin et al. [9] present data for methane in the high temperature and pressure range.

The BWR equation was used to evaluate the density of both the saturated vapor and the vapor film.

Heat of Vaporization

The function $(H - H^\circ)$ can be derived from an equation

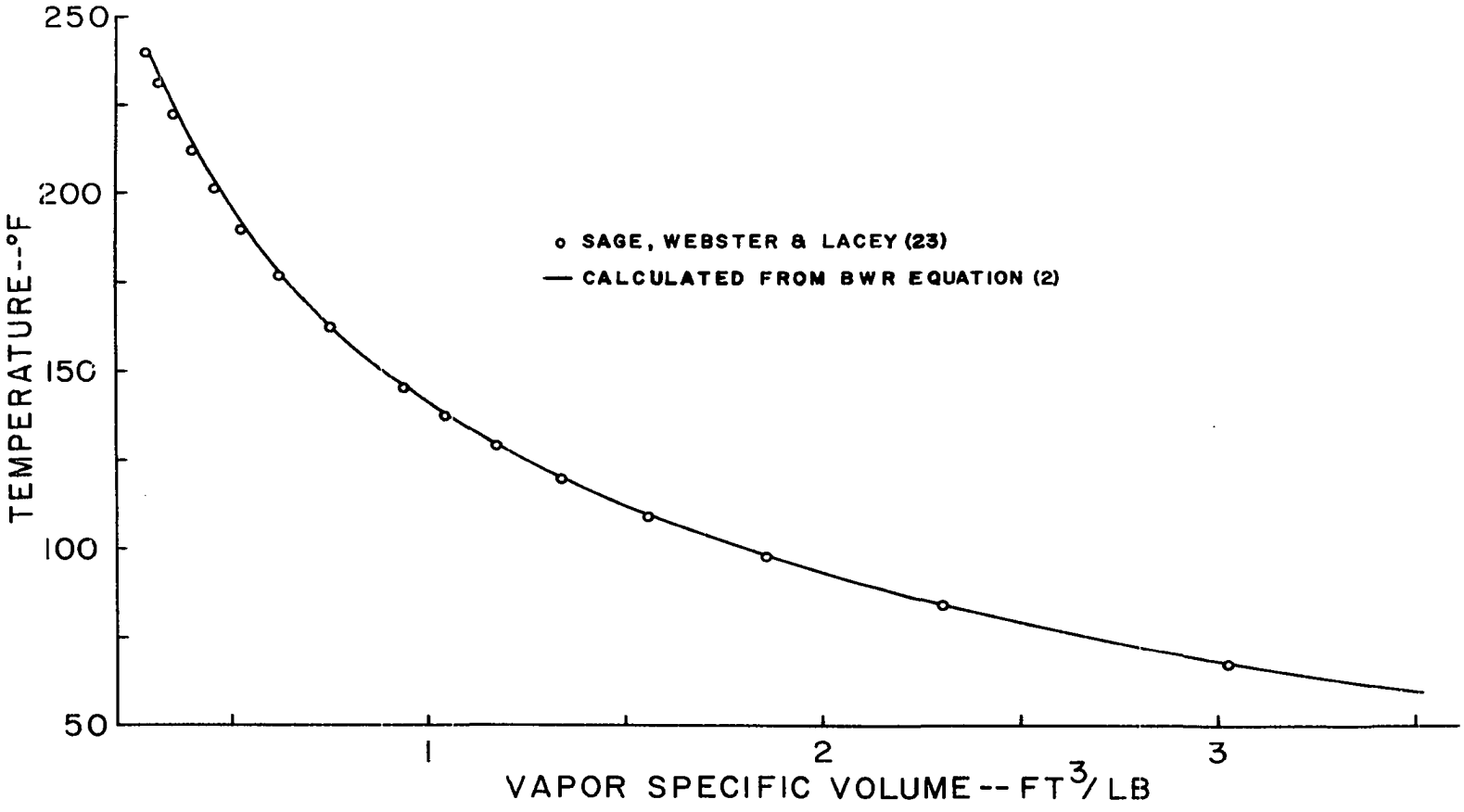

Figure A4
Specific Volume of Saturated n-Butane Vapor Calculated from the Benedict-Webb-Rubin Equation of State

TABLE A-4

CONSTANTS FOR THE BENEDICT-WEBB-RUBIN EQUATION OF STATE*

Constant	Methane	Ethane	Propane	n-Butane
R	10.7335	10.7335	10.7335	10.7335
Molecular Wt	16.031	30.047	44.062	58.078
B_o	0.682401	1.00554	1.55884	1.99211
A_o	6995.25	15670.7	25915.4	38029.6
$C_o \times 10^{-6}$	275.763	2194.27	6209.93	12130.5
b	0.867325	2.85393	5.77355	10.2636
a	2984.12	20850.2	57248.0	113705.0
$c \times 10^{-6}$	498.106	6413.14	25247.8	61925.6
α	0.511172	1.00044	2.49577	4.52693
γ	1.53961	3.02790	5.64524	8.72447

*Constants are from Reference [2].
Temperature is T(°F) + 459.63.
Pressure is in psia.
Density is in lb-mole per cubic foot.

of state. For the BWR equation, it is given by the expression

$$(H - H^\circ) = \left(B_oRT - 2A_o - \frac{4C_o}{T^2}\right)\rho + \frac{1}{2}(2bRT - 3a)\rho^2 + \frac{6}{5}a\alpha\rho^5$$

$$+ \frac{c\rho^2}{T^2}\left[\frac{3(1 - e^{-\gamma\rho^2})}{\gamma\rho^2} - \frac{1}{2}e^{-\gamma\rho^2} + \gamma\rho^2 e^{-\gamma\rho^2}\right] \qquad \text{(A-14)}$$

The units, using constants from Table A-3, are (psia · ft^3 per lb-mole) so that a conversion factor is also required. Then the heat of vaporization is found from the values

$(H - H^\circ)$ for the saturated liquid and vapor.

$$\lambda_{BWR} = (H - H^\circ)_v - (H - H^\circ)_\ell \qquad \text{(A-15)}$$

Following the suggestion of Benedict, the BWR value of ρ_ℓ was used in equation (A-8) and not that found from the Francis equation.

Values obtained in this manner were not in very good agreement with experimental data, especially at low temperatures, so first-order corrections were applied. The corrections brought the values of λ within 1% of those quoted by Perry [23]. The corrections applied are shown in Table A-5.

Heat Capacity at Constant Pressure of the Vapor and Vapor Film

The heat capacity at constant pressure, defined by the equation

$$C_p \equiv \left(\frac{\partial H}{\partial T} \right)_P \qquad \text{(A-16)}$$

can be obtained from an equation of state by evaluating the integral

$$C_p - C_p^* = \int_o^P -T \left(\frac{\partial^2 V}{\partial T^2} \right) dP \qquad \text{(A-17)}$$

An alternate procedure is available. Equation (A-10) gave $P = f(\rho,T)$ and equation (A-14) gave $(H - H^*) = f(\rho,T)$. Then $(C_p - C_p^*)$ can be evaluated from the Benedict-Webb-Rubin equation as follows:

$$C_p - C_p^* = \left[\frac{\partial (H - H^*)}{\partial T} \right]_\rho - \left[\frac{\partial (H - H^*)}{\partial \rho} \right]_T \frac{\left(\frac{\partial P}{\partial T} \right)_\rho}{\left(\frac{\partial P}{\partial \rho} \right)_T} \qquad \text{(A-18)}$$

TABLE A-5

CORRECTIONS TO HEATS OF VAPORIZATION CALCULATED FROM THE BENEDICT-WEBB-RUBIN EQUATION OF STATE

Methane

$$\lambda = \left[\frac{\lambda_{BWR}}{1 + \frac{\delta}{100}} \right]$$

$t < -215°F$	$\log_{10} \delta = -0.0098992t - 1.09784$
$-215°F \leq t \leq -180°F$	$\delta = -0.198t - 33.0$
$t > -180°F$	$\delta = -0.1318t - 21.05$

Ethane

$t \leq -85°F$	$\lambda = \lambda_{BWR} - 10.0^{(0.56989 - 0.00761538t)}$
$t > -85°F$	$\lambda = \lambda_{BWR} + 0.0933t \left(1 - \frac{t}{120} \right)$

Propane

$t < 65°F$	$\lambda = \lambda_{BWR} + (8.59375 \times 10^{-6})t^3 - (1.65625 \times 10^{-3})t^2 + 0.21925t^2 - 7.1$
$65°F \leq t \leq 160°F$	$\lambda = \lambda_{BWR} + 0.04t - 0.4$
$t > 160°F$	$\lambda = \lambda_{BWR} - 0.1625t + 32.0$

n-Butane

$t < 118°F$	$\lambda = \lambda_{BWR} - 9.5 + 0.0805t$
$t \geq 118°F$	$\lambda = \lambda_{BWR}$

Let

$$X \equiv e^{-\gamma\rho^2} \tag{A-19}$$

$$Z \equiv \gamma\rho^2 \tag{A-20}$$

Then the necessary expressions are:

$$\left[\frac{\partial(H - H^*)}{\partial\bar{T}}\right]_\rho = (B_oR + \frac{8C_o}{\bar{T}^2})\rho + bR\rho^2 - \frac{2c\rho^2}{\bar{T}^3}\left[\frac{3(1 - X)}{Z} + X(Z - \frac{1}{2})\right] \tag{A-21}$$

$$\left[\frac{\partial(H - H^*)}{\partial\rho}\right]_T = B_oR\bar{T} - 2A_o - \frac{4C_o}{\bar{T}^2} + (2bR\bar{T} - 3a)\rho + 6a\alpha\rho^4 - \frac{c\rho X}{\bar{T}^2}(2Z^2 - 5Z - 5) \tag{A-22}$$

$$\left(\frac{\partial P}{\partial\bar{T}}\right)_\rho = R\rho + (B_oR + \frac{2C_o}{\bar{T}^3})\rho^2 + bR\rho^3 - \frac{2c\rho^3}{\bar{T}^3}X(1 + Z) \tag{A-23}$$

$$\left(\frac{\partial P}{\partial\rho}\right)_T = R\bar{T} + 2\rho(B_oR\bar{T} - A_o - \frac{C_o}{\bar{T}^2}) + 3\rho^2(bR\bar{T} - a) + 6a\alpha\rho^5 + \frac{c\rho^2}{\bar{T}^2}X(3 + 3Z - 2Z^2) \tag{A-24}$$

The coefficient of volume expansion, defined by the equation

$$\beta \equiv \frac{1}{V}\left(\frac{\partial V}{\partial\bar{T}}\right)_P \tag{A-25}$$

can be rearranged to the form

$$\beta = \frac{1}{\rho} \frac{\left(\frac{\partial P}{\partial T} \right)_\rho}{\left(\frac{\partial P}{\partial \rho} \right)_T} \qquad \text{(A-26)}$$

so that equation (A-18) becomes

$$C_p = C_p^* + \left[\frac{\partial (H - H^*)}{\partial T} \right]_\rho - \rho\beta \left[\frac{\partial (H - H^*)}{\partial \rho} \right]_T \qquad \text{(A-27)}$$

The heat capacity at infinite attenuation, C_p^*, is determined by experiment. In the temperature range above 32°F, constants for the equation

$$C_p^* = a + bT + cT^2 + dT^3$$

where T is in degrees Kelvin, have been presented by Kobe et al. and collected by Hougen and Watson [13]. The constants are:

	a	b x 10^2	c x 10^5	d x 10^9
Methane	4.750	1.200	3.030	-2.630
Ethane	1.648	4.124	-1.530	1.740
Propane	-0.966	7.279	-3.755	7.580
n-Butane	0.945	8.873	-4.380	8.360

Temperatures above 32°F comprise the range of interest for n-butane, but additional data were required for the other

substances. Figures A5 and A6 show the correlations used at low temperatures.

This method is the best available to calculate C_p over the required range of temperatures and pressures. As mentioned above, it was not used to calculate $(C_p)_\ell$ because of excessive error.

The calculated values for C_p of methane were compared in detail with data presented by Din et al. [7] and Jones et al. [15]. A sample comparison is shown in Figure A7. Generally the calculated values are higher than the experimental data by less than 3% at temperatures above -50°F with pressures up to 1,000 psia. Near the critical point, percentage deviations become larger, but also the experimental data are less accurate. As temperatures drop below -170°F, the calculated values in the dense region begin to increase, rather than decrease, and become useless. In this work, values lying in the compressed liquid region were not used, so their accuracy is unimportant. Above the critical pressure, C_p's calculated for temperatures below -170°F will be high by more than 30%. For a surface as complicated as the $C_p(P,T)$, the calculated values represent the data very well.

Thermal Conductivity of Vapor and Vapor Film

The thermal conductivity of the vapor at one atmosphere, k^*, is found in several sources [5,14,17,19,26] and is plotted in Figure A8. A comprehensive list of references is also given by Katz et al. [16]. The equations for k^* were:

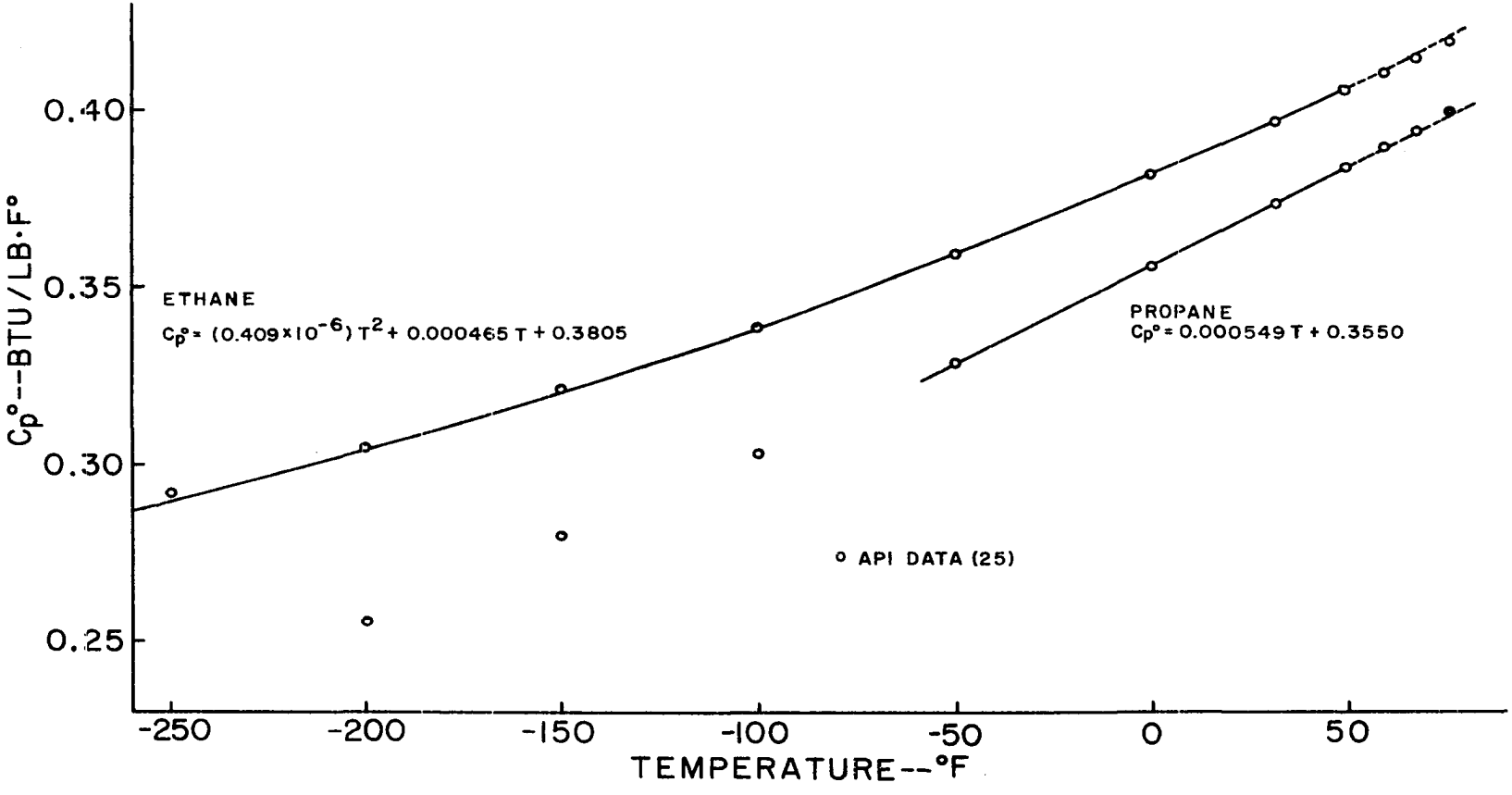

Figure A5
Heat Capacity of Ethane and Propane in the Ideal Gas State

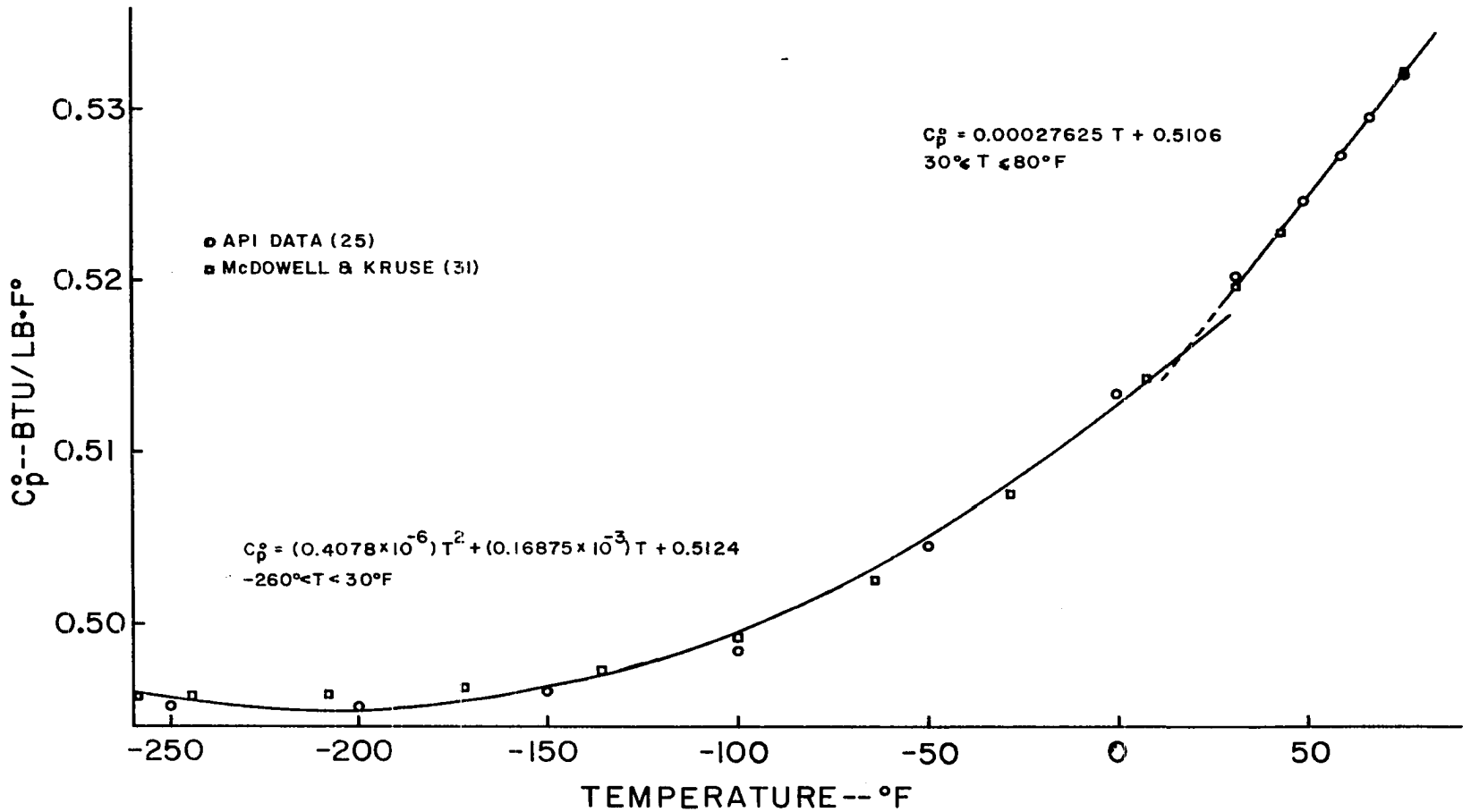

Figure A6
Heat Capacity of Methane in the Ideal Gas State

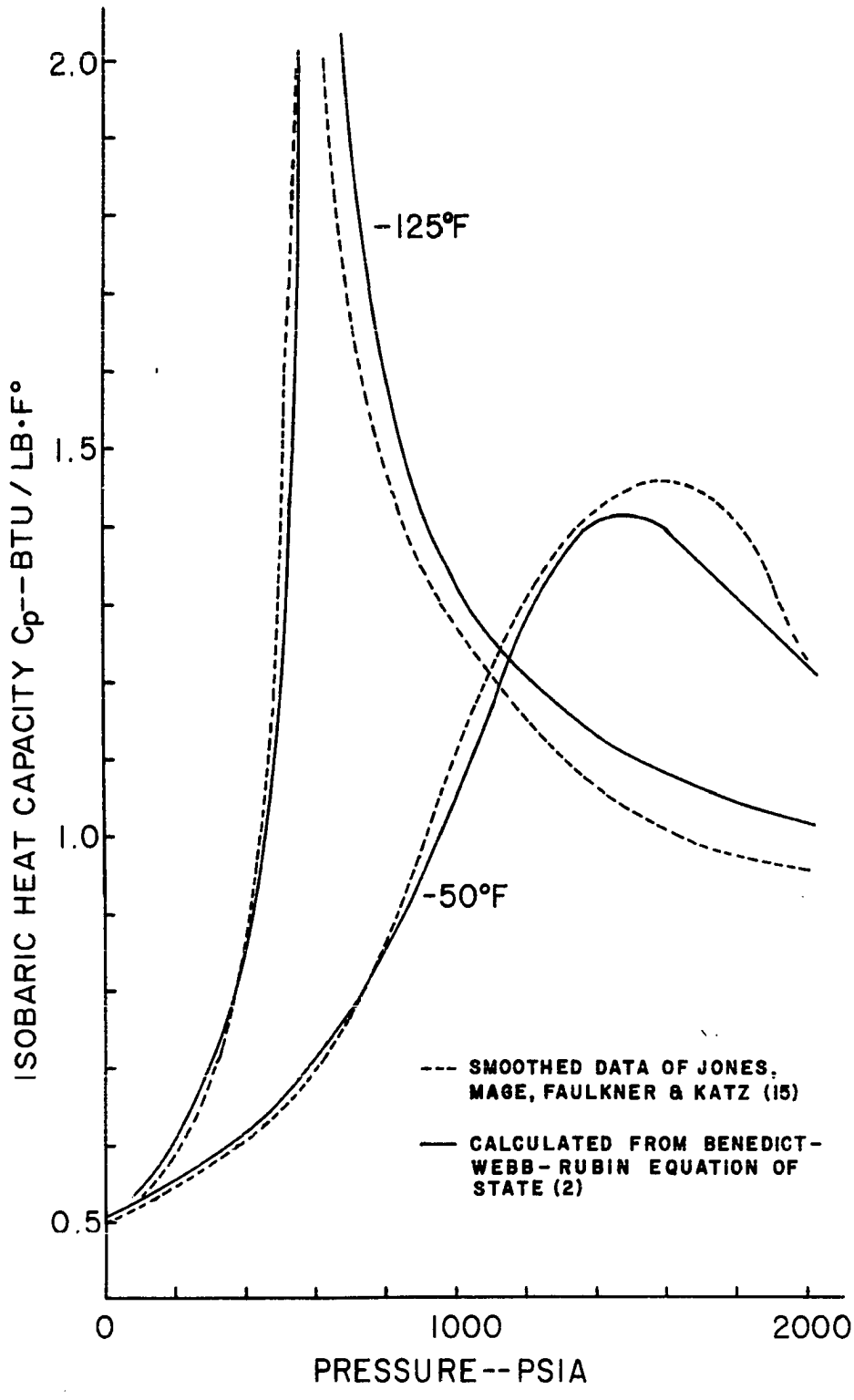

Figure A7
Isobaric Heat Capacity of Methane at -125°F and -50°F

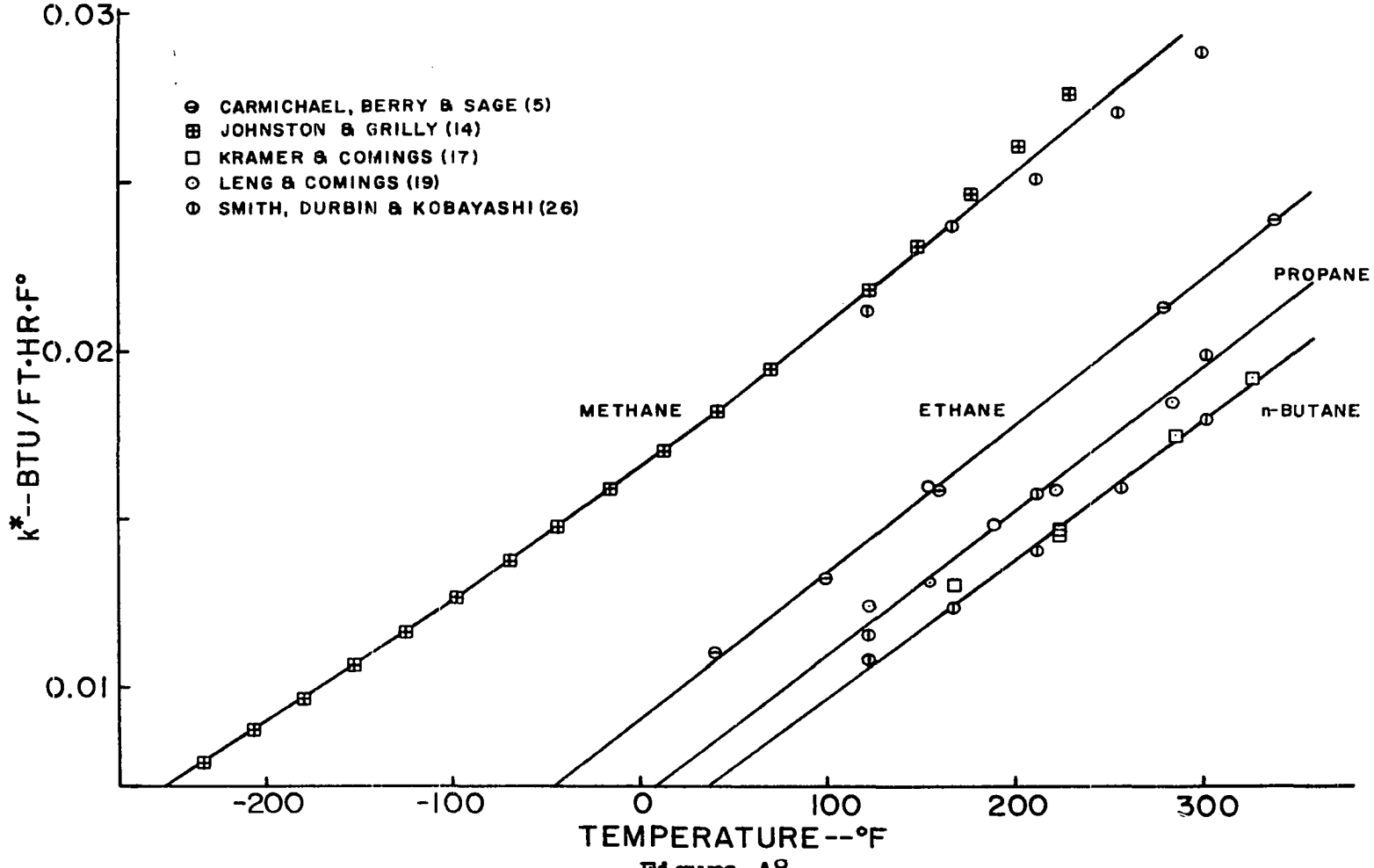

Figure A8
Thermal Conductivity of Hydrocarbons in the Ideal Gas State

Methane: $k^* = 0.01611 + (3.568 \times 10^{-5})T$ $T < -110°F$

$k^* = 0.01651 + (3.928 \times 10^{-5})T$ $T \leq 42°F$

$k^* = 0.01630 + (4.408 \times 10^{-5})T$ $42°F < T$

Ethane: $k^* = 0.00903 + (4.324 \times 10^{-5})T$

Propane: $k^* = 0.00665 + (4.238 \times 10^{-5})T$

n-Butane: $k^* = 0.00563 + (4.065 \times 10^{-5})T$

A convenient method of correlating thermal conductivity k is to plot the residual conductivity $(k - k^*)$ vs. density. The residual method is an especially compact way to represent the vapor film conductivity. It does not appear to work very well for very dense fluids, however, and it was not used to calculate k_l.

The residual thermal conductivity was calculated as a function of density, using the data of Carmichael, Berry and Sage [5], Leng and Comings [19], Kramer and Comings [17], Lenoir and Comings [20], and Lenoir, Junk, and Comings [21]. Generally speaking, the lower the density the more accurate is this method because k^* is known accurately and $(k - k^*) << k^*$ at low densities.

The equations were:

Methane: $\log (k - k^*) = 1.226 \log \rho - 3.0088$

Ethane: $(k - k^*) = (2.875 \times 10^{-6})\rho^3 - (5.25 \times 10^{-5})\rho^2 + 0.001088\rho$

Propane: $(k - k^*) = (5.9 \times 10^{-4})\rho$ if $\rho < 3.7$

$(k - k^*) = 0.00124\rho - 0.00248$ otherwise

n-Butane: $\log (k - k^*) = 1.27198 \log \rho - 3.30103$

Critical Properties

The critical properties used in this analysis are listed below.

Component	Critical Pressure, P_c psia	Critical Temperature, T_c, degrees F
Methane	673.1	-115.78
Ethane	709.08	90.32
Propane	617.4	206.26
n-Butane	550.7	305.62

Data are from Reference Data for Hydrocarbons and Petro-Sulfur Compounds, Special Products Division of the Phillips Petroleum Company. Bulletin No. 521 (1962).

Summary

Tables A-7 through A-14 present values of properties calculated by the procedures described above. In addition, the thermal diffusivity $\alpha \equiv k/\rho C_p$, kinematic viscosity $\nu \equiv \mu/\rho$, Prandtl number $Pr^* \equiv \mu C_p/k$, and reduced temperature and pressure are tabulated.

Table A-6 gives the nomenclature and units for the listings of Tables A-7 through A-14.

TABLE A-6

EXPLANATION OF FLUID PROPERTY TABLES A-7 THROUGH A-14

C_p	specific heat at constant pressure, Btu/lb_m
C_p^*	heat capacity at infinite attenuation
k	thermal conductivity, Btu/ft-hr-F°
k^*	thermal conductivity at attenuation
P_c	critical pressure
Pr	reduced pressure (P/P_c), dimensionless
Pr^*	Prandtl number, $\mu C_p/k$, dimensionless
P_s	saturation pressure, psia
T	temperature, degrees F
T_c	critical temperature
Tr	reduced temperature (T/T_c), dimensionless
α	thermal diffusivity, $k/\rho C_p$, ft^2/hr
λ	heat of vaporization, Btu/lb_m
μ	viscosity, $lb_m/ft\text{-}hr$
ν	kinematic viscosity, μ/ρ, ft^2/hr
ρ	density, lb_m/ft^3
σ	surface tension, lb_f/ft

TABLE A-7

PROPERTIES OF SATURATED LIQUID METHANE
(See Table A-6 for Definitions of Symbols and Units)

T	P_s	ρ_ℓ	λ	$\sigma \times 10^3$	$C_{p\ell}$	k_ℓ	μ_ℓ	ν_ℓ	$\alpha_\ell \times 10^3$	Pr^*_ℓ	Tr	Pr
-270	8.6	27.03	224.7	1.0443	.800	.1128	.3222	.01192	5.216	2.285	.5514	.0128
-260	14.0	26.55	220.8	.9622	.800	.1076	.2821	.01062	5.065	2.098	.5805	.0208
-250	21.5	26.06	216.3	.8813	.822	.1024	.2483	.00953	4.777	1.994	.6096	.0320
-240	31.9	25.55	211.2	.8017	.845	.0972	.2195	.00859	4.502	1.908	.6387	.0474
-230	45.9	25.02	205.4	.7235	.867	.0920	.1950	.00779	4.239	1.839	.6678	.0681
-220	64.0	24.46	198.9	.6469	.890	.0874	.1754	.00717	4.014	1.786	.6969	.0951
-210	86.9	23.87	193.6	.5719	.912	.0833	.1607	.00673	3.824	1.761	.7259	.1292
-200	115.4	23.25	185.7	.4986	.935	.0792	.1474	.00634	3.645	1.740	.7550	.1715
-190	150.1	22.58	177.8	.4272	.957	.0751	.1351	.00598	3.476	1.722	.7841	.2230
-180	191.8	21.86	169.4	.3580	.980	.0711	.1237	.00566	3.317	1.705	.8132	.2849
-170	241.1	21.16	159.2	.2911	1.089	.0670	.1140	.00539	2.907	1.853	.8423	.3582
-160	298.9	20.29	147.8	.2269	1.200	.0605	.1036	.00511	2.485	2.055	.8714	.4441
-150	366.0	19.30	134.6	.1658	1.311	.0541	.0934	.00484	2.140	2.262	.9005	.5437
-140	443.0	18.11	118.5	.1087	1.422	.0478	.0832	.00459	1.856	2.474	.9296	.6582
-130	530.9	16.58	97.2	.0567	1.730	.0410	.0722	.00435	1.429	3.046	.9586	.7888
-120	630.6	14.09	59.5	.0128	2.470	.0240	.0472	.00335	.690	4.855	.9877	.9368

TABLE A-8

PROPERTIES OF SATURATED METHANE VAPOR
(See Table A-6 for Definitions of Symbols and Units)

T	P_s	ρ_v	C_{pv}	C_p^*	k_v	k^*	μ_v	ν_v	α_v	Pr_v^*	Tr	Pr
-270	8.6	.070	.526	.4966	.0065	.0065	.00958	.13759	.17800	.773	.5514	.0128
-260	14.0	.109	.536	.4961	.0069	.0068	.01016	.09332	.11825	.789	.5805	.0208
-250	21.5	.162	.549	.4957	.0073	.0072	.01073	.06625	.08210	.807	.6096	.0320
-240	31.9	.233	.564	.4954	.0077	.0075	.01131	.04861	.05879	.827	.6387	.0474
-230	45.9	.326	.582	.4952	.0082	.0079	.01189	.03647	.04293	.849	.6678	.0681
-220	64.0	.446	.605	.4950	.0086	.0083	.01248	.02796	.03195	.875	.6969	.0951
-210	86.9	.598	.632	.4949	.0091	.0086	.01308	.02189	.02419	.905	.7259	.1292
-200	115.4	.786	.665	.4950	.0097	.0090	.01371	.01743	.01855	.939	.7550	.1715
-190	150.1	1.020	.706	.4951	.0103	.0093	.01436	.01408	.01435	.981	.7841	.2230
-180	191.8	1.308	.758	.4952	.0110	.0097	.01506	.01151	.01114	1.034	.8132	.2849
-170	241.1	1.664	.828	.4955	.0119	.0100	.01583	.00951	.00862	1.103	.8423	.3582
-160	298.9	2.108	.924	.4958	.0128	.0104	.01670	.00792	.00659	1.202	.8714	.4441
-150	366.0	2.668	1.070	.4963	.0140	.0108	.01772	.00664	.00491	1.353	.9005	.5437
-140	443.0	3.395	1.318	.4968	.0155	.0111	.01899	.00559	.00346	1.615	.9296	.6582
-130	530.9	4.389	1.823	.4974	.0175	.0115	.02072	.00472	.00218	2.161	.9586	.7888
-120	630.6	6.367	4.602	.4980	.0213	.0118	.02427	.00381	.00073	5.241	.9877	.9368

TABLE A-9

PROPERTIES OF SATURATED LIQUID ETHANE
(See Table A-6 for Definitions of Symbols and Units)

T	P_s	ρ_ℓ	λ	$\sigma \times 10^3$	$C_{p\ell}$	k_ℓ	μ_ℓ	ν_ℓ	$\alpha_\ell \times 10^3$	Pr^*_ℓ	Tr	Pr
-140	10.0	34.74	215.5	1.1808	.593	.0907	.4601	.01325	4.405	3.007	.5812	.0140
-130	13.6	34.31	212.0	1.1184	.596	.0879	.4192	.01222	4.302	2.840	.5993	.0192
-120	18.3	33.88	208.2	1.0567	.599	.0851	.3845	.01135	4.198	2.703	.6175	.0258
-110	24.1	33.44	204.3	.9956	.601	.0823	.3550	.01062	4.094	2.593	.6357	.0340
-100	31.3	33.00	200.3	.9352	.604	.0796	.3300	.01000	3.989	2.507	.6539	.0441
-90	39.9	32.54	196.1	.8755	.607	.0768	.3086	.00948	3.885	2.441	.6721	.0563
-80	50.2	32.08	194.4	.8165	.610	.0740	.2904	.00905	3.780	2.395	.6903	.0708
-70	62.5	31.60	189.6	.7583	.613	.0712	.2748	.00869	3.674	2.366	.7085	.0881
-60	76.8	31.11	184.9	.7009	.616	.0689	.2614	.00840	3.595	2.337	.7266	.1083
-50	93.5	30.61	180.1	.6443	.619	.0670	.2500	.00817	3.535	2.311	.7448	.1318
-40	112.7	30.09	175.3	.5887	.635	.0650	.2329	.00774	3.403	2.274	.7630	.1589
-30	134.7	29.55	170.3	.5339	.665	.0631	.2172	.00735	3.210	2.290	.7812	.1899
-20	159.6	28.99	165.1	.4802	.695	.0611	.2027	.00699	3.035	2.305	.7994	.2251
-10	187.9	28.40	159.5	.4276	.725	.0592	.1893	.00667	2.875	2.318	.8176	.2650
0	219.6	27.78	153.6	.3761	.755	.0573	.1767	.00636	2.730	2.330	.8358	.3097
10	255.1	27.27	147.3	.3258	.785	.0553	.1677	.00615	2.585	2.380	.8539	.3598
20	294.6	26.59	140.3	.2770	.815	.0634	.1566	.00589	2.463	2.392	.8721	.4154
30	338.3	25.84	132.6	.2296	.845	.0514	.1458	.00564	2.356	2.395	.8903	.4772
40	386.6	25.01	123.9	.1840	.875	.0495	.1350	.00540	2.262	2.387	.9085	.5453
50	439.8	24.07	114.0	.1403	.905	.0476	.1241	.00516	2.183	2.362	.9267	.6202
60	498.0	22.96	102.3	.0991	1.106	.0456	.1128	.00491	1.796	2.735	.9449	.7024
70	561.7	21.58	87.9	.0607	1.478	.0409	.1006	.00466	1.281	3.637	.9630	.7922
80	631.2	19.64	68.2	.0265	1.850	.0377	.0860	.00438	1.037	4.222	.9812	.8901
90	706.7	13.94	2.1	.0004	3.850	.0345	.0532	.00382	.642	5.945	.9994	.9967

TABLE A-10

PROPERTIES OF SATURATED ETHANE VAPOR
(See Table A-6 for Definitions of Symbols and Units)

T	P_s	ρ_v	C_{pv}	C_p^*	k_v	k^*	μ_v	ν_v	α_v	Pr_v^*	Tr	Pr
-140	10.0	.090	.341	.3234	.0031	.0030	.01326	.14767	.10046	1.470	.5812	.0140
-130	13.6	.120	.348	.3270	.0035	.0034	.01373	.11420	.08450	1.351	.5993	.0192
-120	18.3	.158	.357	.3306	.0040	.0038	.01420	.08987	.07120	1.262	.6175	.0258
-110	24.1	.204	.366	.3343	.0045	.0043	.01467	.07184	.06017	1.194	.6357	.0340
-100	31.3	.260	.376	.3381	.0050	.0047	.01514	.05824	.05105	1.141	.6539	.0441
-90	39.9	.327	.386	.3420	.0055	.0051	.01562	.04782	.04349	1.099	.6721	.0563
-80	50.2	.406	.398	.3459	.0060	.0056	.01610	.03967	.03716	1.067	.6903	.0708
-70	62.5	.499	.411	.3500	.0065	.0060	.01659	.03324	.03186	1.043	.7085	.0881
-60	76.8	.608	.425	.3541	.0071	.0064	.01709	.02810	.02740	1.026	.7266	.1083
-50	93.5	.735	.440	.3583	.0076	.0069	.01760	.02394	.02360	1.014	.7448	.1318
-40	112.7	.883	.457	.3626	.0082	.0073	.01813	.02054	.02037	1.009	.7630	.1589
-30	134.7	1.053	.476	.3669	.0088	.0077	.01868	.01774	.01758	1.009	.7812	.1899
-20	159.6	1.250	.498	.3714	.0094	.0082	.01926	.01540	.01517	1.015	.7994	.2251
-10	187.9	1.478	.523	.3759	.0101	.0086	.01987	.01345	.01307	1.029	.8176	.2650
0	219.6	1.741	.552	.3805	.0108	.0090	.02053	.01179	.01122	1.051	.8358	.3097
10	255.1	2.046	.586	.3852	.0115	.0095	.02124	.01038	.00958	1.084	.8539	.3598
20	294.6	2.401	.629	.3900	.0122	.0099	.02203	.00917	.00811	1.131	.8721	.4154
30	338.3	2.819	.683	.3948	.0130	.0103	.02292	.00813	.00677	1.201	.8903	.4772
40	386.6	3.315	.756	.3998	.0139	.0108	.02394	.00722	.00554	1.303	.9085	.5453
50	439.8	3.916	.862	.4048	.0148	.0112	.02516	.00642	.00439	1.464	.9267	.6202
60	498.0	4.666	1.033	.4100	.0158	.0116	.02668	.00572	.00329	1.739	.9449	.7024
70	561.7	5.649	1.360	.4161	.0170	.0121	.02873	.00509	.00222	2.292	.9630	.7922
80	631.2	7.074	2.239	.4221	.0186	.0125	.03188	.00451	.00117	3.842	.9812	.8901
90	706.7	9.744	8.067	.4281	.0212	.0129	.03873	.00397	.00027	14.743	.9994	.9967

TABLE A-11

PROPERTIES OF SATURATED LIQUID PROPANE
(See Table A-6 for Definitions of Symbols and Units)

T	P_s	ρ_ℓ	λ	$\sigma \times 10^3$	$C_{p\ell}$	k_ℓ	μ_ℓ	ν_ℓ	$\alpha_\ell \times 10^3$	Pr^*_ℓ	Tr	Pr
-50	12.5	36.51	184.9	1.0895	.532	.0568	.5282	.01447	2.923	4.950	.6151	.0203
-40	16.0	36.10	182.6	1.0378	.534	.0560	.4914	.01361	2.906	4.684	.6302	.0260
-30	20.3	35.69	180.2	.9865	.536	.0552	.4583	.01284	2.884	4.453	.6452	.0329
-20	25.4	35.27	177.7	.9357	.540	.0544	.4283	.01214	2.856	4.252	.6602	.0411
-10	31.3	34.85	175.0	.8854	.545	.0536	.4010	.01151	2.822	4.077	.6752	.0508
0	38.3	34.42	172.2	.8356	.551	.0528	.3760	.01092	2.784	3.924	.6902	.0621
10	46.5	33.98	169.3	.7864	.558	.0520	.3531	.01039	2.741	3.791	.7052	.0753
20	55.8	33.54	166.2	.7377	.567	.0512	.3320	.00990	2.694	3.675	.7203	.0904
30	66.5	33.08	163.0	.6896	.576	.0504	.3124	.00944	2.643	3.572	.7353	.1078
40	78.7	32.62	159.7	.6421	.587	.0496	.2943	.00902	2.590	3.483	.7503	.1275
50	92.5	32.14	156.3	.5952	.599	.0488	.2773	.00863	2.535	3.403	.7653	.1498
60	107.9	31.65	152.9	.5490	.612	.0480	.2614	.00826	2.478	3.333	.7803	.1748
70	125.2	31.15	148.7	.5035	.626	.0472	.2465	.00791	2.420	3.269	.7954	.2028
80	144.5	30.62	144.4	.4587	.641	.0464	.2323	.00759	2.362	3.212	.8104	.2340
90	165.9	30.07	140.0	.4147	.668	.0456	.2188	.00728	2.270	3.205	.8254	.2686
100	189.4	29.50	135.4	.3715	.690	.0448	.2059	.00698	2.200	3.172	.8404	.3068
110	215.4	28.90	130.6	.3292	.718	.0440	.1935	.00669	2.120	3.158	.8554	.3489
120	243.9	28.26	125.6	.2879	.749	.0432	.1814	.00642	2.040	3.146	.8704	.3950
130	275.0	27.58	120.2	.2477	.783	.0424	.1696	.00615	1.963	3.133	.8855	.4453
140	308.9	26.83	114.4	.2086	.823	.0416	.1581	.00589	1.884	3.126	.9005	.5003
150	345.7	26.02	108.0	.1708	.873	.0407	.1465	.00563	1.794	3.138	.9155	.5600
160	385.7	25.16	101.0	.1344	.937	.0391	.1355	.00538	1.658	3.248	.9305	.6247
170	429.0	24.17	90.9	.0998	1.019	.0374	.1241	.00513	1.519	3.380	.9455	.6948
180	475.7	23.00	79.3	.0673	1.119	.0358	.1120	.00487	1.390	3.504	.9606	.7705
190	526.1	21.49	65.2	.0375	1.319	.0341	.0985	.00459	1.203	3.811	.9756	.8521
200	580.2	19.17	45.0	.0117	2.117	.0324	.0813	.00424	.799	5.309	.9906	.9398

TABLE A-12

PROPERTIES OF SATURATED PROPANE VAPOR
(See Table A-6 for Definitions of Symbols and Units)

T	P_s	ρ_v	C_{pv}	C_p^*	k_v	k^*	μ_v	ν_v	α_v	Pr_v^*	Tr	Pr
-50	12.5	.130	.343	.3275	.0046	.0045	.01468	.11261	.10298	1.094	.6151	.0203
-40	16.0	.164	.352	.3330	.0051	.0050	.01509	.09191	.08748	1.051	.6302	.0260
-30	20.3	.204	.361	.3385	.0055	.0054	.01550	.07582	.07460	1.016	.6452	.0329
-20	25.4	.252	.370	.3440	.0060	.0058	.01592	.06318	.06388	.989	.6602	.0411
-10	31.3	.308	.379	.3495	.0064	.0062	.01634	.05312	.05492	.967	.6752	.0508
0	38.3	.372	.389	.3550	.0069	.0066	.01676	.04505	.04740	.950	.6902	.0621
10	46.5	.447	.400	.3605	.0073	.0071	.01719	.03846	.04103	.937	.7052	.0753
20	55.8	.533	.411	.3660	.0078	.0075	.01763	.03309	.03566	.928	.7203	.0904
30	66.5	.631	.423	.3715	.0083	.0079	.01807	.02865	.03107	.922	.7353	.1078
40	78.7	.743	.436	.3770	.0088	.0083	.01853	.02495	.02714	.919	.7503	.1275
50	92.5	.870	.449	.3824	.0093	.0088	.01900	.02184	.02376	.919	.7653	.1498
60	107.9	1.015	.464	.3881	.0098	.0092	.01949	.01921	.02081	.923	.7803	.1748
70	125.2	1.178	.481	.3948	.0103	.0096	.01999	.01697	.01822	.932	.7954	.2028
80	144.5	1.363	.499	.4014	.0108	.0100	.02052	.01505	.01595	.944	.8104	.2340
90	165.9	1.573	.519	.4080	.0114	.0105	.02108	.01340	.01396	.960	.8254	.2686
100	189.4	1.811	.541	.4145	.0120	.0109	.02168	.01197	.01220	.981	.8404	.3068
110	215.4	2.081	.567	.4210	.0125	.0113	.02232	.01073	.01064	1.008	.8554	.3489
120	243.9	2.388	.596	.4274	.0131	.0117	.02302	.00964	.00923	1.044	.8704	.3950
130	275.0	2.741	.631	.4338	.0138	.0122	.02379	.00868	.00797	1.089	.8855	.4453
140	308.9	3.148	.674	.4402	.0144	.0126	.02465	.00783	.00681	1.151	.9005	.5003
150	345.7	3.622	.730	.4465	.0151	.0130	.02564	.00708	.00573	1.236	.9155	.5600
160	385.7	4.184	.806	.4528	.0161	.0134	.02680	.00640	.00478	1.339	.9305	.6247
170	429.0	4.865	.920	.4590	.0174	.0139	.02821	.00580	.00389	1.491	.9455	.6948
180	475.7	5.721	1.112	.4652	.0189	.0143	.03002	.00525	.00297	1.767	.9606	.7705
190	526.1	6.864	1.512	.4714	.0207	.0147	.03255	.00474	.00200	2.373	.9756	.8521
200	580.2	8.586	2.742	.4775	.0233	.0151	.03672	.00428	.00099	4.322	.9906	.9398

TABLE A-13

PROPERTIES OF SATURATED LIQUID BUTANE
(See Table A-6 for Definitions of Symbols and Units)

T	P_s	ρ_ℓ	λ	$\sigma \times 10^3$	$C_{p\ell}$	k_ℓ	μ_ℓ	ν_ℓ	$\alpha_\ell \times 10^3$	Pr^*_ℓ	Tr	Pr
30	14.3	37.53	173.1	1.0224	.540	.0792	.5004	.01333	3.906	3.414	.6398	.0260
40	17.6	37.16	169.4	.9772	.550	.0788	.4725	.01272	3.857	3.297	.6529	.0320
50	21.5	36.78	165.9	.9324	.560	.0785	.4468	.01215	3.811	3.187	.6659	.0390
60	26.0	36.40	162.6	.8881	.570	.0782	.4229	.01162	3.768	3.084	.6790	.0472
70	31.2	36.01	159.4	.8441	.580	.0778	.4008	.01113	3.727	2.986	.6921	.0566
80	37.1	35.61	156.4	.8005	.590	.0775	.3802	.01068	3.689	2.894	.7051	.0674
90	43.9	35.21	153.5	.7573	.600	.0772	.3609	.01025	3.653	2.805	.7182	.0797
100	51.5	34.80	150.6	.7146	.610	.0769	.3428	.00985	3.620	2.721	.7313	.0936
110	60.1	34.39	147.8	.6724	.620	.0765	.3258	.00947	3.590	2.639	.7444	.1092
120	69.8	33.96	144.9	.6306	.630	.0762	.3097	.00912	3.562	2.561	.7574	.1267
130	80.5	33.53	141.3	.5894	.640	.0756	.2945	.00879	3.524	2.493	.7705	.1461
140	92.4	33.08	137.8	.5486	.650	.0746	.2801	.00847	3.472	2.439	.7836	.1678
150	105.6	32.62	134.2	.5084	.666	.0737	.2663	.00816	3.391	2.408	.7966	.1917
160	120.1	32.14	130.5	.4688	.682	.0727	.2531	.00787	3.316	2.375	.8097	.2182
170	136.1	31.64	126.8	.4297	.698	.0717	.2404	.00760	3.246	2.340	.8228	.2472
180	153.7	31.13	123.0	.3913	.714	.0707	.2281	.00733	3.182	2.303	.8358	.2790
190	172.8	30.59	119.0	.3536	.730	.0697	.2162	.00707	3.123	2.263	.8489	.3138
200	193.7	30.02	114.9	.3166	.746	.0688	.2046	.00682	3.070	2.220	.8620	.3517
210	216.4	29.42	110.5	.2803	.762	.0678	.1932	.00657	3.023	2.172	.8750	.3930
220	241.1	28.77	105.9	.2449	.778	.0668	.1819	.00632	2.984	2.119	.8881	.4378
230	267.8	28.08	101.0	.2104	.794	.0658	.1707	.00608	2.952	2.060	.9012	.4864
240	296.8	27.32	95.7	.1769	.810	.0645	.1596	.00584	2.914	2.004	.9142	.5389
250	328.0	26.49	89.9	.1446	.826	.0625	.1483	.00560	2.856	1.959	.9273	.5956
260	361.7	25.56	83.4	.1135	.842	.0605	.1368	.00535	2.811	1.903	.9404	.6568
270	398.0	24.53	76.0	.0839	.858	.0585	.1254	.00511	2.779	1.839	.9535	.7227
280	437.1	23.35	67.1	.0561	.874	.0565	.1136	.00486	2.769	1.757	.9665	.7936
290	479.0	21.82	55.6	.0306	.890	.0545	.1002	.00459	2.806	1.637	.9796	.8699
300	524.1	19.43	37.2	.0088	1.604	.0525	.0827	.00426	1.685	2.528	.9927	.9517

TABLE A-14

PROPERTIES OF SATURATED BUTANE VAPOR
(See Table A-6 for Definitions of Symbols and Units)

T	P_B	ρ_v	C_{pv}	C_p^*	k_v	k^*	μ_v	ν_v	α_v	Pr_v^*	Tr	Pr
30	14.3	.165	.392	.3789	.0069	.0068	.01569	.09496	.10650	.892	.6398	.0260
40	17.6	.201	.401	.3853	.0073	.0073	.01606	.08005	.09107	.879	.6529	.0320
50	21.5	.242	.409	.3916	.0077	.0077	.01644	.06801	.07828	.869	.6659	.0390
60	26.0	.289	.418	.3979	.0082	.0081	.01682	.05820	.06763	.861	.6790	.0472
70	31.2	.343	.427	.4042	.0086	.0085	.01720	.05013	.05869	.854	.6921	.0566
80	37.1	.405	.437	.4104	.0090	.0089	.01759	.04346	.05117	.849	.7051	.0674
90	43.9	.475	.448	.4166	.0095	.0093	.01798	.03786	.04475	.846	.7182	.0797
100	51.5	.554	.456	.4227	.0099	.0097	.01838	.03318	.03931	.844	.7313	.0936
110	60.1	.643	.466	.4288	.0104	.0101	.01879	.02922	.03465	.843	.7444	.1092
120	69.8	.743	.477	.4348	.0109	.0105	.01920	.02585	.03064	.844	.7574	.1267
130	80.5	.855	.488	.4409	.0113	.0109	.01963	.02297	.02716	.846	.7705	.1461
140	92.4	.980	.499	.4468	.0118	.0113	.02007	.02048	.02413	.849	.7836	.1678
150	105.6	1.120	.512	.4528	.0123	.0117	.02053	.01833	.02148	.853	.7966	.1917
160	120.1	1.276	.525	.4587	.0128	.0121	.02100	.01646	.01915	.859	.8097	.2182
170	136.1	1.451	.538	.4646	.0133	.0125	.02149	.01482	.01709	.867	.8228	.2472
180	153.7	1.646	.553	.4704	.0139	.0129	.02202	.01338	.01525	.877	.8358	.2790
190	172.8	1.864	.570	.4762	.0145	.0134	.02257	.01210	.01361	.889	.8489	.3138
200	193.7	2.110	.588	.4819	.0151	.0138	.02316	.01098	.01214	.904	.8620	.3517
210	216.4	2.386	.608	.4877	.0157	.0142	.02380	.00997	.01080	.923	.8750	.3930
220	241.1	2.699	.632	.4934	.0163	.0146	.02449	.00907	.00958	.947	.8881	.4378
230	267.8	3.055	.660	.4990	.0170	.0150	.02526	.00827	.00845	.978	.9012	.4864
240	296.8	3.465	.695	.5046	.0178	.0154	.02613	.00754	.00740	1.019	.9142	.5389
250	328.0	3.940	.739	.5102	.0187	.0158	.02712	.00688	.00640	1.075	.9273	.5956
260	361.7	4.504	.801	.5157	.0196	.0162	.02829	.00628	.00543	1.157	.9404	.6568
270	398.0	5.188	.894	.5212	.0207	.0166	.02973	.00573	.00446	1.286	.9535	.7227
280	437.1	6.054	1.056	.5267	.0220	.0170	.03158	.00522	.00343	1.519	.9665	.7936
290	479.0	7.241	1.421	.5321	.0236	.0174	.03425	.00473	.00230	2.061	.9796	.8699
300	524.1	9.235	3.099	.5375	.0263	.0178	.03919	.00424	.00092	4.622	.9927	.9517

Literature Cited in Appendix A

1. Benedict, M., G. B. Webb and L. C. Rubin. "An Empirical Equation for Thermodynamic Properties of Light Hydrocarbons and Their Mixtures," Journal of Chemical Physics, 8 (1940), 334.

2. Benedict, M., G. B. Webb and L. C. Rubin. "An Empirical Equation for Thermodynamic Properties of Light Hydrocarbons and Their Mixtures," Chemical Engineering Progress, 47, No. 8 (August, 1951), 419.

3. Brock, J. R. and R. Byron Bird. "Surface Tension and the Principle of Corresponding States," A.I.Ch.E. Journal, 1, No. 2 (June, 1955), 174.

4. Carmichael, L. T. and B. H. Sage. "Viscosity of Ethane at High Pressures," Journal of Chemical and Engineering Data, 8, No. 1 (January, 1963), 94.

5. Carmichael, L. T., Virginia Berry and B. H. Sage. "Thermal Conductivity of Fluids. Ethane," Journal of Chemical and Engineering Data, 8, No. 3 (July, 1963), 281.

6. Carmichael, L. T., V. M. Berry and B. H. Sage. "Viscosity of Hydrocarbons. Propane," Journal of Chemical and Engineering Data, 9, No. 3 (July, 1964), 411.

7. Din, F. (ed.). Thermodynamic Functions of Gases. Vol. 2: Air, Acetylene, Ethylene, Propane and Argon (1956). Vol. 3: Methane, Nitrogen, Ethane (1961). London: Butterworths Scientific Publications.

8. Dolan, J. P., K. E. Starling, A. L. Lee, B. E. Eakin and R. T. Ellington. "Liquid, Gas, and Dense-Fluid Viscosity of n-Butane," Journal of Chemical and Engineering Data, 8, No. 3 (July, 1963), 396.

9. Douslin, D. R., R. H. Harrison, R. T. Moore and J. P. MuCullough. "p-V-T Relations for Methane," Journal of Chemical and Engineering Data, 9, No. 3 (July, 1964), 358.

10. Eakin, B. E., K. E. Starling, J. P. Dolan and R. T. Ellington. "Liquid, Gas, and Dense Fluid Viscosity of Ethane," Journal of Chemical and Engineering Data, 7, No. 1 (January, 1962), 33.

11. Francis, A. W. "Pressure-Temperature-Liquid Density Relations of Pure Hydrocarbons," Industrial and Engineering Chemistry, 49, No. 10 (October, 1957), 1779.

12. Frost, A. A. and D. R. Kalkwarf. "A Semi-Empirical Equation for the Vapor Pressure of Liquids as a Function of Temperature," Journal of Chemical Physics, 21, No. 2 (February, 1953), 264.

13. Hougen, O. A. and K. M. Watson. Chemical Process Principles. Part I. New York: John Wiley and Sons, Inc., 1947.

14. Johnston, H. L. and E. R. Grilly. "The Thermal Conductivities of Eight Common Gases between 80° and 380°K," Journal of Chemical Physics, 14, No. 4 (April, 1946), 233.

15. Jones, M. L. Jr., D. T. Mage, R. C. Faulkner, Jr. and D. L. Katz. "Measurement of Thermodynamic Properties of Gases at Low Temperature and High Pressure--Methane," Chemical Engineering Progress Symposium Series, 59, No. 44 (1963), 52.

16. Katz, Donald L., D. Cornell, R. Kobayashi, F. H. Poettmann, J. A. Vary, J. R. Elenbaas and C. F. Weinaug. Handbook of Natural Gas Engineering. New York: McGraw-Hill Book Company, Inc., 1959.

17. Kramer, F. R. and E. W. Comings. "Thermal Conductivity of Butane at High Pressure: Correlation with Other Gases," Journal of Chemical and Engineering Data, 5, No. 4 (October, 1960), 462.

18. Lee, A. L., K. E. Starling, J. P. Dolan and R. T. Ellington. "Viscosity Correlation for Light Hydrocarbon Systems," A.I.Ch.E. Journal, 10, No. 5 (September, 1964), 694.

19. Leng, D. E. and E. W. Comings. "Thermal Conductivity of Propane," Industrial and Engineering Chemistry, 49, No. 12 (December, 1957), 2042.

20. Lenoir, J. M. and E. W. Comings. "Thermal Conductivity of Gases," Chemical Engineering Progress, 47, No. 5 (May, 1951), 223.

21. Lenoir, J. M., W. A. Junk and E. W. Comings. "Measurement and Correlation of Thermal Conductivities of Gases at High Pressure," Chemical Engineering Progress, 49, No. 10 (October, 1953), 539.

22. Opfell, J. B., W. G. Schlinger and B. H. Sage. "Benedict Equation of State," Industrial and Engineering Chemistry, 46, No. 6 (June, 1954), 1286.

23. Perry, John H. (ed.). Chemical Engineers' Handbook. 3rd Ed. New York: McGraw-Hill Book Company, Inc., 1950.

24. Pratt and Whitney Division of United Aircraft Corporation. Investigation of Light Hydrocarbon Fuels with Flox Mixtures as Liquid Rocket Propellants: Quarterly Progress Report No. 1. Contract NA53-4195, Pratt and Whitney No. PWA FR-1164, October, 1964. (Subsequent reports are classified.)

25. Rossini, F. D. (ed.). Selected Values of Physical and Thermodynamic Properties of Hydrocarbons and Related Compounds. Pittsburgh: Carnegie Press, 1953.

26. Smith, W. J. S., L. D. Durbin and R. Kobayashi. "Thermal Conductivity of Light Hydrocarbons and Methane-Propane Mixtures at Low Pressures," Journal of Chemical and Engineering Data, 5, No. 3 (July, 1960), 316.

27. Starling, K. E., B. E. Eakin and R. T. Ellington. "Liquid, Gas, and Dense-Fluid Viscosity of Propane," A.I.Ch.E. Journal, 6, No. 3 (September, 1960), 438.

28. Starling, K. E. and R. T. Ellington. "Viscosity Correlations for Nonpolar Dense Fluids," A.I.Ch.E. Journal, 10, No. 1 (January, 1964), 11.

29. Swift, G. W., J. Lohrenz and F. Kurata. "Liquid Viscosities above the Normal Boiling Point for Methane, Ethane, Propane and n-Butane," A.I.Ch.E. Journal, 6, No. 3 (September, 1960), 415.

30. Thodos, G. "Vapor Pressures of Normal Saturated Hydrocarbons," Industrial and Engineering Chemistry, 42, No. 8 (August, 1950), 1514.

31. Canjar, Lawrence N. and Francis S. Manning. "Thermo Properties of Hydrocarbons," Petroleum Refiner, 41, No. 8 (p. 121), No. 9 (p. 253), No. 10 (p. 149), No. 11 (p. 203), No. 12 (p. 115), 1962.

32. Carmichael, L. T., H. H. Reamer and B. H. Sage. "Thermal Conductivity of Fluids. Methane." Journal of Chemical and Engineering Data, 11, No. 1 (January, 1966), p. 52.

APPENDIX B

END LOSSES AND THEIR EFFECT ON THE FLUX AT THE MEASURED ΔT

Introduction

The end insulation on the heater was shown in Figures 5 and 6. The cross-section is shown again in Figure B1.

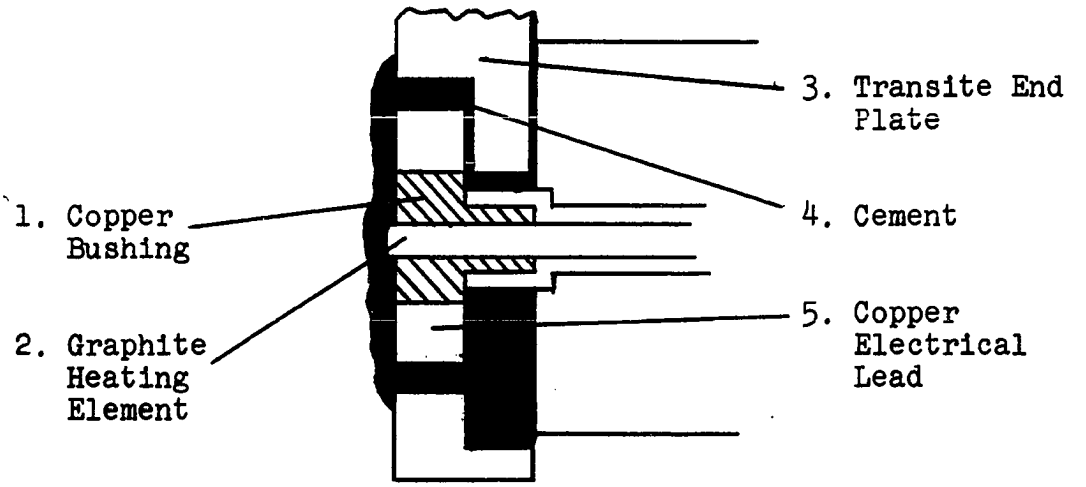

Figure B1. End Insulation of Heater

The graphite rod will always be the hottest part of the heater. It can be seen in Figure B1 that the primary path for end losses is axially down the graphite rod and its boron nitride insulator, which are in good contact with the copper electrical lead. It was found that the pieces 1 and 5 in Figure B1 were hotter than the iron heater body at the same radial distance from the center. Therefore, losses from the end of the iron heater body are completely negligible.

Two questions arise: (1) What are the heat losses down the graphite rod and boron nitride insulator? (2) How

much do these losses affect the flux near the center of the heater where the ΔTs are measured?

The theory is developed below. The conclusions were that although end losses averaged about 6%, the effect near the center of the heater is negligible. Therefore, the measured fluxes were not corrected for end losses.

End Losses

Figure B2 shows the end plate and copper lead, with the location of three thermocouples. It was assumed that end losses would be the same at either end of the heater. Essentially all of the heat either flows down the copper lead or radiates from the round copper surface.

In brief, the calculational method was:

(1) Use T_9, T_{10} and T_f to calculate the heat loss down the rectangular lead, $\dot{Q}_L$ (Figure B3).

(2) Extract the heat transfer coefficient h from this equation and assume that it applies also to the round part of the lead. (Figure B4).

(3) Use T_8, T_f and the calculated h to calculate the heat loss from the round surface, $\dot{Q}_E$.

(4) Assume that the total end losses are $2(\dot{Q}_L + \dot{Q}_E)$.

Calculation of Lead Loss $\dot{Q}_L$

The rectangular portion of the lead can be treated as a fin, as shown in Figure B3.

The equation for heat loss is obtained by assuming that the lead temperature is a function only of z. If no

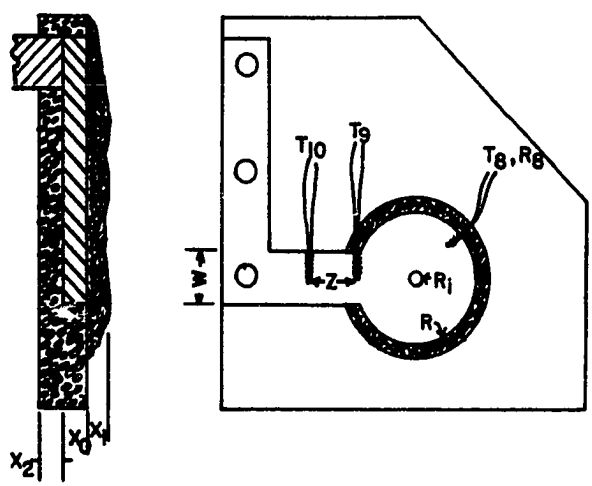

	X_o = 0.125 inch	R_i = 0.063 inch
W = 0.25 inch	X_1 = 0.063 inch	R_8 = 0.25 inch
Z = 0.25 inch	X_2 = 0.125 inch	R = 0.32 inch

Figure B2. Detail of End of Heater Showing Points of Measurement T_8, T_9, and T_{10}

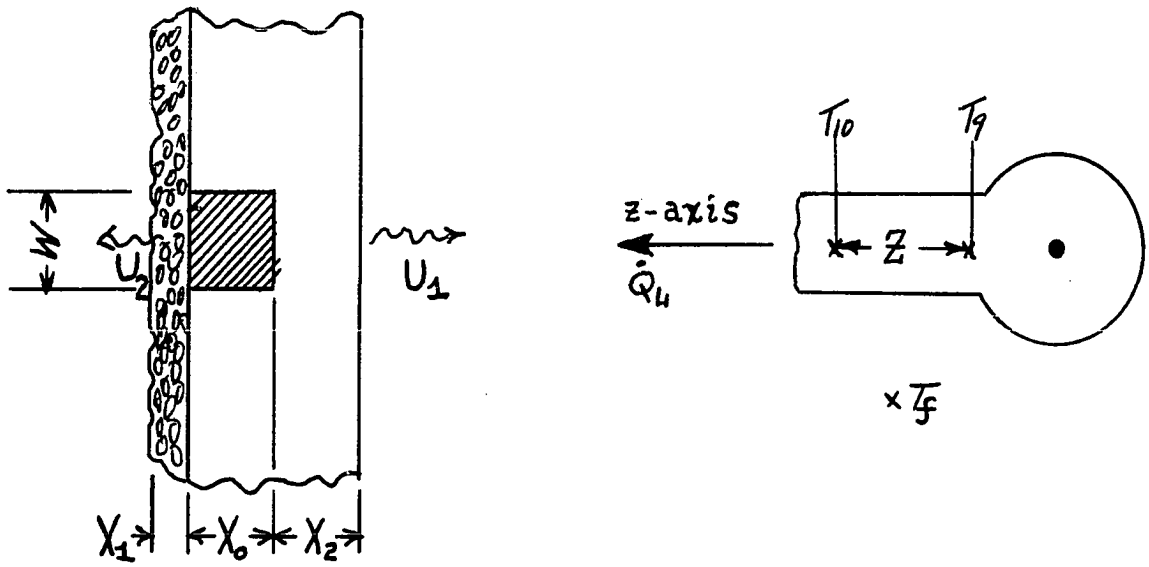

Figure B3. Cross Section of Rectangular Lead

heat is lost from the top and bottom faces, and a temperature θ is defined by (B-1),

$$\theta \equiv T - T_f \tag{B-1}$$

The differential equation to be solved is

$$\frac{d^2\theta}{dz^2} - \left(\frac{U_1 + U_2}{k_o X_o} \right) \theta = 0 \tag{B-2}$$

with boundary conditions

$$\begin{aligned} Z &= 0 \quad \text{at} \quad T = T_9 \\ Z &= \infty \quad \text{at} \quad T = T_f \end{aligned} \tag{B-3}$$

Define

$$B \equiv \frac{U_1 + U_2}{k_o X_o} \tag{B-4}$$

The solution to (B-2) and (B-3) is

$$\theta = \theta_9 e^{-\sqrt{B}\, z} \tag{B-5}$$

Since the temperature θ_{10} was measured at $z = Z$, the unknown B can be calculated from (B-6).

$$\sqrt{B} = -\left[\frac{1}{Z} \ln \frac{\theta_{10}}{\theta_9} \right] \tag{B-6}$$

The heat loss is equal to the amount of heat crossing the plane at $z = 0$:

$$\dot{Q}_L = -k_o (WX_o) \left. \frac{d\theta}{dz} \right|_{z=0} \tag{B-7}$$

which becomes

$$\dot{Q}_L = \theta_9 (Wk_o X_o) \sqrt{B} \tag{B-8}$$

Extracting h from B

It can be assumed that the heat transfer coefficient h is the same on both faces of the plate. In this event, equation (B-4) can be written:

$$k_o X_o B = U_1 + U_2 = \left(\frac{1}{h} + \frac{X_1}{k_1} \right)^{-1} + \left(\frac{1}{h} + \frac{X_2}{k_2} \right)^{-1} \tag{B-9}$$

Make the following substitutions:

$$\begin{aligned} c &\equiv Bk_o X_o \\ a &\equiv X_1/k_1 \\ b &\equiv X_2 k_2 \end{aligned} \qquad \text{(B-10)}$$

Equation (B-9) becomes:

$$c = \frac{h}{1 + ah} + \frac{h}{1 + bh} \qquad \text{(B-11)}$$

Some algebra results in equation (B-12):

$$h = \frac{2c}{2 - c(a + b) + \sqrt{c^2 (a - b)^2 + 4}} \qquad \text{(B-12)}$$

Having obtained h, U_1 can be calculated and assumed to hold constant over the circular part of the copper lead.

Calculation of Heat Loss $\dot{Q}_E$

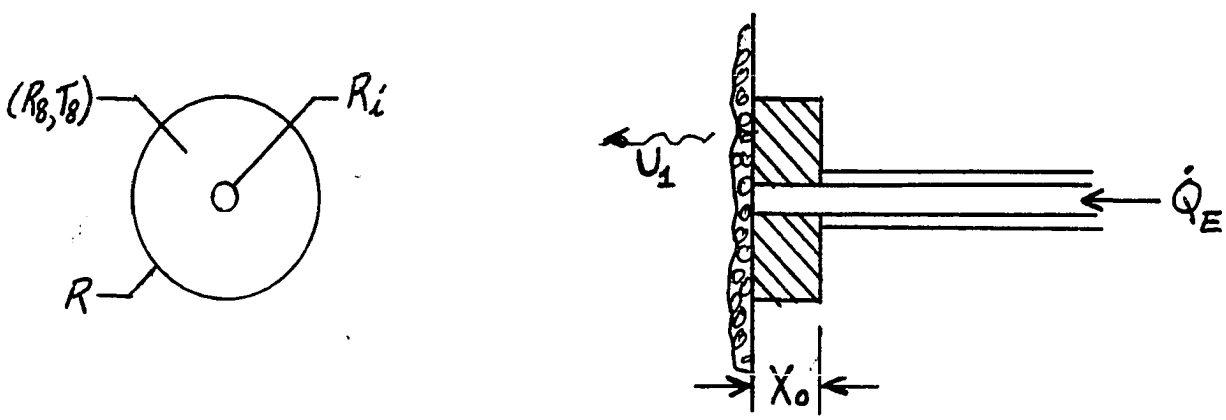

Figure B4. Idealization of Circular Part of Electrical Lead

To approximate the loss from the circular part of the lead, the presence of the rectangular part is neglected. This approximation will lead to a conservative (high) estimate of the total end losses. It is assumed that heat is lost from the face according to the same coefficient U_1 calculated for the rectangular part. It is also assumed that no heat is lost from the edge of the lead (through the transite block). The equation for heat transfer through an annular ring is

$$d\dot{Q}_E = -U_1 \theta (2\pi r\, dr) \tag{B-13}$$

Fourier's law is

$$\dot{Q}_E = -k_o (2\pi r X_o) \frac{d\theta}{dr} \tag{B-14}$$

so that the differential equation to be solved is

$$\frac{d^2\theta}{dr^2} + \frac{1}{r}\frac{d\theta}{dr} - \left(\frac{U_1}{X_o k_o}\right)\theta = 0 \tag{B-15}$$

with boundary conditions

$$\begin{aligned} r &= R_8 \quad \text{at} \quad \theta = \theta_8 \\ r &= R \quad \text{at} \quad \frac{d\theta}{dr} = 0 \end{aligned} \tag{B-16}$$

Define

$$B_1 = \frac{U_1}{k_o X_o} \tag{B-17}$$

The general solution of (B-15) with positive B_1 is

$$\theta = c_1 I_o(r\sqrt{B_1}) + c_2 K_o(r\sqrt{B_1}) \qquad \text{(B-18)}$$

where I_n and K_n are modified Bessel functions of order n of the first and second kinds, respectively.

From the second boundary condition,

$$0 = c_1 I_1(R\sqrt{B_1}) - c_2 K_1(R\sqrt{B_1}) \qquad \text{(B-19)}$$

and from the first boundary condition,

$$\theta_8 = c_1 I_o(R_8\sqrt{B_1}) + c_2 K_o(R_8\sqrt{B_1}) \qquad \text{(B-20)}$$

The constants can be calculated from equations (B-21) and (B-22)

$$c_1 = \frac{\theta_8 K_1(R\sqrt{B_1})}{I_o(R_8\sqrt{B_1})K_1(R\sqrt{B_1}) + K_o(R_8\sqrt{B_1})I_1(R\sqrt{B_1})} \qquad \text{(B-21)}$$

$$c_2 = \frac{c_1 I_1(R\sqrt{B_1})}{K_1(R\sqrt{B_1})} \qquad \text{(B-22)}$$

The end loss $\dot{Q}_E$ is obtained from equation (B-23):

$$\dot{Q}_E = -k\,(2\pi R_1)\chi_o \left(\frac{d\theta}{dr}\right)\Big|_{r=R_1} \qquad \text{(B-23)}$$

which is equivalent to:

$$\dot{Q}_E = -k_o X_o (2\pi R_i) \sqrt{B_1} \left[c_1 I_1 (R_i \sqrt{B_1}) - c_2 K_1 (R_i \sqrt{B_1}) \right] \tag{B-24}$$

The total losses from the heater are $2(\dot{Q}_E + \dot{Q}_L)$, where $\dot{Q}_L$ was given by (B-8) and $\dot{Q}_E$ by (B-24).

An example of some of the results is shown in Table B-1. The percentage loss peaks just before the ends go into film boiling. Since the portion of the lead near the graphite rod is hotter than the boiling surface, the peak in end losses occurs considerably before the heater surface goes into film boiling.

TABLE B-1

EXAMPLE OF RESULTS OF END LOSS CALCULATIONS

Data No.	$\dot{Q}_E$ Btu/hr	$\dot{Q}_L$ Btu/hr	Total Losses Btu/hr	Percent Losses
702	23.8	20.0	87.7	3.36
703	3.7	0	7.4	0.78
704	57.6	37.0	189.2	7.20
705	107.6	75.1	365.4	6.76
706	132.7	94.6	454.7	6.72
707	8.0	0	16.0	1.66
708	95.4	52.1	295.1	11.24
709	132.2	89.4	443.2	8.17
710	147.4	101.6	498.0	7.06
711	142.8	106.8	499.2	6.31
712	13.2	0	26.3	2.75

Effect of End Losses on the Flux Near the Center of the Heater

A problem of this type has been developed by Jacob (Heat Transfer, Vol. 1 (1949), Sec. 12-13). Figure B5

illustrates the model. This development is similar as far as equation (B-30).

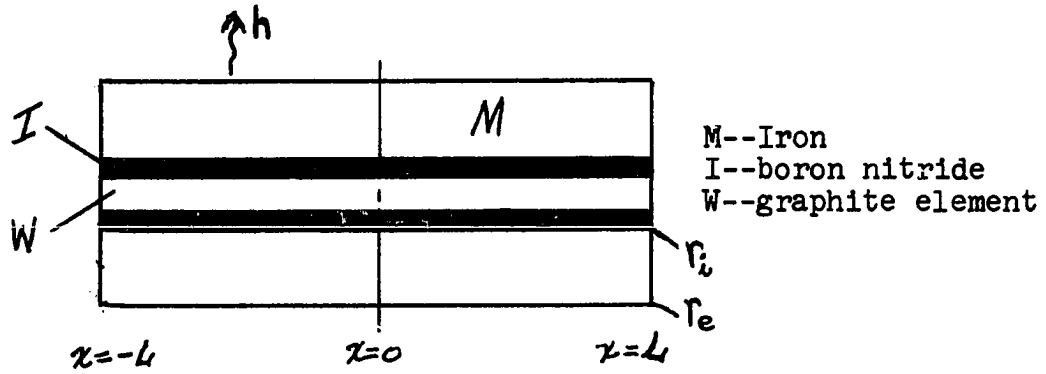

Figure B5. Diagram of Heater

Assume that the axial heat loss from M is negligible but that the loss from the heating element and boron nitride must be considered. The justification for this assumption is that the round part of the lead (#5 in Figure B1) was always observed to be hotter than the heater body M at the same radius. Also assume that temperature is only a function of x.

If the surface heat transfer coefficient, h, is uniform, and the mean conductivity of the iron is k_m, the following term may be defined:

$$(hc)_a = \frac{k_m(2\pi)}{\ln (r_e/r_i)} \qquad \text{(B-25)}$$

Also define

$$(kA)_a = k_I A_I + k_W A_W \qquad \text{(B-26)}$$

where A is axial cross-sectional area, and define the <u>total</u>

rate of heat production per unit time in the rod length 2L as $\dot{Q}_T/2L$.

The basic equation is then, according to Jacob,

$$-(kA)_a \frac{dT}{dx} + \frac{\dot{Q}_T}{2L} dx = -(kA)_a \left(\frac{dT}{dx} + \frac{d^2T}{dx^2} dx \right) + (hc)_a (T - T_W) dx \tag{B-27}$$

where T_W is the surface temperature (at $r = r_e$).

Now define

$$\theta \equiv T - T_W \tag{B-28}$$

where the region of W and I is assumed to be at temperature T(x), and

$$M_a^2 = \frac{(hc)_a}{(kA)_a} \tag{B-29}$$

Equation (B-27) becomes

$$\frac{d^2\theta}{dx^2} = M_a^2 \theta - \frac{(\dot{Q}_T/2L)}{(kA)_a} \tag{B-30}$$

The boundary conditions are:

$$\frac{d\theta}{dx} = 0 \text{ at } x = 0 \tag{B-31}$$

because the temperature profile is symmetric about the center (x = 0), and, because heat is <u>conducted</u> from the region (I,W) at the ends,

$$\frac{d\theta}{dx} = -\frac{\dot{Q}}{(kA)_a} \text{ at } x = L \tag{B-32}$$

where $\dot{Q}$ is the end loss from the areas W and I at one end. The solution to (B-30) is

$$\theta = Me^{-M_a x} + Ne^{M_a x} + \frac{(\dot{Q}_T/2L)}{(kA)_a M_a^2} \qquad \text{(B-33)}$$

which combines with (B-31) and (B-32) to give (B-34).

$$\theta = \frac{-\dot{Q}}{M_a(kA)_a} \frac{\cosh (M_a x)}{\sinh (M_a L)} + \frac{(\dot{Q}_T/2L)}{(kA)_a M_a^2} \qquad \text{(B-34)}$$

Now suppose that the fraction of the end loss, $\mathfrak{L}$, is known:

$$\mathfrak{L} \equiv \frac{2\dot{Q}}{Q_T} \qquad \text{(B-35)}$$

Then (B-34) becomes

$$\theta = \frac{(\dot{Q}_T/2)}{(kA)_a M_a} \left\{ \frac{1}{M_a L} - \mathfrak{L} \frac{\cosh (M_a x)}{\sinh (M_a L)} \right\} \qquad \text{(B-36)}$$

at $x = 0$, $\theta = \theta_o$, so that (B-36) gives (B-37),

$$\theta_o = \frac{(\dot{Q}_T/2)}{(kA)_a M_a} \left\{ \frac{1}{M_a L} \quad \frac{\mathfrak{L}}{\sinh (M_a L)} \right\} \qquad \text{(B-37)}$$

Dividing (B-36) by (B-37) gives

$$\frac{\theta}{\theta_o} = \frac{(1/M_aL)\ \sinh\ (M_aL) - \mathfrak{L}\ \cosh\ (M_ax)}{(1/M_aL)\ \sinh\ (M_aL) - \mathfrak{L}} \qquad \text{(B-38)}$$

Example Calculation

(1) $\dot{Q} = 10{,}700$ Btu/hr $\qquad L = 0.167$ ft

$\dot{Q}/2L = 32{,}100$ Btu/ft-hr

(2) $k_M = 42$ Btu/ft-hr-F° $\qquad A_W = 0.0000213\ ft^2$

$k_I = 15$ Btu/ft=hr-F° $\qquad A_I = 0.0000437\ ft^2$

$k_W = 79$ Btu/ft-hr-F° $\qquad (A_W + A_I) = 0.0000650\ ft^2$

$r_e = 0.0338$ ft

$r_i = 0.00455$ ft

(3) $(kA)_a = 0.00234$ Btu-ft/hr-F° (from B-26)

(4) $(hc)_a = 132$ Btu/ft-hr-F° (from B-25)

(5) $M_a^2 = 56{,}400/ft^2$ (from B-29)

(6) $M_a = 238/ft$; $\qquad (1/M_aL) = 0.0252$; $\qquad M_aL = 39.8$

(7) $\sinh\ (M_aL) \approx \frac{e^{39.8}}{2}$

Now equation (B-38) becomes

$$\frac{\theta}{\theta_o} = \left[\frac{0.0126\ e^{39.8} - \mathfrak{L}\ \cosh\ (238x)}{0.0126\ e^{39.8} - \mathfrak{L}} \right]$$

$\mathfrak{L}$ is a fraction (usually less than 0.10), and negligible in comparison with e^{40}. Therefore, (B-38) can be simplified:

$$\frac{\theta}{\theta_o} \approx 1 - (M_a L)\mathfrak{L} \exp [M_a x - M_a L]$$

as long as exp $(-M_a x)$ is much smaller than exp $(+M_a x)$. The temperatures were measured at about x = 2/3 inch, or 0.0555 ft, so that

$$\frac{\theta}{\theta_o} \approx 1 - (39.8)(\mathfrak{L})e^{-26.6}$$

It can be seen that an end loss of even 10% does not affect the temperatures near the center of the heater.

APPENDIX C

THERMOCOUPLE CALIBRATION

Calibration of the thermocouples was done in two parts. First, one fluid temperature thermocouple (No. 2) was standardized against the vapor pressure curves. Then all other thermocouples were calibrated against No. 2.

Standardization of No. 2 Thermocouple

The data in this work were recorded in groups of up to ten points at a given pressure. For about two hundred of these sets of measurements, T_2 was averaged. The difference

$$\Delta_2 \equiv \langle T_2 \rangle - T_{sat} \qquad \text{(C-1)}$$

was plotted vs. T_{sat}, where $\langle\ \rangle$ denotes an averaged temperature and T_{sat} was calculated from the vapor pressure relationship described in Appendix A.

A curve was drawn through these points which is described by equations (C-2) and (C-3). Temperatures are in degrees Fahrenheit.

$$\Delta_2 = 0.025\ T_{sat} + 1.5 \qquad T_{sat} \leq -50°F \qquad \text{(C-2)}$$

$$\Delta_2 = -0.003367\ T_{sat} - 0.17 \qquad T_{sat} > -50°F \qquad \text{(C-3)}$$

The scatter of these points ranged from $\pm$ 1°F at -260°F to $\pm$ 0.5°F at +260°F. This scatter reflects errors in the pressure readings as well as measuring instrument errors.

Correction of T_2

Each "data point" consisted of 15-16 temperatures. The temperature T_2 was corrected by a simple algorithm. For example, if $T_2 < -50°F$:

$$\Delta_2 \leftarrow 0.025T_2^o + 1.5$$

$$T^* \leftarrow T_2^o - \Delta_2$$

$$\Delta_2 \leftarrow 0.025T^* + 1.5$$

$$T_2 \leftarrow T_2^o - \Delta_2$$

The symbol "←" means "is replaced by." This algorithm comes from an alternate way of defining Δ_2:

$$\Delta_2 \equiv T_2^o - T_2 \qquad \text{(C-4)}$$

where T_2^o is the observed temperature and T_2 is the correct temperature. Equation (C-4) is equivalent to (C-1) if T_{sat} is the correct temperature and only one reading T_2^o is taken.

Correction of Other Temperatures

The other two fluid temperature thermocouples (T_1 and T_3) were not corrected since their only function was to confirm that the fluid in the vessel was at a uniform temperature: e.g., that the system was in equilibrium.

The remaining thirteen thermocouples were corrected using the same algorithm, but their deltas were defined by (C-5), where T_2 is the corrected value.

$$\Delta_i \equiv T_i^o - T_2 \qquad (4 \leq i \leq 16) \qquad \text{(C-5)}$$

These Δ_is were measured at five temperatures by periodically comparing T_2 with T_1. Table C-1 lists the average values. The location of each measurement is shown in Table C-2.

TABLE C-1

DIFFERENCES OF THERMOCOUPLES FROM THE STANDARD THERMOCOUPLE

i	Correct Temperature -256°F	-121°F	-43°F	+74°F	+171°F
			Δ_i		
4	-6.58	-2.20	-0.24	-0.45	-0.66
5	0.92	1.01	0.26	-0.56	-0.72
6	1.34	1.34	-0.35	-0.41	-0.79
7	----	2.05	0.43	-0.54	-1.21
8	0	0.92	-0.69	-0.57	-1.04
9	-12.98	-6.66	-1.68	0.15	-0.05
10	-9.89	-5.32	-1.40	0.06	-0.29
11	-0.99	-1.83	0.82	0.10	-0.58
12	-11.11	-5.82	-0.85	0.07	-0.05
13	-10.98	-5.12	-1.01	-0.06	-0.12
14	-11.20	-4.99	-1.02	0.16	-0.21
15	-9.64	-3.90	-0.77	0.10	----
16	-10.73	-4.37	-0.74	-0.19	-0.25

TABLE C-2

LOCATION OF THERMOCOUPLES
(See Figure 4 for Dimensions)

Position in Inner Ring	i	Position in Outer Ring	i	End Bracket (See Appendix B)	i
12 o'clock	4	2 o'clock	11	nearest heater	
3 o'clock	5	4 o'clock	12	center	8
6 o'clock	6	6 o'clock	13	center	9
9 o'clock	7	8 o'clock	14	outermost	10
		10 o'clock	15		
		12 o'clock	16		

The proper Δ_i was determined by linear interpolation between the tabular values.

All of these corrections were done on the computer, of course, since about 10,000 temperatures had to be corrected in this way.

APPENDIX D

DATES OF EXPERIMENTAL RUNS AND COMMENTS

Runs 1 through 5 were primarily to check out the system, and after run 5 the heater was removed and two thermocouple pins were drilled out and replaced. Data on runs 1-5 were discarded, since they were not on a consistent basis with the remaining data.

Nucleate boiling runs are listed in Table D-1 and film boiling runs in Table D-2.

Position of the thermocouples referred to in the tables was as follows:

	O'clock Position	
	All runs except 39 and 40	Runs 39 and 40 (Heater rotated and switched end for end)
Inner Ring		
4	12	6
5	3	3
6	6	12
7	9	9
Outer Ring		
11	2	4
12	4	2
13	6	12
14	8	10
15	10	8
16	12	6

TABLE D-1

NUCLEATE BOILING RUNS

Run No.	Date (1966)	Component	Comments
6	Feb. 8	n-butane	Discarded points 1-4; insufficient surface preparation.
7	Feb. 10	propane	
8	Feb. 11	propane	Switched from potentiometer to digital voltmeter to measure temperature
9	Feb. 18	propane	Switched from water to liquid nitrogen cooling.
10	Feb. 20	propane	
11	Feb. 22	propane	
12	Feb. 24	ethane	
13	Feb. 25	ethane	
14	Feb. 26	ethane	
15	Feb. 28	ethane	
16	March 1	ethane	
17	March 2	ethane	
18	March 4	n-butane	
19	March 6	n-butane	
20	March 8	methane	
21	March 12	methane	T.C. #5 and #16 shorted to electrical system. Had to replace extension wires but not thermocouples. Heater not removed.
22	March 14	methane	

TABLE D-1--Continued

Run No.	Date (1966)	Component	Comments
23	March 15	methane	
24	March 17	methane	Deleted Point No. 19--leak dropped liquid level.
25	March 25	methane	Ended nucleate boiling data with Point No. 9.
38	April 17	n-butane	Run to check for hysteresis effects. Reversed direction of current through heater.
39	April 20	n-butane	Inner ring (T.C. #4,5,6, 7) cut off; heater rotated 180° and switched end for end.

TABLE D-2

FILM BOILING RUNS

Run No.	Date (1966)	Component	Comments
25	March 8	methane	film boiling points 10-23. Film boiling has caused surface to darken in color. Heating element failed and was replaced.
26	March 22	methane	Heating element failed and was replaced.
27	March 29	methane	Extension wires on T.C. #15 had to be repaired.
28	April 1	methane	
29	April 2	ethane	Extension wire on T.C. #15 repaired again.
30	April 3	ethane	
31	April 4	ethane	
32	April 6	propane	Heating element failed and was replaced.
33	April 9	propane	
34	April 11	propane	Heating element failed and was replaced. T.C. #13 was broken permanently.
35	April 14	propane	
36	April 15	butane	
37	April 16	butane	
40	April 29	methane	run to recheck methane low temperature data

APPENDIX E

MAXIMUM NUCLEATE BOILING (BURNOUT) DATA

TABLE E-1

METHANE BURNOUT DATA

Run No.	Data Point No.	Reduced Pressure P/P_c	Critical Flux q_{lc} M Btu/ft^2-hr
22	B1	.354	147
22	B2	.409	112
23	B1	.050	101
23	B2	.092	117
23	B3	.150	148
23	B4	.131	131
24	B1	.199	144
24	B2	.400	130
24	B3	.360	138
24	B4	.533	105
24	B5	.475	120
24	B6	.631	93
24	B7	.770	65
25	B1	.089	122
25	B2	.776	63
25	B3	.820	54
25	B4	.874	39
25	B5	.920	27

TABLE E-2

ETHANE BURNOUT DATA

Run No.	Data Point No.	Reduced Pressure P/P_c	Critical Flux q_{lc} M Btu/ft^2-hr
12	B1	.021	85
12	B2	.050	111
13	B1	.570	131
13	B2	.451	150
13	B3	.313	159
14	B1	.100	129
14	B2	.150	139
14	B3	.204	147
15	B1	.300	155
15	B2	.496	141
16	B1	.472	147
16	B2	.441	152
16	B3	.539	132
16	B4	.677	104
17	B1	.599	121
17	B2	.691	99
17	B3	.810	66
17	B4	.853	51
17	B5	.890	38

TABLE E-3

PROPANE BURNOUT DATA

Run No.	Data Point No.	Reduced Pressure P/P_c	Critical Flux q_{1c} M Btu/ft^2-hr
7	B1	.538	108
7	B2	.500	117
7	B3	.478	115
7	B4	.591	96
7	B5	.682	77
7	B6	.700	70
7	B7	.774	54
7	B8	.849	37.3
7	B9	.935	18.1
8	B1	.476	121
9	B1	.400	132
9	B2	.275	135
10	B1	.021	66
10	B2	.050	94
10	B3	.100	114
11	B1	.146	121
11	B2	.196	126
11	B3	.300	136

TABLE E-4

n-BUTANE BURNOUT DATA

Run No.	Data Point No.	Reduced Pressure P/P_c	Critical Flux q_{1c} M Btu/ft^2-hr
1*	B1	.734	86
3*	B1	.500	97
4*	B1	.301	126
4*	B2	.399	92
6	B1	.150	100
6	B2	.200	101
6	B3	.147	93
6	B4	.202	102
6	B5	.300	109
6	B6	.400	109
6	B7	.500	107
6	B8	.600	83
6	B9	.700	65
6	B10	.800	46.2
6	B11	.919	19.9
8	B1	.143	104
8	B2	.200	111
8	B3	.147	100
8	B4	.151	101
9	B1	.100	96
9	B2	.027	65
9	B3	.050	82
9	B4	.027	67
9	B5	.300	117
9	B6	.459	108

*Burnout data were kept for runs 1-4 even though the nucleate boiling data were discarded. This is because surface changes are not supposed to affect the critical flux but do affect the nucleate boiling ΔT.

APPENDIX F

MINIMUM FILM BOILING DATA

The true minimum film boiling flux will lie somewhere between the lowest observed film boiling flux q_F and the flux q_T when the transition occurred. The minimum film boiling temperature difference, ΔT_{2c}, was not always observed.

Table F-1 presents the data. The nomenclature and units used in the table are:

Data No.	Run Number plus the point in the run. For example, 30M4 is the fourth observed transition in run 30.	
K	1--methane	2--ethane
	3--propane	4--n-butane
P	pressure, psia	
q_T, q_F	Btu/ft^2-hr; see above for explanation	
ΔT_{2c}	degrees F	

TABLE F-1

MINIMUM FILM BOILING DATA

Data No.	K	P	q_T	q_F	ΔT_{2c}
25M1	1	538	6,600	10,300	---
26M1	1	33	7,000	11,000	---
26M2	1	135	13,300	19,700	---
28M1	1	336	13,200	13,200	125
29M1	2	65	9,300	10,800	---
30M1	2	75	11,100	14,900	---
30M2	2	135	15,700	15,700	---
30M3	2	145	17,300	17,300	---
30M4	2	290	21,600	26,000	---
31M1	2	213	17,100	19,700	218
33M1	3	450	13,000	17,200	94
33M2	3	370	18,000	31,900	---
34M1	3	345	20,700	22,900	204
35M1	3	31	12,400	16,400	89
35M2	3	93	18,600	21,500	---
35M3	3	124	20,200	27,200	---
35M4	3	200	24,300	26,500	---
35M5	3	265	23,300	24,800	---
35M6	3	247	22,100	26,700	226
36M1	4	28	12,600	18,100	---
36M2	4	55	16,500	20,300	---
36M3	4	110	20,400	27,100	253
36M4	4	165	22,900	27,300	252
36M5	4	220	25,000	25,000	240
37M1	4	345	17,500	27,700	145
37M2	4	300	20,700	20,700	177

APPENDIX G

CORRECTIONS TO NUCLEATE BOILING DATA FOR THE EFFECT OF FLUX ON THERMOCOUPLE READINGS

Introduction

As mentioned in Chapter VI, some of the individual temperatures show regular deviations with increasing flux, even though many precautions were taken to minimize this effect.

The relevant equation was developed in Chapter IV. It is assumed that whatever the reason that thermocouple "i" is giving incorrect readings, the difference will manifest itself in the same way as a small displacement of the thermocouple bead. In other words,

$$(T_i^* - T_i) = (r_i - r_i^*)\left[\frac{q(D/D_i)}{k}\right] \qquad (4\text{-}19)$$

where the observed temperature T_i^* is at some unknown radius r_i^* and the "correct" temperature T_i is at the known radius r_i. D is the heater diameter, q is the surface flux (known) and k is the thermal conductivity of the metal. The derivation of this equation assumed that r_i and r_i^* were very near each other.

The difficulty with (4-19) is that neither T_i nor r_i^* is known, but only one equation is available to work with.

There are, however, several temperature measurements around each ring. As a first approximation it is assumed that the average temperature $\langle T \rangle$ of that ring is the correct value. Now a plot of $(T_i^* - \langle T \rangle)$ vs. $\left[\frac{q(D/D_i)}{k}\right]$ is made.

Figure G1 shows such a graph for the four inner-ring

thermocouples during Run 18. (Run 18 was selected because it was a butane run made in about the middle of the data-taking. Butane is better for this purpose because thermocouple calibration corrections (Appendix C) are negligible at these temperatures.) All of the thermocouples except No. 6 do show a linear relationship, although the intercepts are not all zero. (This discrepancy is because $\langle T \rangle$ is not really the correct temperature.)

To correct the temperatures, one need only find the slopes $m_i \equiv (r_i - r_i^*)$. Then

$$T_i = T_i^* - m_i \left[\frac{q(D/D_i)}{k} \right] \qquad \text{(G-1)}$$

The correction can subsequently be improved by correcting only the largest deviations and repeating the process with the new $\langle T \rangle$.

The slopes used to make the final corrections are listed in Table G-1, with their equivalent displacement error expressed in thousandths of an inch. One bead diameter is about 0.010 inch. It is apparent that these errors, on average, were small: negligible change for the inner ring and -0.0125 inch on average for the outer ring.

The smoothing effect of these changes is very important if not all temperatures are measured at a given point. For example, thermocouples No. 15 and No. 7 were sometimes used as a monitor and were not recorded. The uncorrected average would then not be on the same basis as the rest of

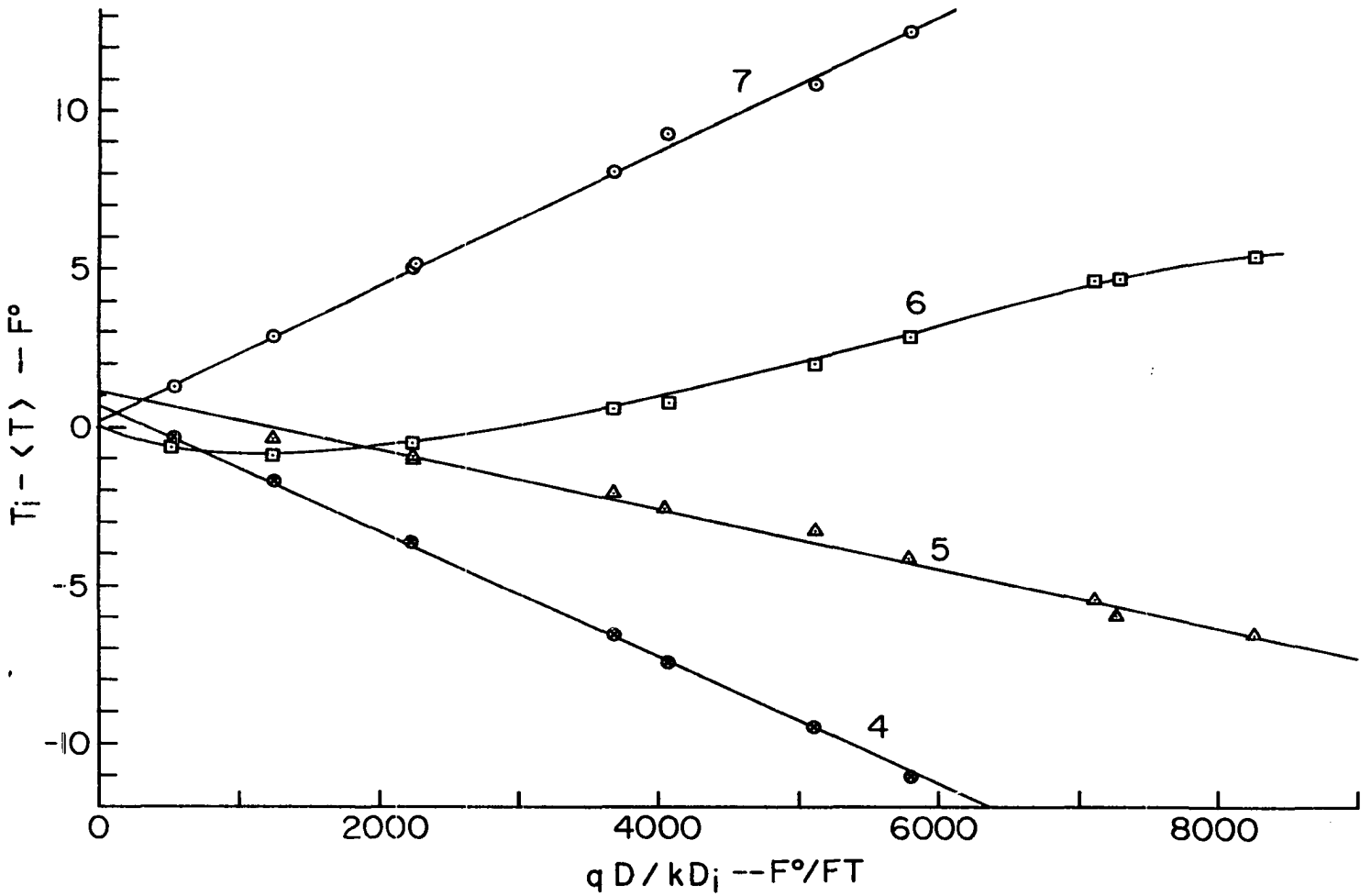

Figure G1. Deviations of Inner Ring Thermocouples from the Average Inner Ring Temperature during Run 18

the data, but the corrected values are. The procedure is not merely a smoothing procedure, however, since the averages were changed slightly. The net effects are: (a) The slope of the log q vs. log ΔT lines in nucleate boiling are slightly increased. (b) Individual temperatures are smoothed so that the absence of one or more individual measurements will not distort the average.

TABLE G-1

SLOPES m_i USED WITH EQUATION (G-1)
TO CORRECT THERMOCOUPLE READINGS

Thermo-couple	Clock Position	m_i (feet)	Apparent Displacement Error in Thousandths of an Inch
		Inner Ring	
4	12	-0.00199	+23.9
5	3	-0.000944	+11.3
6	6	+0.00075	-9.0
7	9	+0.00212	-25.4
		Outer Ring	
11	2	-0.00055	+6.6
12	4	-------	0
13	6	+0.00320	-38.4
14	8	+0.00135	-16.2
15	10	+0.00170	-20.4
16	12	-------	0

Examples of the data before and after the changes are given in Tables G-2 and G-3. It should be emphasized that these changes were not a cure-all. Not all runs were affected the same. However, a considerable smoothing effect

was seen for all runs.

For other examples, see Appendix K.

TABLE G-2

EXAMPLE OF SMOOTHING EFFECT OF EQUATION (G-1) APPLIED TO INNER RING THERMOCOUPLES*

Data No.	$\frac{q(D/D_i)}{k}$		$T_4 - \langle T \rangle$	$T_5 - \langle T \rangle$	$T_6 - \langle T \rangle$	$T_7 - \langle T \rangle$
1301	447	Before	0.3	-0.8	-0	+0.5
		After	1.2	-0.4	-0.3	-0.5
1302	1032	Before	-1.0	-0.4	-0.8	2.2
		After	1.0	0.6	-1.6	0
1303	2044	Before	-2.7	-0.7	-0.9	4.3
		After	1.4	1.2	-2.5	-0.1
1304	3513	Before	-6.0	-1.5	1.9	5.7
		After	0.9	1.8	-0.8	-1.8
1305	5124	Before	-11.3	-4.2	1.6	13.9
		After	-1.2	0.6	-2.3	2.9
1306	5041	Before	-11.1	-2.0	3.7	9.5
		After	-1.2	2.7	-0.1	-1.3
1307	6725	Before	-15.0	-3.1	5.4	12.6
		After	-1.8	3.2	0.3	-1.8

*m_i used are listed in Table G-1. The m_i were determined from Run 18.

TABLE G-3

EXAMPLE OF SMOOTHING EFFECT OF EQUATION (G-1) APPLIED TO OUTER RING THERMOCOUPLES*

Data No.	$\frac{q(D/D_i)}{k}$		$T_{xx} - \langle T \rangle$				
			T_{11}	T_{12}	T_{13}	T_{14}	T_{16} **
1301	179	Before	0.5	-1.0	-0.4	0.5	0.5
		After	0.7	-0.9	-0.9	0.4	0.7
1302	409	Before	0.7	-1.1	0.1	0.5	-0.2
		After	1.2	-0.8	-0.9	0.3	0.1
1303	791	Before	0.0	-2.1	1.8	1.3	-0.9
		After	1.1	-1.5	-0.1	0.9	-0.3
1304	1310	Before	-0.4	-2.4	3.4	1.6	-2.2
		After	1.3	-1.4	0.3	0.9	-1.1
1305	1905	Before	-2.4	-3.7	5.6	1.5	-1.0
		After	0.2	-2.2	0.9	0.5	0.6
1306	1874	Before	-0.3	-2.7	4.5	1.2	-2.7
		After	2.2	-1.2	-0.1	0.2	-1.2
1307	2496	Before	-0.6	-3.1	6.5	1.2	-4.0
		After	2.8	-1.1	0.4	-0.2	-2.0

*m_i used are listed in Table G-1. The m_i were determined principally from Run 18.

**T_{15} was not measured--used as monitor during this run.

APPENDIX H

NUCLEATE BOILING DATA

Tables H-1 through H-5 list the nucleate boiling data in the following form:

Data No.	Run Number plus data point in run: 2008 means run 20, point number 8.
P	Pressure, psia
Pr	Reduced Pressure
T_w	Average surface temperature in degrees F, calculated from the outer ring thermocouples
q	Average flux, Btu/ft^2-hr
ΔT	$T_w - T_{sat}$, degrees F

T_w has been slightly corrected at high fluxes as explained in Appendix G.

The surface referred to in Table H-5 was fouled during film boiling, which deposited some carbon on the surface.

TABLE H-1

METHANE NUCLEATE BOILING DATA

Data No.	P	Pr	T_w	q	ΔT
2001	14.7	.022	-245.6	7110	13.2
2002	14.7	.022	-239.5	16800	19.3
2003	14.7	.022	-235.4	29000	23.4
2004	14.7	.022	-232.8	43400	26.0
2005	14.7	.022	-232.4	49600	26.4
2006	33.7	.050	-228.7	6800	9.7
2007	33.7	.050	-223.5	16500	14.9
2008	33.7	.050	-220.0	29800	18.5
2009	33.7	.050	-216.3	47200	22.2
2010	33.7	.050	-216.8	65100	21.7
2011	33.7	.050	-216.1	79900	22.4
2012	67.3	.100	-209.2	6620	9.2
2101	14.7	.022	-243.4	7050	15.4
2102	14.7	.022	-239.7	16200	19.1
2103	14.7	.022	-239.2	28200	19.6
2104	14.7	.022	-240.0	16100	18.8
2105	14.7	.022	-238.3	28100	20.5
2106	14.7	.022	-237.8	44200	21.0
2201	202.0	.300	-171.6	6910	6.1
2202	202.0	.300	-170.6	16800	7.1
2203	202.0	.300	-169.0	27800	8.7
2204	202.0	.300	-166.9	45300	10.8
2205	202.0	.300	-166.3	62900	11.4
2206	202.0	.300	-166.3	92600	11.4
2207	202.0	.300	-164.7	117000	13.0
2208	202.0	.300	-165.0	134000	12.7
2209	202.0	.300	-164.4	140000	13.3
2210	269.0	.400	-158.9	6890	6.0
2211	269.0	.400	-156.6	18800	8.3
2212	269.0	.400	-155.4	34400	9.5
2213	269.0	.400	-155.2	52600	9.7
2214	269.0	.400	-153.2	80300	11.7
2215	269.0	.400	-151.2	104000	13.7
2301	14.7	.022	-244.1	6760	14.7
2302	14.7	.022	-239.7	15600	19.1
2303	14.7	.022	-237.2	27500	21.6
2304	14.7	.022	-233.8	50500	25.0
2305	14.7	.022	-231.9	64200	26.9
2306	33.7	.050	-227.1	6680	11.3
2307	33.7	.050	-223.5	17700	14.9
2308	33.7	.050	-220.9	33200	17.6
2309	33.7	.050	-216.4	77000	22.1
2310	33.7	.050	-215.0	94100	23.5
2311	67.3	.100	-210.2	6630	8.1

TABLE H-1--Continued

Data No.	P	Pr	T_w	q	ΔT
2312	67.3	.100	-207.1	18100	11.2
2313	67.3	.100	-205.3	32700	13.0
2314	67.3	.100	-203.2	56200	15.1
2315	67.3	.100	-201.5	86300	16.8
2316	67.3	.100	-200.6	109000	17.8
2317	101.0	.150	-197.5	6800	7.2
2318	101.0	.150	-194.9	18500	9.8
2319	101.0	.150	-193.3	33800	11.4
2320	101.0	.150	-191.2	54500	13.5
2321	101.0	.150	-188.9	82200	15.8
2322	101.0	.150	-187.3	106000	17.4
2323	101.0	.150	-186.1	126000	18.6
2324	134.6	.200	-188.2	6680	5.9
2325	134.6	.200	-185.7	18100	8.5
2326	134.6	.200	-184.5	33700	9.6
2327	134.6	.200	-181.3	59600	12.9
2328	134.6	.200	-179.4	82200	14.7
2401	134.6	.200	-186.9	6660	7.2
2402	134.6	.200	-185.1	18600	9.0
2403	134.6	.200	-183.8	34100	10.4
2404	134.6	.200	-181.0	58100	13.2
2405	134.6	.200	-179.0	80800	15.2
2406	134.6	.200	-176.9	108000	17.2
2407	134.6	.200	-175.1	132000	19.1
2408	269.0	.400	-159.2	6830	5.7
2409	269.0	.400	-157.8	18200	7.1
2410	269.0	.400	-156.4	32800	8.5
2411	269.0	.400	-154.2	60200	10.7
2412	269.0	.400	-151.5	85800	13.4
2413	269.0	.400	-149.4	119000	15.5
2414	336.5	.500	-148.0	16600	6.2
2415	336.5	.500	-147.1	31700	7.0
2416	336.5	.500	-145.1	58700	9.0
2420	404.0	.600	-140.2	7050	4.6
2421	404.0	.600	-140.4	16500	4.4
2422	404.0	.600	-139.8	27800	5.0
2423	404.0	.600	-139.0	42100	5.8
2424	404.0	.600	-137.9	55700	6.9
2425	404.0	.600	-137.2	70200	7.6
2426	404.0	.600	-136.2	84800	8.6
2427	471.0	.700	-133.2	7150	3.4
2428	471.0	.700	-133.1	16500	3.5
2429	471.0	.700	-133.8	27800	2.8
2430	471.0	.700	-132.2	45900	4.4
2431	471.0	.700	-131.3	65100	5.2
2432	538.5	.800	-126.9	6970	2.2

TABLE H-1--Continued

Data No.	P	Pr	T_w	q	ΔT
2433	538.5	.800	-126.7	16500	2.5
2501	538.5	.800	-125.4	6800	3.7
2502	538.5	.800	-125.2	16500	3.9
2503	538.5	.800	-125.4	27300	3.7
2504	538.5	.800	-125.1	37800	4.0
2505	538.5	.800	-125.0	53800	4.1
2506	606.0	.900	-120.3	7000	2.0
2507	606.0	.900	-121.1	16600	1.2
2508	606.0	.900	-121.1	22200	1.2
2509	606.0	.900	-121.1	27000	1.2

TABLE H-2

ETHANE NUCLEATE BOILING DATA

Data No.	P	Pr	T_w	q	ΔT
1201	14.7	.021	-108.9	7170	18.6
1202	14.7	.021	-103.1	14100	24.4
1203	14.7	.021	-100.7	21300	26.7
1204	14.7	.021	-98.2	29400	29.3
1205	14.7	.021	-93.6	44800	33.8
1206	14.7	.021	-92.2	60100	35.2
1207	14.7	.021	-92.0	72000	35.5
1208	35.5	.050	-79.8	7380	15.0
1209	35.5	.050	-76.4	16300	18.3
1210	35.5	.050	-72.4	29100	22.4
1211	35.5	.050	-68.4	59100	26.4
1212	35.5	.050	-66.9	80600	27.9
1213	35.5	.050	-64.4	94800	30.4
1214	70.9	.100	-54.2	7480	9.6
1215	70.9	.100	-51.0	16200	12.8
1216	70.9	.100	-49.0	30300	14.8
1217	70.9	.100	-45.1	66200	18.7
1301	70.9	.100	-54.1	7130	9.7
1302	70.9	.100	-51.5	16100	12.4
1303	70.9	.100	-48.9	30900	15.0
1304	70.9	.100	-46.6	50600	17.3
1305	70.9	.100	-44.1	72600	19.7
1306	70.9	.100	-44.1	71500	19.7
1307	70.9	.100	-43.0	94300	20.8
1308	106.4	.150	-36.0	7130	7.1
1309	106.4	.150	-33.3	16800	9.7
1310	106.4	.150	-31.8	29600	11.2
1311	106.4	.150	-28.5	65300	14.6
1312	106.4	.150	-26.4	81000	16.6
1401	70.9	.100	-52.8	9210	11.1
1402	70.9	.100	-49.1	23300	14.7
1403	70.9	.100	-45.5	44800	18.3
1404	70.9	.100	-43.9	65300	19.9
1405	70.9	.100	-41.5	94900	22.3
1406	106.4	.150	-34.9	12700	8.1
1407	106.4	.150	-32.0	29700	11.1
1408	106.4	.150	-29.6	53300	13.4
1409	106.4	.150	-28.5	82800	14.5
1410	106.4	.150	-28.0	109000	15.0
1411	141.8	.200	-20.3	13300	6.6
1412	141.8	.200	-18.9	29600	8.0
1413	141.8	.200	-16.9	54300	10.0
1414	141.8	.200	-14.5	86700	12.4
1415	141.8	.200	-13.9	120000	13.0

TABLE H-2--Continued

Data No.	P	Pr	T_w	q	ΔT
1501	213.0	.300	2.5	7270	4.5
1502	213.0	.300	3.8	17000	5.8
1503	213.0	.300	4.6	31000	6.6
1504	213.0	.300	4.6	43900	6.6
1505	213.0	.300	5.4	65800	7.4
1506	213.0	.300	5.6	87500	7.6
1507	213.0	.300	7.5	110000	9.5
1508	213.0	.300	9.2	138000	11.2
1509	213.0	.300	9.0	151000	11.0
1510	284.0	.400	21.4	12600	3.9
1511	284.0	.400	22.5	29400	5.1
1512	284.0	.400	22.9	65300	5.5
1513	284.0	.400	24.1	89200	6.6
1514	284.0	.400	25.1	116000	7.7
1601	354.0	.500	35.1	7390	1.7
1602	354.0	.500	35.8	17100	2.4
1603	354.0	.500	35.9	29500	2.6
1604	354.0	.500	36.0	45900	2.6
1605	354.0	.500	36.8	64200	3.5
1606	354.0	.500	37.8	88500	4.4
1607	354.0	.500	39.6	117000	6.2
1608	425.0	.600	48.5	7300	1.2
1609	425.0	.600	48.7	16700	1.4
1610	425.0	.600	48.6	30600	1.3
1611	425.0	.600	48.6	49300	1.3
1612	425.0	.600	49.1	71700	1.8
1701	425.0	.600	49.2	7090	1.9
1702	425.0	.600	49.0	15800	1.7
1703	425.0	.600	49.4	28800	2.1
1704	425.0	.600	49.7	46300	2.4
1705	425.0	.600	50.2	64600	2.9
1706	425.0	.600	51.4	91300	4.0
1707	425.0	.600	51.9	105000	4.6
1708	425.0	.600	52.7	117000	5.4
1709	496.0	.700	61.3	6950	1.6
1710	496.0	.700	61.3	17800	1.6
1711	496.0	.700	60.9	32800	1.3
1712	496.0	.700	61.4	50300	1.7
1713	496.0	.700	61.1	65700	1.5
1714	496.0	.700	62.6	91500	2.9
1715	567.0	.800	71.5	6930	.7
1716	567.0	.800	71.2	18400	.4
1717	567.0	.800	71.1	30900	.3
1718	567.0	.800	70.8	44400	0.0
1719	567.0	.800	71.3	59800	.5
1720	567.0	.800	71.6	65600	.8

TABLE H-2--Continued

Data No.	P	Pr	T_w	q	ΔT
1721	638.0	.900	80.6	6800	-.3
1722	638.0	.900	80.4	16500	-.5
1723	638.0	.900	80.6	29000	-.2

TABLE H-3

PROPANE NUCLEATE BOILING DATA

Data No.	P	Pr	T_w	q	ΔT
701	185.0	.300	105.8	13500	7.6
702	185.0	.300	108.9	36900	10.7
703	247.0	.400	127.4	13500	6.3
704	247.0	.400	129.8	37200	8.7
705	247.0	.400	132.8	76400	11.8
706	246.0	.400	134.4	95600	13.7
707	309.0	.500	145.7	13600	5.7
708	309.0	.500	147.9	37100	7.8
709	309.0	.500	150.7	76700	10.7
710	309.0	.500	152.6	99600	12.5
711	309.0	.500	154.0	112000	14.0
712	370.0	.600	160.6	13500	4.4
713	370.0	.600	162.2	37200	6.0
714	370.0	.600	165.5	77100	9.3
715	370.0	.600	166.7	90100	10.5
716	432.0	.700	174.0	13400	3.3
717	432.0	.700	176.1	37400	5.4
718	432.0	.700	176.6	51500	5.9
719	432.0	.700	177.6	70000	7.0
720	494.0	.800	185.8	13300	2.0
721	494.0	.800	189.2	27700	5.5
722	494.0	.800	188.3	37300	4.6
801	247.0	.400	125.3	7340	4.2
802	247.0	.400	128.1	15000	7.0
803	247.0	.400	129.2	29200	8.1
804	247.0	.400	131.5	65800	10.4
805	247.0	.400	133.7	95600	12.7
806	247.0	.400	138.5	121000	17.4
901	247.0	.400	125.4	7420	4.3
902	247.0	.400	127.1	13100	6.0
903	247.0	.400	129.1	29400	8.0
904	247.0	.400	131.0	49100	10.0
905	247.0	.400	131.2	74600	10.2
906	247.0	.400	124.5	7710	3.4
907	247.0	.400	127.4	17400	6.3
908	247.0	.400	128.9	30100	7.9
909	247.0	.400	130.1	45700	9.0
910	247.0	.400	132.0	65800	11.0
911	247.0	.400	134.7	94700	13.6
912	247.0	.400	139.7	114000	18.7
913	247.0	.400	140.0	123000	18.9
914	247.0	.400	140.8	129000	19.8
915	185.0	.300	104.1	7630	5.9
916	185.0	.300	106.2	14500	8.1
917	185.0	.300	107.7	23700	9.5

TABLE H-3--Continued

Data No.	P	Pr	T_w	q	ΔT
918	185.0	.300	109.5	45300	11.3
919	185.0	.300	111.3	65900	13.1
920	185.0	.300	111.8	92700	13.6
921	185.0	.300	114.5	106000	16.3
922	185.0	.300	115.6	122000	17.4
1001	14.7	.024	-28.6	7580	14.9
1002	14.7	.024	-21.0	15200	22.5
1003	14.7	.024	-15.5	29600	28.0
1004	14.7	.024	-9.9	45700	33.6
1005	14.7	.024	-4.9	66400	38.6
1006	30.9	.050	2.3	7670	12.9
1007	30.9	.050	7.6	17200	18.3
1008	30.9	.050	11.4	29500	22.1
1009	30.9	.050	15.4	45500	26.0
1010	30.9	.050	16.4	66000	27.1
1011	30.9	.050	19.3	83700	30.0
1012	30.9	.050	24.5	87700	35.2
1013	61.7	.100	34.3	7790	8.7
1014	61.7	.100	39.1	17400	13.4
1015	61.7	.100	41.9	29700	16.3
1016	61.7	.100	47.2	65800	21.6
1017	61.7	.100	48.8	86200	23.2
1018	61.7	.100	49.9	104000	24.2
1019	92.6	.150	57.5	7720	7.4
1020	92.6	.150	61.1	15900	11.0
1021	92.6	.150	64.3	29200	14.2
1022	92.6	.150	66.7	65800	16.6
1101	92.6	.150	58.0	7850	7.9
1102	92.6	.150	61.3	16200	11.2
1103	92.6	.150	64.2	29400	14.1
1104	92.6	.150	66.2	46300	16.2
1105	92.6	.150	66.7	65400	16.6
1106	92.6	.150	67.9	87000	17.8
1107	92.6	.150	70.6	110000	20.5
1108	123.5	.200	76.6	7670	7.6
1109	123.5	.200	81.6	29600	12.6
1110	123.5	.200	84.2	65400	15.1
1111	123.5	.200	86.2	91600	17.2
1112	123.5	.200	89.5	118000	20.5
1113	123.5	.200	87.6	118000	18.5
1114	185.0	.300	104.5	7460	6.3
1115	185.0	.300	107.8	29800	9.6
1116	185.0	.300	110.4	65900	12.2
1117	185.0	.300	110.8	89200	12.6
1118	185.0	.300	113.7	118000	15.5
1119	185.0	.300	115.6	132000	17.4

TABLE H-4

n-BUTANE NUCLEATE BOILING DATA

Data No.	P	Pr	T_w	q	ΔT
605	82.6	.150	146.2	13500	14.3
606	82.6	.150	149.6	37900	17.8
607	82.6	.150	150.8	53300	19.0
608	82.6	.150	153.2	76100	21.3
609	82.8	.150	155.0	91200	23.0
610	110.1	.200	165.0	13300	11.8
611	110.1	.200	168.5	37800	15.3
612	110.1	.200	170.9	76400	17.7
613	110.1	.200	172.7	93800	19.5
614	82.6	.150	151.5	37600	19.7
615	82.6	.150	154.9	76500	23.0
616	82.6	.150	156.0	91300	24.2
617	110.1	.200	172.0	76200	18.8
618	110.1	.200	173.9	99100	20.7
619	165.0	.300	195.9	13300	9.8
620	165.0	.300	197.5	37700	11.5
621	165.0	.300	199.5	76700	13.5
622	165.0	.300	201.1	96700	15.0
623	220.0	.400	220.9	37700	9.4
624	220.0	.400	222.4	76300	10.9
625	220.0	.400	223.9	90000	12.4
626	220.0	.400	225.2	102000	13.7
627	275.0	.500	239.4	6610	6.9
628	275.0	.500	239.1	37600	6.6
629	275.0	.500	240.8	54100	8.3
630	275.0	.500	242.9	76800	10.3
631	275.0	.500	244.5	90600	11.9
632	275.0	.500	246.1	98400	13.5
633	330.0	.600	254.7	12700	4.1
634	330.0	.600	256.7	37400	6.1
635	330.0	.600	261.8	77000	11.1
636	385.0	.700	270.9	12900	4.4
637	385.0	.700	272.8	37500	6.3
638	385.0	.700	274.6	54600	8.1
639	441.0	.800	284.4	12700	3.4
640	441.0	.800	285.6	24800	4.6
641	441.0	.800	286.1	30400	5.1
642	441.0	.800	285.6	37300	4.7
643	441.0	.800	286.2	43500	5.2
1801	110.1	.200	161.7	6910	8.5
1802	110.1	.200	164.7	16400	11.5
1803	110.1	.200	165.2	29100	12.0
1804	110.1	.200	168.0	47600	14.8
1805	110.1	.200	169.9	65100	16.7

TABLE H-4--Continued

Data No.	P	Pr	T_w	q	ΔT
1806	110.1	.200	172.4	89500	19.2
1807	110.1	.200	174.8	103000	21.6
1808	82.6	.150	142.1	7010	10.2
1809	82.6	.150	146.3	16100	14.5
1810	82.6	.150	149.9	29500	18.0
1811	82.6	.150	153.2	52500	21.3
1812	82.6	.150	155.3	74100	23.4
1813	82.6	.150	157.2	92100	25.3
1901	55.1	.100	118.2	6550	13.9
1902	55.1	.100	123.5	16100	19.2
1903	55.1	.100	127.6	28700	23.3
1904	55.1	.100	131.6	46600	27.3
1905	55.1	.100	133.9	65200	29.6
1906	55.1	.100	136.7	83800	32.4
1907	55.1	.100	137.8	89900	33.5
1908	27.5	.050	80.5	6870	17.5
1909	27.5	.050	86.6	16400	23.5
1910	27.5	.050	91.5	29200	28.5
1911	27.5	.050	95.7	43800	32.7
1912	27.5	.050	100.8	65600	37.8
1913	27.5	.050	104.2	74900	41.2
1914	14.7	.027	55.4	6460	24.2
1915	14.7	.027	57.7	15600	26.5
1916	14.7	.027	64.0	28200	32.8
1917	14.7	.027	69.1	42400	37.9
1918	14.7	.027	74.4	56600	43.2
1919	14.7	.027	76.9	63400	45.7

TABLE H-5

n-BUTANE NUCLEATE BOILING ON A FOULED SURFACE

Data No.	P	Pr	T_w	q	ΔT
3801	110.1	.200	161.9	13500	8.7
3802	110.1	.200	162.4	19400	9.2
3803	110.1	.200	163.1	27700	9.9
3804	110.1	.200	164.1	36400	10.9
3805	110.1	.200	164.9	45900	11.7
3806	110.1	.200	165.5	54900	12.3
3807	110.1	.200	166.3	65800	13.1
3808	110.1	.200	166.3	76600	13.1
3809	110.1	.200	168.1	92500	14.9
3810	110.1	.200	166.2	67700	13.0
3811	110.1	.200	164.9	50200	11.7
3812	110.1	.200	164.3	32100	11.1
3813	110.1	.200	162.4	18900	9.2
3814	110.1	.200	162.7	29800	9.5
3815	110.1	.200	164.5	47300	11.3
3816	110.1	.200	166.9	62200	13.7
3901	110.1	.200	163.1	7400	9.9
3902	110.1	.200	164.4	15100	11.2
3903	110.1	.200	164.4	27400	11.2
3904	110.1	.200	164.0	38200	10.8
3905	110.1	.200	165.1	51000	11.9
3906	110.1	.200	167.0	67300	13.8
3907	110.1	.200	168.1	80700	14.9
3908	110.1	.200	169.3	97100	16.1
3909	110.1	.200	168.2	78600	15.0
3910	110.1	.200	167.4	58000	14.2
3911	110.1	.200	165.9	26700	12.7
3912	110.1	.200	164.5	13500	11.3

APPENDIX I

FILM BOILING DATA

Tables I-1 through I-4 list the film boiling data. The averages have not been corrected or modified except for thermocouple calibration. The form of the tables is:

Data No.	Run Number plus data point in run: 3727 means run 37, point number 27.
P	Pressure, psia
Pr	Reduced Pressure
T_w	Average surface temperature in degrees F, calculated from the outer ring thermocouples
q	Average flux, Btu/ft^2-hr
ΔT	$T_w - T_{sat}$, degrees F

TABLE I-1

METHANE FILM BOILING DATA

Data No.	P	Pr	T_w	q	ΔT
2510	673	1.00	-88.0	6730	28.0
2511	673	1.00	-22.3	16400	93.7
2512	673	1.00	75.6	26400	192
2513	673	1.00	203	40100	319
2514	673	1.00	405	61900	521
2515	606	.900	-69.7	6660	52.5
2516	606	.900	34.3	16100	157
2517	606	.900	163	27200	285
2518	606	.900	388	45800	511
2519	606	.900	557	62100	679
2520	606	.900	747	81200	870
2521	539	.800	-54.8	8920	74.3
2522	539	.800	54.2	17700	183
2523	539	.800	282	35400	411
2601	14.7	.022	-136	6620	123
2602	14.7	.022	72.1	12500	331
2603	14.7	.022	220	18600	479
2604	16.5	.025	407	26700	663
2605	33.7	.050	-10.4	11000	228
2606	33.7	.050	145	17500	384
2607	33.7	.050	414	29700	652
2608	33.7	.050	668	42300	906
2609	33.7	.050	833	50500	1070
2610	67.3	.100	13.6	13600	232
2611	67.3	.100	146	20300	364
2612	67.3	.100	272	27000	491
2613	67.3	.100	522	40100	740
2614	67.3	.100	640	47000	858
2615	67.3	.100	772	54800	990
2616	101	.150	-37.3	12100	167
2617	101	.150	136	20600	341
2618	101	.150	330	31500	535
2619	101	.150	527	43300	732
2620	101	.150	753	57800	957
2621	135	.200	102	19700	297
2701	135	.200	74.4	15700	269
2702	135	.200	297	27100	491
2703	135	.200	561	42500	755
2704	135	.200	788	58000	982
2705	202	.300	52.4	15600	230
2706	202	.300	284	27700	462
2707	202	.300	474	40100	651
2708	202	.300	723	58300	901
2709	202	.300	813	65000	991

TABLE I-1--Continued

Data No.	P	Pr	T_w	q	ΔT
2710	269	.400	50.5	15700	216
2711	269	.400	262	27900	427
2712	269	.400	424	38700	589
2713	269	.400	640	54800	805
2714	269	.400	820	69000	984
2715	337	.500	47.0	15500	201
2716	337	.500	238	27000	392
2717	337	.500	410	39300	564
2718	337	.500	647	57400	802
2719	337	.500	849	73300	1000
2801	404	.600	42.4	15900	187
2802	404	.600	215	27800	360
2803	404	.600	374	38900	519
2804	404	.600	553	53200	698
2805	404	.600	723	68000	868
2806	404	.600	794	74600	939
2807	471	.700	12.2	12900	149
2808	471	.700	63.3	16500	200
2809	471	.700	211	27300	347
2810	471	.700	372	39200	509
2811	471	.700	570	56600	707
2812	471	.700	783	76600	920
2813	538	.800	11.1	12600	140
2814	538	.800	69.5	17200	199
2815	538	.800	237	30200	367
2816	538	.800	415	44700	545
2817	538	.800	628	63300	757
2818	538	.800	827	84000	956
2819	606	.900	-13.1	11100	109
2820	606	.900	86.8	19500	209
2821	606	.900	318	38300	440
2822	606	.900	544	58500	667
2823	606	.900	802	86000	925
2824	337	.500	22.0	14800	176
2825	337	.500	-15.7	13200	138
4001	14.7	.022	397	26200	656
4002	14.7	.022	688	41100	947
4003	14.7	.022	181	18400	440
4004	14.7	.022	42.7	12600	302
4005	14.7	.022	-47.2	10600	212
4006	33.6	.050	96.9	16500	336
4007	33.6	.050	238	23900	476
4008	33.6	.050	361	29600	600
4009	33.6	.050	605	41200	844
4010	33.6	.050	828	52100	1066
4011	67.3	.100	707	52000	925

TABLE I-1--Continued

Data No.	P	Pr	T_w	q	ΔT
4012	67.3	.100	928	65000	1146
4013	67.3	.100	453	36300	671
4014	67.3	.100	276	25200	495
4015	67.3	.100	160	19300	379
4016	101	.150	135	19400	340
4017	101	.150	292	28200	496
4018	101	.150	480	41500	684
4019	101	.150	714	58400	919
4020	101	.150	886	69100	1090
4021	135	.200	663	55100	858
4022	135	.200	319	29800	513

TABLE I-2

ETHANE FILM BOILING DATA

Data No.	P	Pr	T_w	q	ΔT
2901	14.7	.021	78.0	7720	206
2902	14.7	.021	208	11600	335
2903	14.7	.021	357	17000	484
2904	14.7	.021	590	27100	718
2905	14.7	.021	809	37100	936
2906	35.5	.050	93.3	8740	188
2907	35.5	.050	249	14400	344
2908	35.5	.050	514	27300	609
2909	35.5	.050	725	39000	820
2910	35.5	.050	848	46700	942
2911	70.9	.100	122	10900	185
2912	70.9	.100	307	18800	371
3001	70.9	.100	207	14900	271
3002	70.9	.100	429	26100	493
3003	70.9	.100	649	38400	713
3004	70.9	.100	823	50200	887
3005	106	.150	207	15000	250
3006	106	.150	416	26300	459
3007	106	.150	619	39300	662
3008	106	.150	847	55900	890
3009	142	.200	247	18700	274
3010	142	.200	446	29700	473
3011	142	.200	676	45700	703
3012	284	.400	357	26100	340
3013	284	.400	484	35800	466
3014	284	.400	712	54500	695
3015	284	.400	858	69100	841
3016	355	.500	350	25900	316
3017	355	.500	261	19600	227
3101	142	.200	410	27200	437
3102	142	.200	833	58600	860
3103	213	.300	777	58600	779
3104	213	.300	850	64800	852
3105	213	.300	382	26600	384
3106	213	.300	570	40900	572
3107	213	.300	262	19700	264
3108	355	.500	403	30200	369
3109	355	.500	570	44200	537
3110	355	.500	762	62600	729
3111	355	.500	850	71200	816
3112	426	.600	367	27400	320
3113	426	.600	255	18400	207
3114	426	.600	567	46000	520
3115	426	.600	760	65500	713

TABLE I-2--Continued

Data No.	P	Pr	T_w	q	ΔT
3116	426	.600	852	75100	805
3117	497	.700	865	79000	805
3118	497	.700	627	53300	567
3119	497	.700	468	37400	408
3120	497	.700	302	22000	243
3121	497	.700	233	15900	174
3122	567	.800	236	15800	166
3123	567	.800	348	26400	277
3124	567	.800	488	40300	417
3125	567	.800	653	58700	583
3126	567	.800	836	78500	766
3127	638	.900	832	80500	751
3128	638	.900	690	62300	609
3129	638	.900	513	42300	432
3130	638	.900	364	27300	283
3131	638	.900	236	14800	155
3132	638	.900	194	11000	113
3133	638	.900	146	6980	64.8
3134	709	1.00	170	11300	79.9

TABLE I-3

PROPANE FILM BOILING DATA

Data No.	P	Pr	T_w	q	ΔT
3201	556	.900	435	26800	240
3202	556	.900	550	39700	355
3203	556	.900	693	56500	497
3301	494	.800	730	58800	546
3302	494	.800	824	70800	640
3303	494	.800	586	41200	402
3304	494	.800	452	26700	268
3305	556	.900	825	71900	629
3306	556	.900	515	33500	320
3307	494	.800	357	16900	173
3308	432	.700	359	17700	188
3309	432	.700	491	31200	320
3310	432	.700	672	50200	501
3311	432	.700	841	70000	670
3312	370	.600	857	70000	701
3313	370	.600	660	48500	504
3314	370	.600	494	31900	338
3401	370	.600	372	20700	216
3402	309	.500	441	26400	301
3403	309	.500	570	38400	430
3501	14.7	.024	202	10600	245
3502	14.7	.024	432	18200	475
3503	14.7	.024	623	27000	666
3504	14.7	.024	813	36500	857
3505	14.7	.024	920	42700	964
3506	30.9	.050	339	16300	350
3507	30.9	.050	563	26900	573
3508	30.9	.050	729	36900	740
3509	30.9	.050	869	45500	880
3510	61.7	.100	352	19100	326
3511	61.7	.100	487	26100	461
3512	61.7	.100	670	37500	644
3513	61.7	.100	843	50100	817
3514	61.7	.100	901	54400	875
3515	92.6	.150	380	21500	330
3516	92.6	.150	524	29700	474
3517	92.6	.150	671	40400	621
3518	92.6	.150	841	52800	791
3519	124	.200	458	27200	389
3520	124	.200	808	54200	739
3521	124	.200	901	61700	832
3522	124	.200	602	37500	533
3523	185	.300	418	26500	320
3524	185	.300	543	36000	445

TABLE I-3--Continued

Data No.	P	Pr	T_w	q	ΔT
3525	185	.300	721	51100	622
3526	185	.300	842	62100	744
3527	309	.500	817	64900	677
3528	309	.500	896	74000	756
3529	309	.500	659	48400	519
3530	309	.500	513	34400	373
3531	309	.500	396	24800	256
3532	247	.400	830	63300	709
3533	247	.400	666	47800	545
3534	247	.400	507	33700	385
3535	247	.400	417	26700	296

TABLE I-4

n-BUTANE FILM BOILING DATA

Data No.	P	Pr	T_w	q	ΔT
3601	14.7	.027	249	10400	218
3602	14.7	.027	386	15400	355
3603	14.7	.027	636	26700	604
3604	14.7	.027	758	33800	727
3605	14.7	.027	890	41100	859
3606	27.5	.050	813	41300	750
3607	27.5	.050	618	29100	555
3608	27.5	.050	521	23900	458
3609	27.5	.050	407	18200	344
3610	55.1	.100	874	50700	769
3611	55.1	.100	688	37200	584
3612	55.1	.100	508	25700	403
3613	55.1	.100	405	20300	301
3614	82.6	.150	498	27200	366
3615	82.6	.150	586	32900	454
3616	82.6	.150	704	41300	572
3617	82.6	.150	847	52200	715
3618	110	.200	864	56800	711
3619	110	.200	754	46800	601
3620	110	.200	633	36500	480
3621	110	.200	504	27100	351
3622	165	.300	883	62700	697
3623	165	.300	759	50400	573
3624	165	.300	626	38300	440
3625	165	.300	488	27300	302
3626	220	.400	681	45000	470
3627	220	.400	789	55600	578
3628	220	.400	887	66000	676
3629	220	.400	631	40300	419
3630	220	.400	486	27600	275
3631	220	.400	451	25000	240
3701	496	.900	841	68700	547
3702	496	.900	749	56500	456
3703	496	.900	675	46800	381
3704	496	.900	607	38000	313
3705	496	.900	522	27700	228
3706	496	.900	444	17900	150
3707	441	.800	432	17900	151
3708	441	.800	484	24200	203
3709	441	.800	538	30400	257
3710	441	.800	638	41700	357
3711	441	.800	731	53300	450
3712	441	.800	886	73600	605
3713	385	.700	422	17600	155

TABLE I-4--Continued

Data No.	P	Pr	T_w	q	ΔT
3714	385	.700	506	26900	240
3715	385	.700	604	38000	338
3716	385	.700	755	55400	489
3717	385	.700	894	73400	627
3718	330	.600	504	27700	253
3719	330	.600	602	38200	351
3720	330	.600	713	50000	462
3721	330	.600	848	66600	598
3722	330	.600	435	20700	184
3723	275	.500	479	26400	246
3724	275	.500	580	36300	347
3725	275	.500	717	50300	485
3726	275	.500	826	62200	594
3727	275	.500	902	71300	670

APPENDIX J

DETERMINATION OF FLUX BY MEASUREMENT OF TEMPERATURE AT TWO RADII

As explained in Chapter IV, it was desired to measure the heat flux by two independent means. One method was to measure current and voltage drop across the heating element, which is supposedly accurate to about ± 1%. The other method which was tried was to measure the temperature at two radii inside the heater body. The applicable equation, where the conductivity of the metal is $k = \alpha T + \beta$, comes from (4-3):

$$q = \frac{1}{D \ln (D_2/D_1)} \left[\frac{\alpha}{2} (T_1^2 - T_2^2) + \beta(T_1 - T_2) \right] \qquad (J\text{-}1)$$

q = surface heat flux, Btu/ft^2-hr

D = heater diameter

T_1 = temperature at diameter D_1 (17/64 inch)

T_2 = temperature at diameter D_2 (21/32 inch)

Table J-1 lists the flux calculated from (J-1) and the flux measured by electrical means for Run #18. Run 18 was selected because it is a typical nucleate boiling run carried out at temperatures where the constants α and β are most accurately known.

Table J-2 lists the same data for Run 29, a typical film boiling run. Oddly enough, agreement is better for the film data which was not corrected (Appendix G). However, in neither case is agreement good enough to attach much weight to the flux calculated from (J-1).

There are two reasons why (J-1) is known to give the wrong results, rather than the alternate method. First is

TABLE J-1

COMPARISON OF FLUX MEASUREMENTS MADE BY INDEPENDENT MEANS: BUTANE NUCLEATE BOILING

Data No.	Flux, Btu/ft^2-hr		Surface Temperature T_w, °F
	Calculated from Electrical Measurements	Calculated from (J-1)	
1801	6,910	7,590	161.7
1802	16,400	17,000	164.7
1803	29,100	33,100	165.2
1804	47,600	54,500	168.0
1805	65,100	76,100	169.9
1806	89,500	105,200	172.4
1807	103,000	120,000	174.8
1808	7,010	8,280	142.1
1809	16,100	17,600	146.3
1810	29,500	31,100	149.9
1811	52,500	58,500	153.2
1812	74,100	84,900	155.3
1813	92,100	106,600	157.2

the great variation in the inner ring measured temperatures at high fluxes (see Appendix G). The second reason is that (J-1) gives high results at high fluxes. It is difficult to see how the flux could be 15% higher than the power expenditure would indicate. Were the fluxes calculated from (J-1) the lower values, the discrepancy might be rationalized in favor of (J-1).

In order to make this method effective for radial heaters, a better method for measuring temperatures is required.

One question which might be raised is: why (J-1)

TABLE J-2

COMPARISON OF FLUX MEASUREMENTS MADE BY INDEPENDENT MEANS: ETHANE FILM BOILING

Data No.	Flux, Btu/Ft^2-Hr		Surface Temperature T_w, °F
	Calculated from Electrical Measurements	Calculated from (J-1)	
2901	7,720	8,830	78
2902	11,600	14,200	208
2903	17,000	17,100	357
2904	27,100	32,000	590
2905	37,100	26,800	809
2906	8,740	7,990	93
2907	14,400	15,700	249
2908	27,300	29,400	514
2909	39,000	41,800	725
2910	46,700	47,600	848
2911	10,900	10,900	122
2912	18,800	21,900	307

does not work well, when measurements of the same kind made in flat plates do work? The answer is that in a radial configuration the fluxes across the inner thermocouple ring are much higher than those across the outer ring, leading to temperature errors. In flat plate geometry, the flux across every thermocouple bead is the same.

APPENDIX K

CIRCUMFERENTIAL TEMPERATURE VARIATION

It was thought that the six outer ring thermocouples, spaced at 60° intervals, would allow radial variations in ΔT to be reported. The results, however, were disappointing.

Part of the difficulty was caused by the effect of heat flux on the temperature readings, described in Chapter VI and Appendix G. Part was also caused by the necessity of using a digital voltmeter ($\pm$ 0.5°F) rather than a potentiometer. At any rate, no pattern was observed which held constant for all runs.

As a final attempt, nucleate boiling runs 38 and 39 were made. For run 39, the heater was rotated 180° and switched end-for-end. The angular locations of the thermocouples in each case are listed on page D2.

The deviations $T_i - \langle T \rangle$ for runs 38 and 39 are listed in Tables K-1 and K-2. T_i is the individual temperature, and $\langle T \rangle$ is the average of the T_i for the thermocouples in the particular ring, as explained in Appendix G. The corrections listed in Appendix G have been applied. Thermocouple No. 13 was broken.

The results are almost completely patternless. If there is a circumferential temperature variation, it must be rather small.

TABLE K-1

DIFFERENCES $T_i - \langle T \rangle$ FOR OUTER RING BEFORE ROTATING HEATER

Data No.	$\frac{q(D/D_i)}{k}$	$T_i - \langle T \rangle$				
		T_{11}	T_{12}	T_{14}	T_{15}	T_{16}
3801	411	0.2	0.8	-0.5	-0.7	0.2
3802	593	0.1	0.7	-0.3	-0.5	0
3803	847	0.2	1.1	-0.4	-0.8	-0.1
3804	1113	0.3	1.6	-0.6	-1.1	-0.2
3805	1406	0.2	2.2	-0.9	-1.1	-0.4
3806	1684	0	2.7	-0.5	-1.4	-0.7
3807	2020	-0.4	3.0	-0.4	-1.7	-0.5
3808	2355	-0.3	4.4	0.4	-3.9	-0.5
3809	2849	-0.9	4.6	-1.1	-1.7	-0.9
3810	2079	-0.6	3.1	-0.5	-1.4	-0.5
3811	1537	-0.8	2.2	-0.1	-0.7	-0.5
3812	982	-0.4	1.2	-0.4	-0.6	0.1
3813	577	-0.2	0.7	-0.7	-0.4	0.7
3814	912	-0.8	0.9	-0.3	-0.2	0.4
3815	1449	-0.9	2.4	-0.4	-1.0	-0.1
3816	1910	-1.6	2.7	-0.1	-0.8	-0.4
Clock Position:		2	4	8	10	12

TABLE K-2

DIFFERENCES $T_i - \langle T \rangle$ FOR OUTER RING AFTER ROTATING HEATER

Data	$\frac{q(D/D_i)}{k}$	$T_i - \langle T \rangle$				
		T_{11}	T_{12}	T_{14}	T_{15}	T_{16}
3901	226	0.5	0.7	1.8	-2.1	-0.8
3902	462	0.5	0.8	1.7	-2.5	-0.5
3903	839	0.5	0.9	1.7	-2.4	-0.7
3904	1168	0.2	0.8	1.9	-2.0	-0.8
3905	1564	0	1.1	1.8	-2.1	-0.7
3906	2026	-0.1	1.1	1.7	-2.2	-0.8
3907	2484	-0.2	1.2	1.6	-2.3	-0.8
3908	2996	0.1	1.6	1.7	-2.3	-1.1
3909	2420	-0.2	1.2	2.0	-2.2	-0.8
3910	1782	-0.4	0.6	2.6	-2.3	-0.5
3911	816	-0.2	0.8	2.2	-2.4	-0.4
3912	412	0.7	0.6	2.0	-2.6	-0.7
Clock Position		4	2	10	8	6